# Influence of Molecular Orientation and Surface Coverage of ω-Functionalized Mercaptans on Surface Acidity

Charles Douglas Taylor

Dissertation submitted to the Faculty of the Virginia Polytechnic Institute and State University in partial fulfillment of the requirements for the degree of

Doctor of Philosophy
in
Chemistry

Mark R. Anderson, Chair
John D. Dillard
William Ducker
Gary L. Long
Brian Tissue

August 15, 2000
Blacksuburg, Virginia

Keywords: Surface Acidity, RAIRS, Structure Property Relationship, Self-Assembled Monolayer

# Influence of Molecular Orientation and Surface Coverage of ω-Functionalized Mercaptans on Surface Acidity

**Charles Douglas Taylor**

## (ABSTRACT)

The compounds 12-phenoxy-dodecane-1-thiol, 4-dodecyloxymercaptophenol and 3-dodecyloxymercaptophenol have been synthesized using a novel synthesis to investigate the effect that the orientation of the functional group has on surface acidity. 3-dodeycloxymercaptophenol and 4-dodecyloxymercaptophenol differ in that the hydroxyl group is substituted on different carbons of the benzene ring. The difference in substitution patterns should present the hydroxyl group in different orientations in the interface between a self-assembled monolayer of the compound and aqueous solutions buffered over a pH range of 3-13. By preparing self-assembled monolayers of these molecules on gold substrates, the ability of the hydroxyl group to donate its proton was shown to depend on the hydroxyl group substitution pattern on the benzene ring through contact angle titration experiments. 3-dodecyloxymercaptophenol clearly showed plateaus at low and high pH with a broad transition between the two plateaus. 4-dodecyloxymercaptophenol showed a clear plateau at low pH but not at high pH, although a transition was observed. Using infrared spectroscopy, it was further shown that the long molecular axis of the benzene ring in 3-dodecyloxymercaptophenol was tilted from the surface normal by 55°. The short molecular axis of the ring was twisted out of the plane of the surface by 28° for self-assembled monolayers of this molecule on gold substrates. In contrast, the tilt angle of 4-dodecyloxymercatophenol was measured to be 46° and was twisted out of the surface plane by 36°. It was also found from cyclic voltammetry experiments in 0.5 M KOH, that the ionized monolayers of 4-dodecyloxymercaptophenol were 2.3 kJ/mol less stable than monolayers of 3-dodecyloxymercaptophenols. This finding suggests that hydrogen bonding and other intermolecular interactions in 4-dodecyloxymercaptophenol are greater than in 3-dodecyloxymercaptophenol.

# Table of Contents

# Table of Figures

# Table of Equations

# List of Tables

# Index of Acronyms

| | |
|---|---|
| AFM | Atomic force Microscopy |
| ATP | Aminothiophenol |
| ATR-IR | Attenuated Total Reflectance Infrared |
| CAT | Contact angle titration |
| CHES | 2-(Cyclohexylamino)ethanesulfonic acid |
| CV | Cyclic voltammetry |
| DNA | Deoxyribonucleic acid |
| GPI | General purpose interface |
| HEPES | N-(2-hydroxyethyl)piperazine-N'-(2-ethanesulfonic acid) |
| HTP | Hydroxythiophenol |
| LB | Langmuir-Blodgett |
| LV | Liquid-vapor |
| MOPS | 3-(N-morpholino)propanesulfonic acid |
| MP | Mercaptopyridine |
| MPP | Mercaptophenyl-phthalimide |
| NMR | Nuclear magnetic resonance |
| PAC | Photoacoustic calorimetry |
| PCA | Polyethylene carboxylic acid |
| QCM | Quartz crystal microbalance |
| RAIRS | Reflection-adsorption infrared spectroscopy |
| SA | Self-assembly |
| SAM | Self assembled monolayer |
| SERS | Surface enhanced Raman spectroscopy |
| SL | Solid-liquid |
| SV | Solid-vapor |
| TAPS | N-*tris*(Hydroxymethyl)methyl-3-aminopropane sulfonic acid |
| TDM | Transition dipole moment |
| TLC | Thin layer chromatography |
| TSM | Thickness shear mode |

# 1.0 Introduction

## 1.0.1 Conceptual Basis of the Dissertation

One area of particular importance in adhesion science is the bonding of metal substrates to one another. In one solution to this problem that is also relevant to the topic of this thesis, phenol is reacted with an excess of formaldehyde under basic conditions to form a resole (figure 1)[1]. The resole reacts further with an epoxide via the hydroxyl groups to toughen the adhesive thereby reducing brittleness. Bonding metals with adhesives has a fundamental problem in that only van der Waals type interactions occur between the metal and the adhesive. Van der Waals bonding leads to a weak adhesive joint compared to a joint formed through covalent bonds. A method suitable for building a covalent bond from one metal substrate to another metal substrate might exist in the form of self-assembled monolayers (SAMs), figure 2. Using SAMs in applications such as adhesion raises several important questions. In the chemistry presented in figure 1, the phenol molecule has all its rotational and translational degrees of freedom available via which the molecule can orient itself appropriately for a favorable reaction to occur. Using a phenolic group in a SAM removes many of these degrees of freedom, which raises the question, what substitution pattern should be used to prepare the SAM. In other words, should the SAM be prepared from a molecule that has the hydroxyl group in the 2, 3 or 4 position with the functional group forming the covalent bond in the 1 position. Once confined to a surface, the hydroxyl bearing molecule can neither freely

rotate nor can it translate through space. Another problem introduced once the

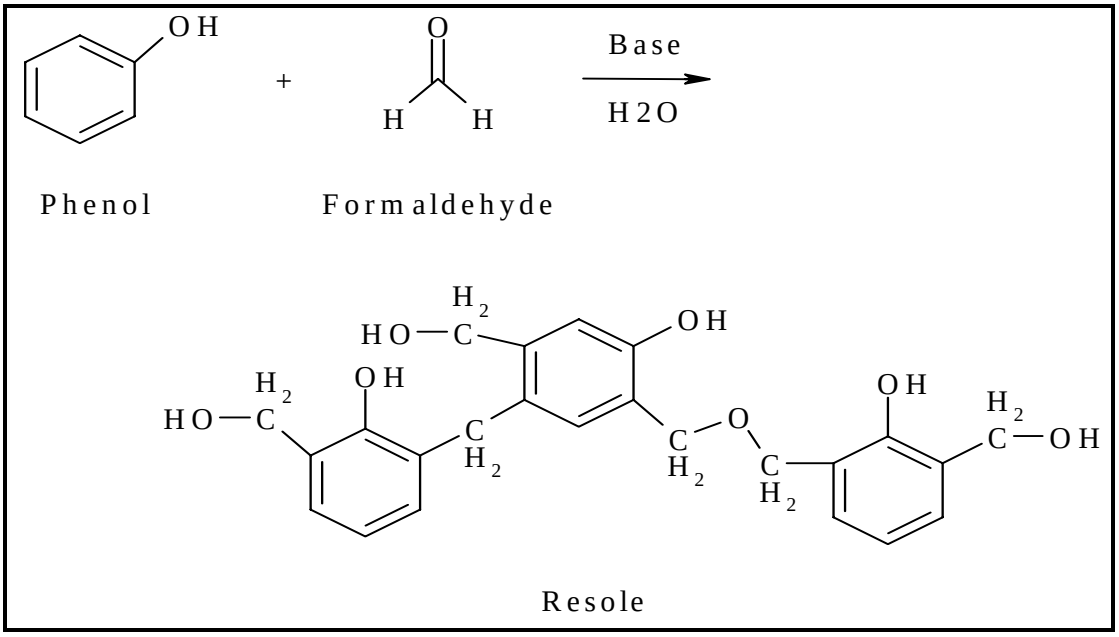


**Figure 1. Reaction scheme used to produce a resole for use as an adhesive to bond metal substrates.**

molecule containing the phenolic group becomes surface bound is steric hindrance. Adjacent molecules that form the SAM may block possible reaction sites. The presence of the metal surface also has an impact because the surface potential of the metal might alter the chemistry of the phenol group. Further complication arises from the directing nature that substituents on benzene rings have in determining what reactive sites are available on benzene rings. The hydroxyl groups may be positioned more or less favorably for hydrogen bonding to occur due to the way the alkyl chains and hydroxyl bearing benzene ring pack in the monolayer. This could impact the ability of the hydroxyl proton to participate in further reactions that toughen the resole. In short, several problems develop that could change the chemical behavior of the phenol in reactions once the phenol containing molecule becomes surface confined. Based upon this reasoning, several experimental objectives are identified which need further study in order to use SAMs as priming agents for adhesive interactions and are the focus of this thesis. Although gold has been used for these studies, SAMs can be prepared on other metals including copper, iron and aluminum.

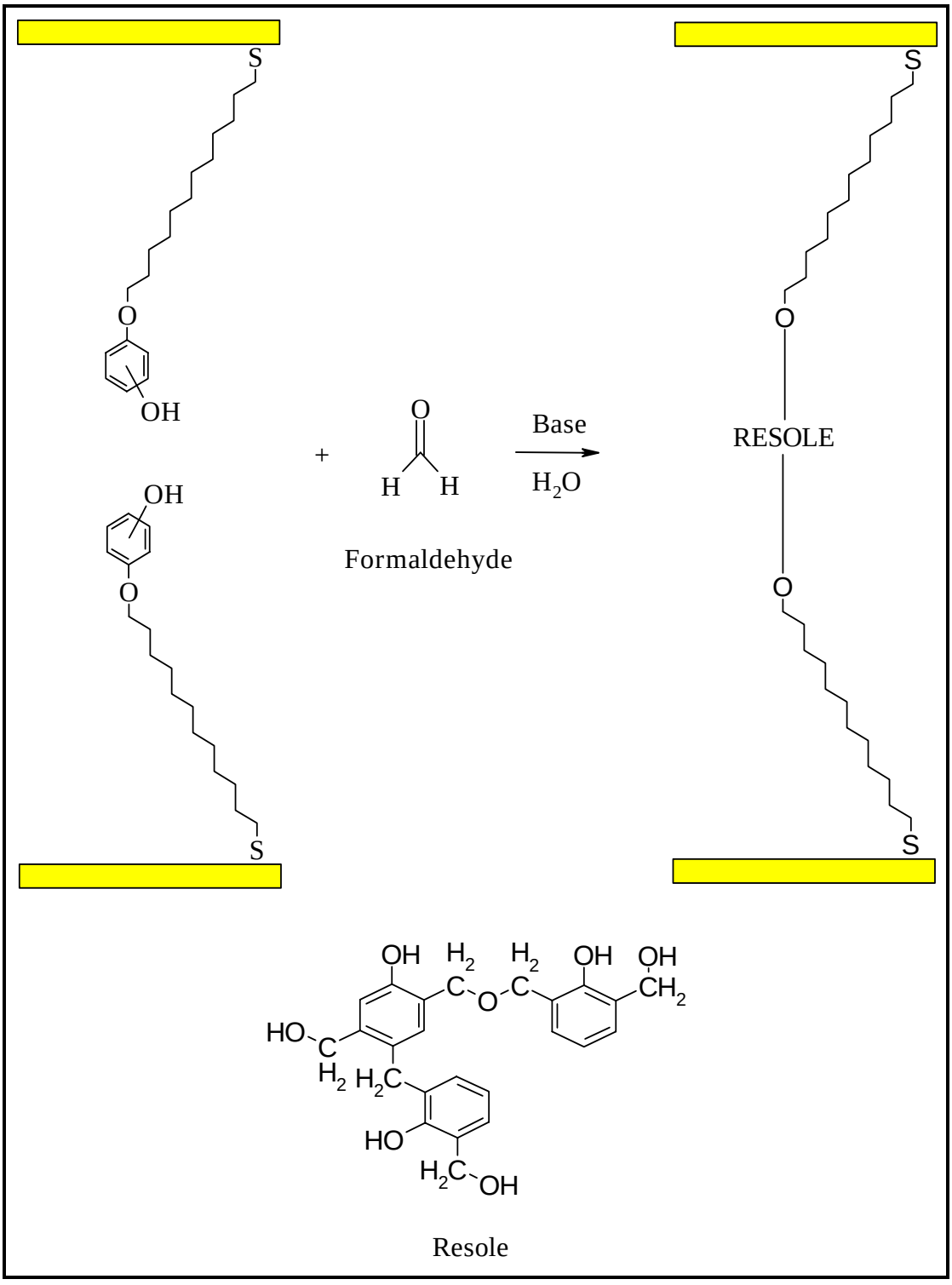


**Figure 2. Conceptual drawing of an adhesive joint formed between gold metal substrates coated with a SAM bearing phenol functionality. Only one molecule of the SAM is shown participating in the resole reaction for clarity.**

Suitable anchor atoms need to be selected for SAM formation, but the use of SAMs as surface primers could be a general technique. The first objective includes synthesizing molecules that are di-functional possessing both the phenol group and an anchor atom capable of forming a covalent bond to the metal. A molecule that is in all other respects identical to the phenol compounds except that it lacks a hydroxyl group must be synthesized to act as a control surface. The second objective involves measuring the acidity of the phenolic proton after confinement to the surface followed by the third objective of measuring the *ex situ* orientation of the phenol group in space. Finally, measuring the intermolecular interactions of the chains composing the SAM and the intermolecular interactions of the hydroxyl group is the fourth objective. In sum, these experiments would provide a well-characterized surface for further studies where actual adhesive bonds are made and broken.

### 1.0.2 Thesis Statement

The overarching research goal presented here is to better understand what effect small perturbations in molecular structure in the solid- liquid interphase have on the properties of the surfaces created from these molecules.

## 1.1 Experimental Approach

Experimental details are presented in those chapters dealing specifically with experimental results. This section intends to foreshadow the experimental methodologies used to make the measurements identified as the experimental objectives in the thesis statement.

Designing molecules to build surfaces suitable to achieve the first objective relies upon synthesizing molecules that meet the requirements of possessing terminal acidic functional groups and other requirements detailed in chapter 2 (figure 3. Panel I). The anchor atom chosen for this project is sulfur since it is now well established that sulfur bonds strongly to gold coated glass substrates[2,3,4,5]. The specific details of the inorganic chemistry involved in the bond formation between gold and sulfur still has unanswered questions[6,7], but it is thought that the hydrogen atom of the thiol is lost and sulfur is oxidized

creating a thiolate moiety. Porter's work using various alkanethiols and sodium

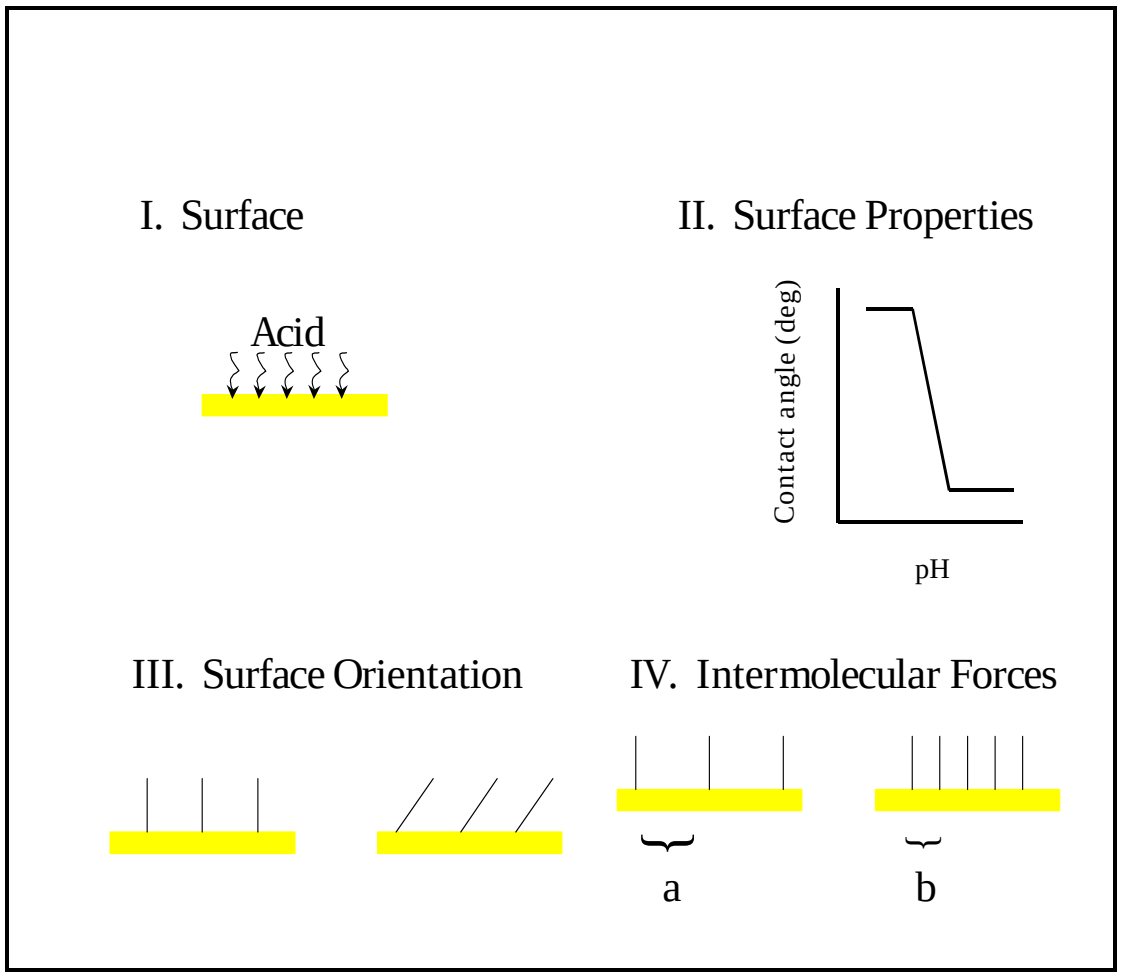


**Figure 3. Diagrammatic illustrati0n of the thesis goals. I. A proposed surface with acid functionality. II. Measurement of the surface acidity using contact angle titration. III. Measuring the average orientation of the molecules making up the SAM. IV. Measuring the intermolecular interactions between the chains of the molecules as a function of their spacing.**

octadecanethiolate shows that when hydrogen is not present, SAMs involving sulfur bonded to gold do not form[8]. Porter's finding requires the synthesis of a compound containing a thiol head group for SAM formation on gold. Several procedures exist in the literature for adding a thiol group to an alkyl chain with varying degrees of success as measured by yield of the final thiol product[9,10,11,12,13,14]. In most all cases reported, yields typically do not exceed 60% when the alkyl chain contains more than ten carbon atoms. Unfortunately, alkyl chains need to contain twelve carbon atoms at a minimum to produce true SAMs[15], so yields involving synthesis of novel compounds containing twelve or

more carbon atoms are expected to be low. This is a particularly acute problem for compounds possessing two functionalities as proposed in this work.

The second objective was to characterize the SAM surface created from the molecules previously synthesized in terms of the acidity of the surface (figure 3. Panel II.). Several reports in the literature have used contact angle titrations (CATs) to make this measurement and CATs have been used here to measure surface acidity. An important distinction is that the measurements made here use a new application of an instrument, the quartz crystal microbalance (QCM), to measure the contact angle. A description of the operating principles of the QCM will be presented along with data demonstrating the equivalence of the QCM method with optical goniometry.

Infrared reflection adsorption spectroscopy provides a convenient tool to measure the orientation of adsorbed molecules on metal mirror substrates, the third objective of the thesis statement (figure 3. Panel III.). Measuring the *ex situ* surface structure of the benzene ring requires knowledge of the normal coordinate vibrations of the entire molecule coupled with intensity measurements of the normal mode infrared bands resulting when light is absorbed. Orientation calculations can then be made using intensity data obtained from the bulk transmission infrared spectrum and the reflection spectrum.

Finally, intermolecular forces have been measured using cyclic voltammetry (CV) electrochemical experiments (figure 3. Panel IV.). By measuring the degree to which the reductive desorption peak potential shifts at nearly constant surface coverage between electrodes coated with 3 and 4-dodecyloxymercaptophenols, a measure of the interaction between the monolayer's chains and functional groups can be made using the current-potential characteristic and the Frumkin adsorption isotherm equation.

Self-assembled monolayers have been widely studied over the past 15 years. Initially these studies were directed toward understanding monolayer structure, and the degree to which the alkyl chains of the monolayer ordered themselves in films of the molecules participating in the self-assembly process. Recent investigations have begun examining how monolayers can be used to

modify surfaces toward specific purposes. The molecules used for forming monolayers range from simple long chain mercaptans such as dodecanethiol or hexadecanethiol, to more complicated molecules possessing terminal functional groups capable of reacting with other species in an adjacent solvent layer.

## 1.2 Self Assembled Monolayer Literature Review

Several reviews of SAMs have been previously reported. Ulman has reviewed monolayers prepared from both Langmuir-Blodgett (LB) and self-assembly (SA) methods[13,16]. Wink[17], Zhong and Porter[18], and Whitesides and Laibinis[19] have written reviews covering various aspects of SAMs. Finklea[20] has reviewed SAMs formed on electrode surfaces, and Nuzzo[21,22] has reviewed SAMs used to prepare model surfaces and their technological applications. Since an extensive review literature already exists describing various SAM studies, only the pertinent literature relevant to the object of this thesis and the general properties of SAMs will be presented.

### 1.2.1 Nature of self assembled monolayers

SAMs are prepared using two primary techniques: Langmuir-Blodgett[13] (LB) and self-assembly methods[23,24,25,26]. LB methods spread an amphiphilic molecule on water and subsequently dip a substrate through the air-water interface or touch a substrate to the amphiphilic layer and remove the monolayer coated substrate for subsequent analysis. In LB monolayers, the amphiphilic molecular film is typically compressed before deposition on the substrate. The SA method offers the advantages of spontaneous adsorption and ordering on the substrate, obviating the need for dipping and compression, and first became widely used after several groups reported experimental results describing SAM properties in the 1980s[21-24,27,28,29]. Figure 4 shows a space filled model of a dodecanethiol SAM supported on a gold substrate. The SAM forms because of

lateral intermolecular interactions between adjacent alkyl chains indicated by the

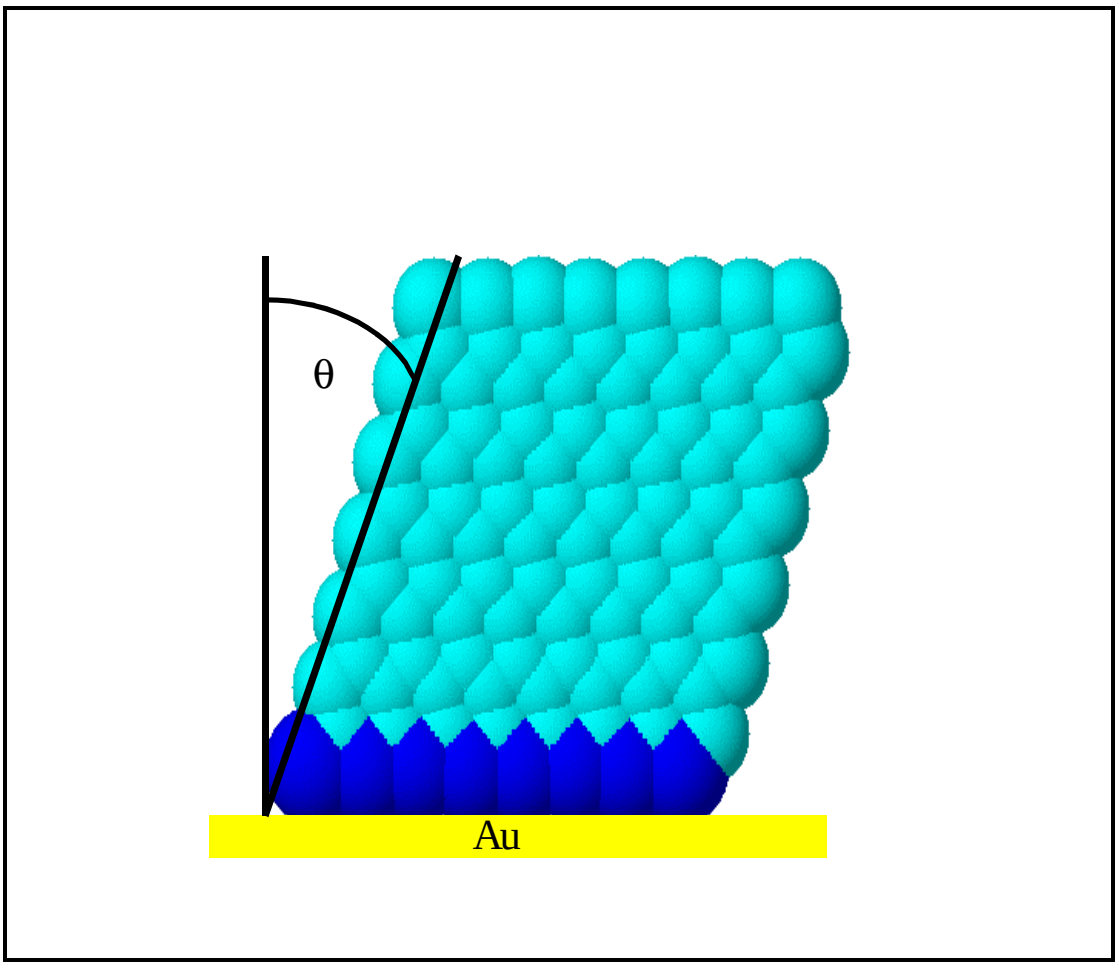


**Figure 4. Space filled model of a dodecanethiol monolayer. The model illustrates the dense packing of the alkyl chains making up the monolayer and the tilt angle, θ, of the alkyl chains measured from the surface normal. Theta depends upon the specific alkyl chain but typically is about 20° to 35° for methyl terminated SAMs on gold substrates.**

all gauche conformation of the chains and strong metal-head group interactions. The SAM properties arise from the strong surface-head group bond, the lateral intermolecular interactions and the packing density of the molecules making up the SAM. SAMs make possible fundamental and technological studies of surfaces ranging from adhesion[30], wetting[17,31,32,46] and DNA sequencing[33] to molecular electronics via nano-scale lithography[34,49] because of the relative simplicity of preparing surfaces from them.

### 1.2.2 Molecules used to make SAMs

SAMs have been prepared from a wide range of molecules. The range of ω-substituted alkanethiols that have been used for SAM preparation include alkanes (linear, branched, fluorinated and deuterated), alcohol, aldehyde, alkenes, alkynes, amide, amine, aromatic, carboxylic acid, ester, ether, halide, or nitrile functional groups[35]. The body of the molecule can contain an equally wide array of functional groups. Literature reports include molecules containing amides[36,37], aromatic groups[38,39,40], conjugated alkynes or alkenes[41,42,43], heteroatoms[44,45,46,47], sulfones or other rigid rod structures[48,49]. The diversity of chemical functional groups that have been used for SAM formation imparts potential widespread technological use of SAMs in diverse fields.

### 1.2.3 Substrates Used to Support SAMs

Gold is the most common substrate used for sulfur head-group SAM support. This is principally because of the strong gold-sulfur bond (167 KJ/mole)[50], and the noble nature of gold allowing it to withstand vigorous cleaning methods. Both single crystal and polycrystalline gold are used with polycrystalline evaporated gold films (1000-2000 Å thick) supported on other substrates such as glass, silicon or cleaved mica being most common. A vapor deposited polycrystalline gold metal film is bound to a supporting substrate such as glass using an adhesive layer of vapor deposited chromium or titanium (50-100 Å thick). This metal under-layer or pure supporting substrate (mica, glass or silicon) can have subtle influences on the structure of the SAM as Walczak[51], Gupta[52] and Caldwell[53] have shown. Electrochemical experimental methods have shown that the metal film surface roughness leads to surface areas about 20%-30% greater than the geometric surface area[8]. Initially, vapor deposited gold has multiple crystal domains, but procedures exist that yield nearly single crystal domains and ultraflat substrates after annealing[54,55]. Golan has reported a comparison of crystallinity and grain size of gold sputtered and vapor deposited on glass, silicon and cleaved mica supporting substrates[56]. Other substrates have been used for SAM support. Along with gold, liquid mercury, platinum, silver and copper have been used for SAM supports of sulfur containing molecules. The

native oxide layer is removed by the adsorption process in the case of silver but not in the case of copper[57,58,59]. High temperature superconducting composites such as Tl-Ba-Cu-O[60] have supported thiol SAMs as have nickel[61,62] and metal alloys such as indium tin-oxide[33,63]. An additional unique substrate used for SAM formation is the underpotential deposition (UPD) of a single or atomic layer of silver or copper on gold or a short alkyl chain surface followed by depositing the SAM atop the metal atomic layer[64,65,66]. These studies show that monolayer stability increases because of the stronger bond between the UPD metal layer and the thiol.

After the substrate has been prepared, it typically is cleaned using different protocols depending on the application. Gold metal films are cleaned in strongly oxidizing solutions such as "piranha" solution (a 1:3 mixture of 30% $H_2O_2$ and concentrated $H_2SO_4$ at a solution mixture generated temperature of 80 °C) (*Caution: this mixture reacts violently with organic material and has been known to explode when stored in closed containers!*)[20]. Alternatively, an oxygen plasma and UV light generated ozone can be used to clean these films[20]. These cleaning methods generate oxide layers that should be removed by an ethanol rinse to avoid the deleterious effects that the oxide layer can have on monolayer structure[67,68].

### 1.2.4 Deposition of the monolayer on the substrate

Most SA methods involve adsorption from a solution of the molecule composing the monolayer at room temperature and various solvents, although vapor deposition of monolayers has been used for some molecules[69,70]. Ethanol is the most common solvent but any solvent capable of dissolving the SAM molecule can be used[5]. Surfactants have been used to disperse insoluble thiols in water for subsequent adsorption of the molecule onto a substrate[71,72]. There is also some evidence suggesting that oxygenated solvents set up equilibrium between adsorption and desorption of the SAM molecule[73]. To achieve the highest quality surface, long deposition times and dilute solutions are required[73]. For millimolar or higher concentrations, a disordered monolayer is deposited in a few seconds, but a period of several hours to days is required for a completely

ordered SAM to form with densest packing between the SAM molecules. Solvent trapping within the SAM can also occur, but an annealing process can be used to remove any trapped solvent as well as removing any kinetically trapped disordered state[74,75,76]. Several different annealing methods exist and include soaking in a hot deposition solution, heating in a gaseous ambient environment after the initial deposition or cycling a SAM coated electrode through a potential range and repeatedly exposing it to a deposition solution.

Other deposition methods exist including vapor deposition under vacuum and ambient pressures if the SAM molecules have a sufficiently high vapor pressure[69,70]. A SAM can be deposited by electrochemical methods by slowly shifting the potential to potentials more positive of the desorption potential[77,78,79].

### 1.2.5 Surface acidity measurements

Several methods have been used to measure surface acidity. Whitesides used CAT[80] and photoacoustic calorimetry (PAC)[81] to study the acidity of carboxylic acid functional groups at the solid-water interphase. Whitesides also used attenuated total reflectance infrared spectroscopy (ATR-IR) and direct potentiometric titration to measure surface acidity of "polyethylene-carboxylic acid" (PCA) obtained from the reaction of polyethylene with chromic acid/sulfuric acid. Other experimental methods used to measure surface acidity include surface enhanced Raman spectroscopy (SERS)[82] and CV[83] as well as interfacial capacitance measurements. Finally, Hu and Bard measured surface confined acid titration curves using atomic force microscopy (AFM)[84].

The most frequently used method to measure surface acidity is the sessile drop contact angle method. In this method, aqueous and non-aqueous solutions buffered over a wide pH range are placed on the surface and allowed to reach thermodynamic equilibrium after which the advancing contact angle is measured goniometricly. The most frequently measured surface used in measuring surface acidity is a carboxylic acid surface prepared from a SAM or from oxidation of polyethylene with a mixture of chromic acid/sulfuric acid. CATs have also been used to measure the basicity of surfaces prepared from amine terminated SAMs. Values of $pK_{1/2}$ obtained from these measurements are invariant with the choice

of buffer. Both inorganic and organic buffer solutions have been used to prepare titration curves of surfaces. The organic buffers used to prepare titration curves include HEPES, N-(2-(hydroxyethyl)piperazine-N'-2-ethane-sulfonic acid; CHES, 2-(cyclohexylamino)ethanesulfonic acid; MOPS, 3-(morpholino)propanesulfonic acid; TAPS, tris[(hydroxymethyl)amino]-methane; and phosphate and triethanolamine. These buffers have a wide range of surface tensions that should cause a noticeable difference in the titration curves if there was a buffer dependent surface free energy effect, but no effect was observed upon the inflection point. This indicates that the buffer components do not act as surfactants[80].

Various spectroscopic techniques have been employed to measure surface acid titration curves. In Whitesides' PAC method, a signal from an acidic surface is measured as a function of pH. The signal measured results from the dissipation energy of a chromophore that has been excited by a short laser light pulse. The dissipation energy heats the surrounding solution producing an acoustic shear wave (the analytical signal) in the liquid film that is measured by a pressure transducer. This method avoids light scattering difficulties introduced by rough surfaces in other spectroscopic methods. In Whitesides' ATR-IR method, a filter paper, initially prepared by immersion in buffer solution of particular pH, is blotted against the acidic surface. Any superficial water is blotted dry and an ATR-IR spectrum of the sample was subsequently obtained after the sample has been vacuum dried under 0.01 torr pressure for one hour. By measuring the area of vibrational bands specifically involved in the ionization process, the degree of acid dissociation can be calculated. Equations 1 and 2 mathematically summarize the procedure for computing the values used to prepare the titration curve.

**Equation 1. Ratio of adsorbencies**

$$R(pH) = \frac{A_{1560}(pH)}{A_{1710}(pH) + A_{1560}(pH)}$$

**Equation 2. Extent of dissociation**

$$\alpha_i(pH) = \frac{R(pH) - R(pH1)}{R(pH13) - R(pH1)}$$

where R(pH) is the ratio of absorbencies (A) at a particular wavenumber and filter paper pH, $\alpha_i$ is the extent of dissociation at each pH and R(pH13) and R(pH1) are used as baseline correction terms and are obtained by measuring the area under each band when the surface is completely ionized, R(pH13) and unionized, R(pH1). The bands used to measure the absorbencies are specific to the system under study and in this system correspond to the carboxylate stretch (the ionization product) at 1560 $cm^{-1}$ and carbonyl stretch (the unionized acid surface) at 1710 $cm^{-1}$. Anderson[85] and Yu have used SERS titrations to measure titration curves. Yu used SAMs of 4-mercaptopyridine deposited on a roughened gold electrode while Anderson used 4-pyridinecarboxaldehyde adsorbed on silver. In essence, the SERS method is identical to Whitesides' method using ATR IR. It has the distinct advantage of being an *in situ* method compared to Whitesides' *ex situ* method. The intensities of bands involved in the ionization process are measured in the presence of buffered aqueous solutions over a wide pH range and compared to the spectrum of the unionized surface. The value obtained initially is further refined by accounting for the effect of surface potential. Values obtained for the surface $pK_{1/2}$ using SERS titration agree to within 10% of values obtained by capacitance measurements.

White *et. al.* used CV to estimate the $pK_{1/2}$ of 11-mercaptoundecanoic acid. By plotting the surface charge density against electrolyte pH, they observed a maximum in the plot. Since the maximum of the plot occurred at a pH that was similar to the $pK_{1/2}$ of the same acid measured by the other experimental methods described in this section of the thesis, they reasoned that the maximum corresponded to the $pK_{1/2}$. The reported value obtained using White's CV method (8.5) differs from the value reported by Creager and Clarke who used CATs to measure the $pK_{1/2}$ (8.0) they report[86]. Significantly, Creager and Clarke used a gold substrate while White *et. al.* used a silver substrate. White suggests that the substrate difference plays a critical role in determining surface acidity because of

the differences between the points of zero charge between the two metal substrates. This difference might also be explained by the different orientation SAM chains make with the surface normal when adsorbed onto silver compared to gold. When adsorbed on silver the alkyls chains are nearly parallel with the surface normal ( tilt angle is 12°), but the chains tilt by approximately 30° when adsorbed on gold[59]. White's experimental method is based upon the reversible protonation-deprotonation of the carboxylic acid functional group of the monolayer.

Bryant and Crooks measured the interfacial capacitance of monolayers of 4-aminothiophenol (4-ATP) and 4-mercaptopyridine (4-MP) using an ac impedance method[87]. Using Smith and White's theoretical model relating the differential interfacial capacitance of a SAM coated metal electrode to the fractional degree of ionization of an acidic or basic monolayer, they calculated $pK_{1/2}$ values of 4.6 and 6.9 for 4-MP and 4-ATP, respectively. The bulk pKa values for 4-MP and 4-ATP are 1.4 and 4.3, respectively. The model developed by Smith and White relates the interfacial capacitance ($C_T$) to the film capacitance ($C_F$), the diffuse layer capacitance ($C_S$) and the degree of protonation (C(f)) through equation three.

**Equation 3. Interfacial Capacitance**

$$\frac{1}{C_T} = \frac{1}{C_F} + \frac{1}{C_S + C(f)}$$

An important finding in these experiments is that the surface pKa is a strong function of the electrode potential. At more positive potentials, the surface pKa shifts to lower values, but the pKa shifts to higher values at more negative potentials.

Hu and Bard used AFM to measure the surface pKa of 3-mercaptopropionic acid (3-MPA) on gold substrates[84]. By using this AFM, Hu and Bard measured the contribution of the surface potential to the broadening of titration curves defined from the onset of dissociation to complete dissociation of the carboxylic acid terminated SAM seen in all surface confined acid titration curves. They made this measurement using Ducker's method of attaching a

silicon colloidal sized probe particle to the tip of a microfabricated AFM cantilever which was rastered across a 3-MPA coated gold substrate under solutions of different pH. Through application of the Gouy-Chapman model of the electrical double layer, they quantitatively determined the pKa of 3-MPA to be 7.7 compared to the bulk pKa of approximately 4. The value they report is in agreement with values obtained from other methods including CATs. CAT experiments give values of 8.0 for the $pK_{1/2}$ of 11-mercaptopropionic acid.

In summary, the researchers described in this section found that the acidity of carboxylic acid terminated SAMs show marked differences compared to bulk solution behavior. The titration curves are broader in the sense that the range of pH units over which ionization begins to complete ionization occurs is greater than in the corresponding range in bulk acid titrations. These groups have also observed that the apparent $pK_{1/2}$ shifts to larger buffer solution pH values (becomes more basic or less acidic) compared to comparable solution $pK_{1/2}$ values. These studies have been limited to carboxylic acid or amine terminated alkane thiols and no reports exist for other terminally functionalized SAMs. No attempt has been made to examine the effect that functional group orientation has on the acidity of surface confined molecules. Answering this question is one of the goals this work.

# 2.0 Organic Synthesis

## 2.1 Synthetic requirements

Synthesizing the compounds needed to measure the influence of the orientation of ionizable functional group on surface acidity proved to be a more difficult aspect of this project than first expected. The molecules used to build the surface via self-assembly had to present an ionizable functional group to the solid-liquid interface such that the spatial position of the functional group at the interface varied in a predictable and reproducible way. The selected molecules also had to have transition dipole moments (TDMs) that were perpendicular and parallel to the long molecular axis of the molecule and were excitable by infrared radiation in the range between 700-3500 $cm^{-1}$. Furthermore, the molecules had to possess alkyl chains of at least twelve carbon atoms so that a well ordered SAM

could be made from them and were soluble in solvents commonly used to prepare SAMs. Finally, the selected molecules had to have bulk solution pKa values that changed little between the substitution positions on the benzene ring. In other words, the pKa of the acidic functional group should not change as a result of being located on the ring in the meta or para position. These requirements limited synthetic options to molecules possessing terminal benzene rings, since choosing other terminal functional groups would not allow the functional group to be oriented with sufficient spatial resolution to affect the pKa.

Figure 5 shows three surfaces prepared via SA supported on gold substrates from molecules that vary only in the substitution position of an ionizable hydroxyl group or the absence of an ionizable functional group. The molecules used to make these surfaces meet all the requirements outlined earlier and are therefore suitable to use in these studies. The essential feature of these surfaces is that the hydroxyl group is located in different positions at the solid-gas or solid-liquid interface. The first surface, prepared from 4-dodecyloxymercaptophenol, shows the hydroxyl group oriented 60° from the surface normal while the second surface, prepared from 3-dodecyloxymercaptophenol, shows the hydroxyl group aligned with the surface normal. This difference in hydroxyl group location should impact the ability of the molecules making up the surface to lose the hydroxyl group proton. The third surface created from self-assembling 12-phenoxy-dodecane-1-thiol on gold has no ionizable terminal functionality and acts as a control surface. The degree to which the hydroxyl group is tilted away from the surface normal in an actual SAM is not expected to be 0° or 60° because of intermolecular interactions and packing effects. However, it is expected that there will be significant differences between the orientation of the hydroxyl groups in the SAM between the two different molecules. A review of the synthetic literature did not find any preparation for the molecules selected for this study nor are the molecules commercially available so a novel synthesis of the needed compounds is presented below.

## 2.2 Retrosynthesis

The absence of prior preparatory procedures or commercial availability of the desired compounds required that a synthetic procedure be developed to prepare 2-, 3-, 4-dodecyloxymercaptophenols and 12-phenoxy-dodecane-1-thiol.

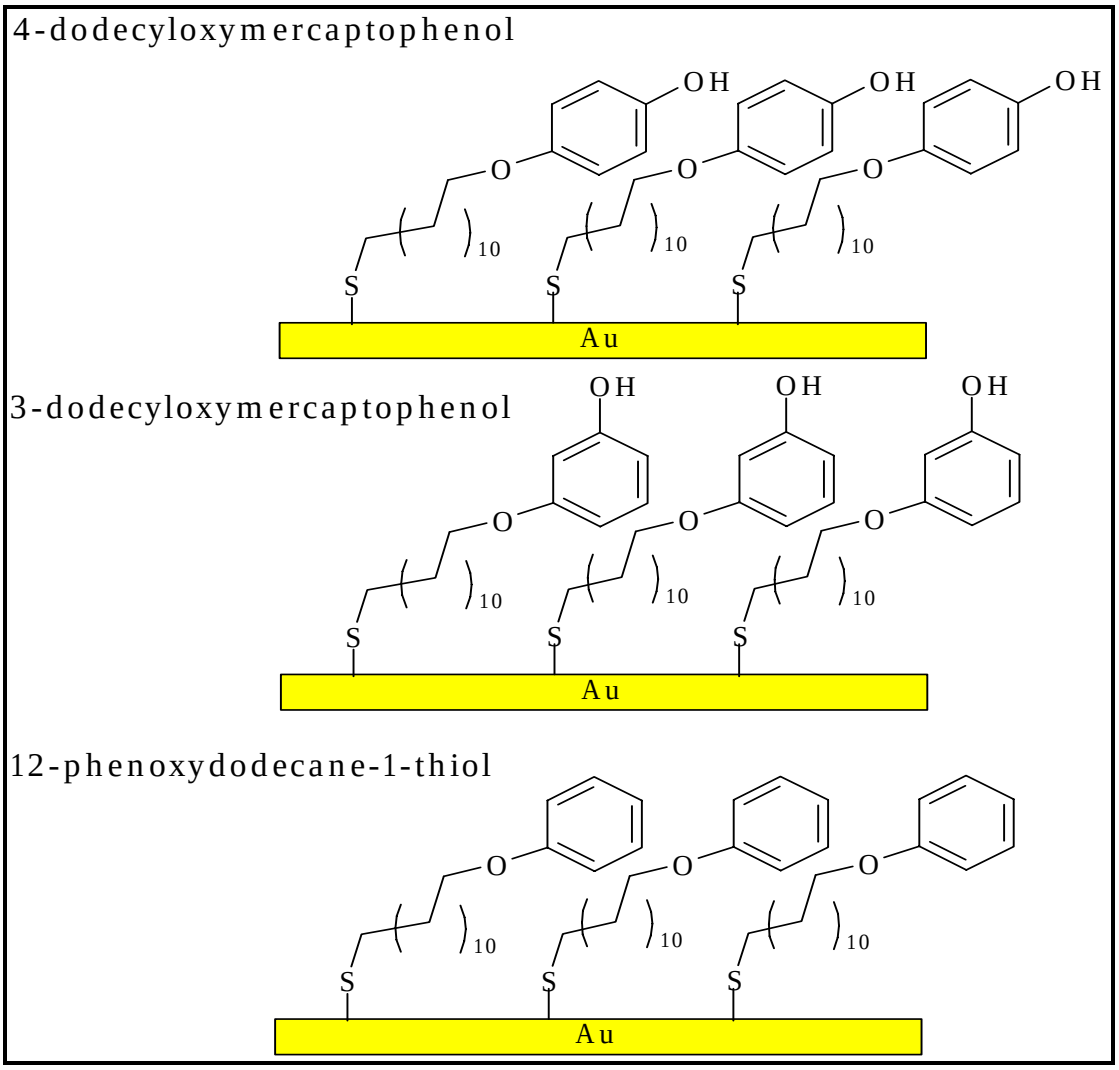


**Figure 5. Three surfaces prepared via self-assembly from molecules meeting the requirements outlined in the text. The first two surfaces show the hydroxyl group oriented at different angles with respect to the surface normal while the last surface does not bear an ionizable functional group making it a good control surface.**

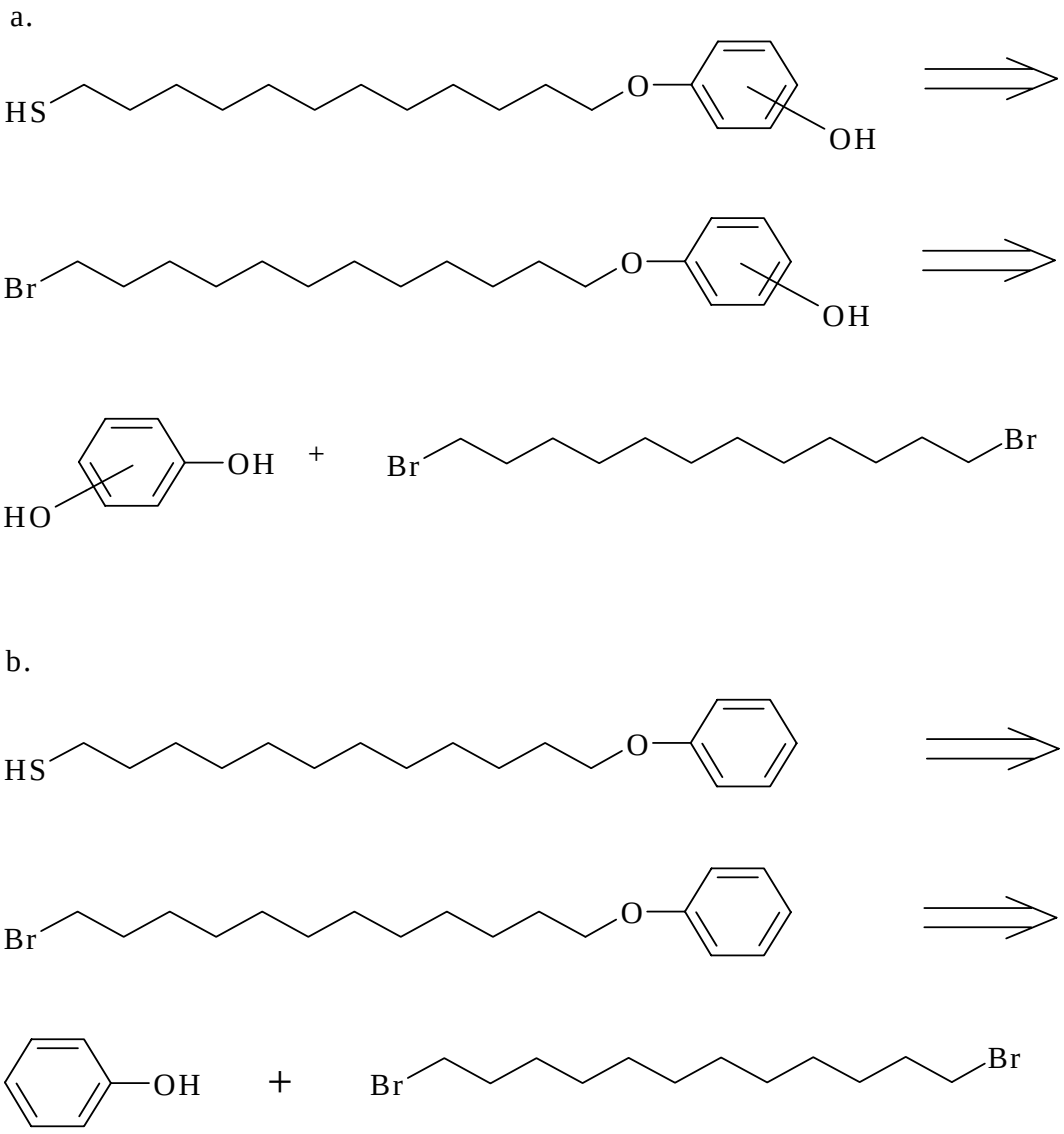


**Figure 6. Retrosynthesis of 3- and 4-dodecyloxymercaptophenols, (a) and 12-phenoxy-dodecane-1-thiol, (b).**

Retrosynthesis (figure 6a) suggests that a suitable pathway for synthesizing 3- and 4-dodecyloxymercaptophenols begins by adding 1,12-dibromododecane to hydroquinone (1,4 substitution on the benzene ring), resorcinol (1,3 substitution) or catechol (1,2 substitution) through nucleophilic substitution at either the one or the twelve carbon atom of the dibromoalkane. A suitable nucleophile could be made from oxidation of hydroquinone, resorcinol or catechol by addition of one equivalent of base to a solution of hydroquinone, resorcinol or catechol creating an oxygen nucleophile. The solvent choice is limited by the requirement that the solvent must promote nucleophilic substitution reactions which forces selection of a polar solvent. Retrosynthetic analysis of 12-phenoxy-dodecane-1-thiol (figure 6b) suggests that a reaction scheme similar to the one used to prepare the phenolic terminated compounds can be used to prepare a surface without ionizable functionality.

## 2.3 Synthetic results and discussion

### 2.3.1 General synthetic methods

Hydroquinone, resorcinol, catechol and 1,12-dibromododecane (Aldrich) were reagent grade and used without further purification. Ethanol (200 proof) was obtained from Midwest Grain products and dried over molecular sieves overnight. Potassium hydroxide and sodium sulfate was obtained from Mallinckrodt and used as received. Hexane and ethyl acetate were obtained from VWR and used as received. IR spectra were collected using a Nicolet model 710 infrared spectrometer equipped with a liquid nitrogen cooled HgCdTe detector set up for transmission mode operation at 2 $cm^{-1}$ resolution. Omnic software (version 3.1, Nicolet) was used to process the interferogram to obtain the transmission infrared spectrum of the new compound. Films of newly synthesized compounds were solvent cast onto NaCl salt plates using 1 mM solutions prepared in dichloromethane (Burdick-Jackson) by depositing 10 μL of a solution of the compound from a micro-liter syringe (Hamilton) onto the salt plate. The solvent was allowed to evaporate leaving a uniformly thick, contiguous film. This method was chosen because film thickness could be reproduced from

sample to sample making quantitative comparison of spectra less difficult. NMR spectra were collected with a Varian 400 MHz nuclear magnetic resonance spectrometer interfaced to a Sun Microsystems Sparcstation workstation and referenced to TMS. Melting points were determined on a Mel-Temp apparatus and are uncorrected. Mass spectra were obtained on a Fison model Quattro GC-MS using electron impact ionization.

### 2.3.2 Synthesis of 3- and 4-dodecyloxymercaptophenols

Resorcinol or hydroquinone (0.30 mol) was added to a boiling heterogeneous mixture of 1,12-dibromododecane (0.13 mol) suspended in water (50 mL) in a three neck round bottom flask with one neck stoppered with a rubber septum (figure 7a). A condenser was placed in the central neck of the flask and stoppered with a rubber septum pierced with a syringe needle to prevent a closed system. A solution of NaOH (4.0 g, 0.10 mol) in water (15 mL) was added to the boiling mixture from a dropping funnel placed in the third neck of the flask over a one-hour period with vigorous stirring. Slow addition of the base solution helped to minimize oxidizing the di-hydroxy compound. A nitrogen

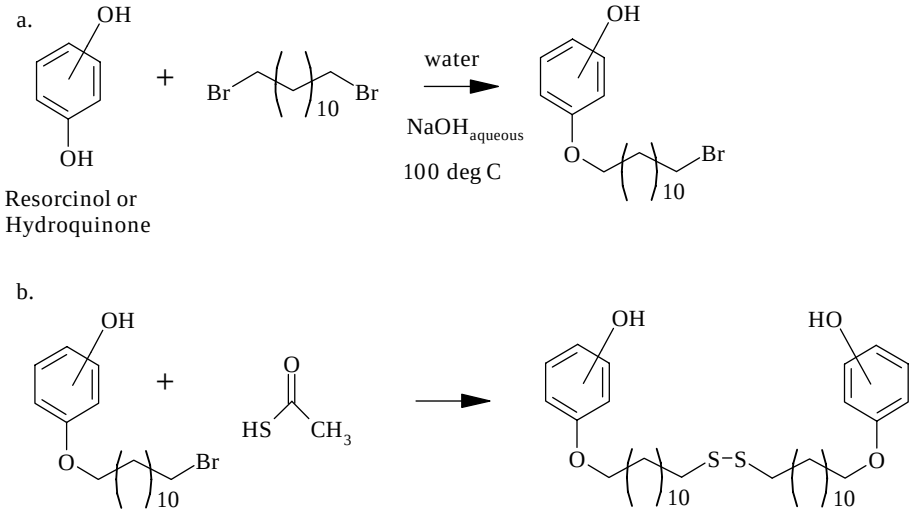


**Figure 7. Reaction used to synthesize 3- and 4-ω-bromoalkoxyphenoxides from resorcinol and hydroquinone, respectively. b. Reaction used to convert the ω-bromoalkoxyphenoxides to a disulfide. Treatment of the disulfide with concentrated HCl leads to the thiol.**

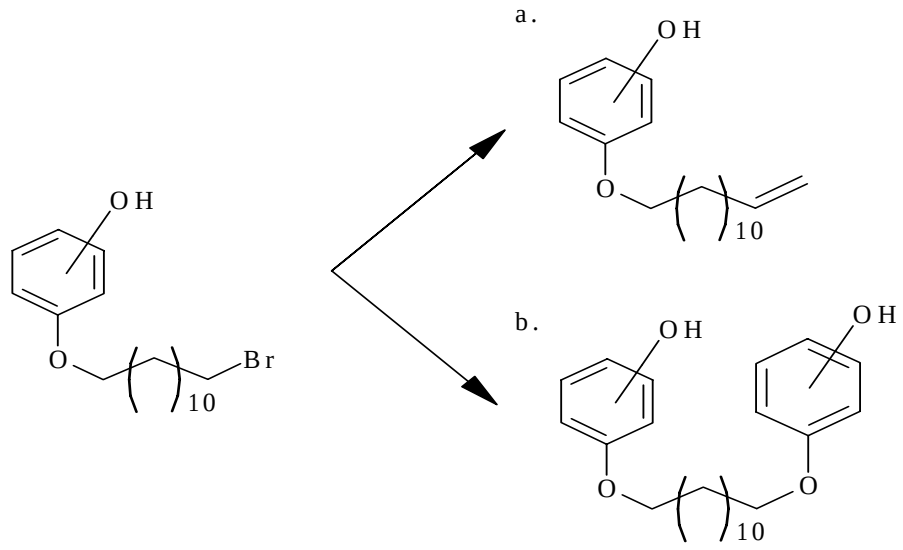


**Figure 8. Two possible side reactions which work together to decrease yields of ω-bromododecyloxyphenoxides. A terminal alkene is formed (a) while 1,12 substitution of dibromoalkane can also occur (b)[88].**

atmosphere was maintained at all times by inserting a needle connected to a nitrogen cylinder through the rubber septum. The nitrogen atmosphere was necessary to minimize oxidation of the di-hydroxy compound in the basic reaction medium. The reaction was left to stir for seven hours while periodically monitoring the progress of the reaction by thin layer chromatography (TLC) (1:1::hexane:ethyl acetate eluent). After cooling in air, the reaction mixture was transferred to a separatory funnel. The dark brown organic phase was separated from the aqueous phase by adding $CCl_4$ (50 mL) followed by with several water washes until a negative test of the wash solution with $FeCl_3$ was obtained indicating that the excess phenol had been removed. The organic phase was dried over $Na_2SO_4$ (anhydrous). The compounds were purified on a silica gel column using flash column chromatography after drying using the same eluent used for TLC analysis.

A broad signal centered at 3377 $cm^{-1}$ in the IR spectrum indicated the presence of the hydroxyl group in 4-bromoalkoxyphenoxide. A similar broad signal at 3490 $cm^{-1}$ confirmed the presence of the hydroxyl group in 3-bromoalkoxyphenoxide. Proton NMR spectra of each compound showed the expected signals consistent with the structure of the desired compound. Proton

NMR signals were observed at δ 3.9 ppm (br t, $OCH_2$), 3.5 ppm (br t, $CH_2Br$), 1.3-2.0 ppm (br m) with a strong signal at δ 1.4 ppm consistent with the alkyl chain. Complex multiplets were observed in the aromatic region consistent with1,3 and 1,4 substitution patterns of the benzene ring. Yields from these reactions were typically 25%-35% relative to theoretical yields calculated from the reaction stoichiometry. Mass spectral data showed parent ion peaks (M+, 357) consistent with the expected molecular weights of the ω-bromoalkoxyphenoxides.

Several attempts to synthesize 2-dodecyloxymercaptophenol were made. NMR spectra of the crude reaction mixture suggested that the desired product formed, but it could not be separated from the reaction mixture despite repeated attempts.

At least two possible side reactions can explain the modest yields obtained when attempting to make these ethers (figure 8). The alkane chain must be terminated with a halide to facilitate subsequent conversion to the thiol. However, terminal alkene formation is a problem via an elimination reaction of the bromoalkane (figure 8a). Another possible side reaction leads to substitution at both the 1 and 12 carbon atoms of the alkane chain by the dianion (figure 8b). Formation of the dianion was minimized by slowly adding the base solution. The elimination reaction is more difficult to prevent and efforts were not made to reduce the alkene formation. The polar solvent needed to support nucleophilic substitution presents another problem because of the long alkyl chain of the dibromoalkane. The chain most likely forms a micelle in the polar solvent that could further inhibit nucleophilic substitution at the carbon alpha to either of the bromine atoms.

### 2.3.3 Synthesis of 12-phenoxy-dodecane-1-thiol

The molecule used to prepare the control surface, 12-phenoxy-dodecane-1-thiol, was prepared by reacting phenol (0.016 mol) with 1,12-dibromododecane (0.021 mol) in ethanol (30 mL) in the presence of a catalytic amount of $CeCl_3$ (10mg). Powdered KOH (0.17 mol) was added to the mixture after all the solid material had dissolved. After fifteen minutes a colorless precipitate developed. The reaction mixture was refluxed gently under nitrogen overnight. After

cooling, the ethanol was removed and water was added to the residual solid. Ethyl acetate was added to extract the organic product from the water and separated in a separatory funnel. The organic layer was washed with water several times until a negative test with $FeCl_3$ indicated that all excess phenol had been removed from the organic layer. Solvent was removed and the crude product was separated on a silica gel column using hexane as the eluent. Recrystallization from hot pentane was induced by cooling to -10° C and yielded 5.1 grams (88% yield) of pure product. Proton NMR of the recrystallized product was consistent with the expected structure. Signals were observed at δ 4.0 ppm (br t, $OCH_2$), 3.4 ppm (br t, $CH_2Br$), 1.3-2.0 ppm (br m) with a strong signal at δ 1.3 ppm consistent with the alkyl chain. Complex multiplets were observed in the aromatic region, δ 7.3 ppm (m) and 6.9 ppm (m), consistent with the substitution pattern of the benzene ring. Mass spectral data showed a parent ion peak (M+, 340) consistent with the expected molecular weights of the 12-phenoxy-dodecane-1-thiol.

2.3.4 Conversion of the ω-bromoalkoxyphenoxides to thiols

Several literature procedures are available for converting haloalkanes to thiols[10,12]. Unfortunately, the literature methods give low yields and appear to be highly dependent on alkyl chain length since most methods tried gave the disulfide product or did not convert the haloalkane to the thiol or disulfide at all. Methods to reduce disulfides to thiols exist which also appear to be low yielding procedures based upon the experimental results obtained in this work. A recent report by Reddy, Rao and Iyengar bears this finding out[89]. They find that the previously published disulfide reduction reactions suffer from long reaction times, low yields, hazardous and expensive reagents and difficult purification procedures. Unfortunately, this work was not published early enough to take advantage of the increased yields (>90%) and chemoselectivity to prepare the molecules used in this work.

To a solution of the ω-bromododecyloxyphenoxides or the ω-bromododecyloxybenzene (0.003 mol) in DMF (10 mL) was added potassium

thioacetate (0.003 mol). The solution became cloudy and was stirred at room temperature for three days. Diethyl ether was added to the reaction mixture to extract the product. The mixture was separated and the ether removed. The crude material was dissolved in acetone (10 mL) and 3 M NaOH (15 mL) was added. Two layers immediately separated and the mixture was stirred for three hours and then neutralized by adding 1 N HCl followed by extraction into diethyl ether and dried over $Na_2SO_4$. The ether was removed and the crude material was recrystallized from hot pentane by decanting the pentane into a separate flask because most of the crude material remained insoluble in pentane. A white solid precipitated from the cooled pentane after 36 hours. A second recrystallization from hot pentane was necessary to obtain the pure thiol (0.150 g) in 15% yield. The only difference between the proton NMR spectra of the isolated pure 3- and 4-dodecyloxymercaptophenols and ω-bromoalkoxyphenoxides was the disappearance of the signal at δ 3.5 ppm ($CH_2Br$) and the appearance of a signal at δ 2.5 ppm ($HSCH_2$). A similar peak was observed in the proton NMR spectrum of 12-phenoxy-dodecane-1-thiol, δ 2.5 ppm ($HSCH_2$) as was the absence of the peak at δ 3.5 ppm ($CH_2Br$). Mass spectral data showed a molecular ion peak consistent with the loss of bromine and addition of the thiol group for all three thiol compounds.

## 3.0 Contact angle titration using the QCM

After preparing the surfaces shown in figure 5 from molecules whose synthesis was detailed in chapter 2, the next goal was to measure the surface acidity of the molecules. While several methods were outlined in chapter 1 for making this measurement, CAT of the surface is the most convenient method to use despite its tedious nature. As the work of the groups referenced in chapter 1 shows, data from CAT produces titration curves similar to the other methods outlined in chapter 1. This might be surprising since CAT was the first method used to measure surface acidity, but surface titration curves measured by CAT agree well with titration curves measured by the other methods discussed in chapter 1. Optical goniometry is the standard method for measuring contact angle, but the contact angle data presented here was determined by applying a

new method based upon the QCM. The QCM method was selected for these experiments because of its novelty and the ease with which the angle could be determined. In conventional goniometry, a cross hair is used to find the tangent line (contact line) between the liquid and gas phases on the solid phase. This is often difficult to measure accurately. The QCM does not suffer from this problem. The QCM could be more easily automated as well at lower cost than image capturing capable goniometer systems. Data will be presented that demonstrates that contact angles determined by the QCM method are equivalent to contact angles measured by optical goniometry. The data was measured using phenol solutions whose surface free energies varied considerably with the weight per cent of phenol in solution. A 2.76% (w/w) $Na_2SO_4$ solution was used to measure the maximum contact angle. Before presenting the data obtained from CAT experiments using the QCM, the general operational principles of the QCM will be presented which will be followed with a discussion of the circuit and experimental apparatus used to make the CAT measurements. The importance of using buffered solutions for measuring surface acidity will then be discussed, and Young's equation will be used to develop a semi-theoretical model of the CAT experiment. Data will also be presented demonstrating that contact angles measured with the QCM are the same as contact angles measured with a goniometer. Finally, data will be presented demonstrating the different acid behaviors of 3- and 4-dodecyloxymercaptophenol surfaces.

### 3.1 The quartz crystal microbalance

The quartz crystal microbalance consists of a quartz crystal coated on both sides with a metal acting as an electrode through which a potential can be established. The disk diameter of the quartz is around one inch with smaller and larger diameters possible depending on the application. The electrodes can be deposited symmetrically or asymmetrically on the opposing faces of the crystal, but usually a symmetrical arrangement is used. Metal tabs are deposited on the quartz crystal at the same time as the central electrode disk, but the tabs are placed so that they extend to opposite edges of the crystal and do not overlap each other as do the electrodes. The tabs are used to establish electrical

connection to the oscillator circuit. The area of the electrode is usually 0.25 $in^2$, but varies depending on the application and whether or not an asymmetrical or

**Figure 9. An image of a quartz crystal used in the quartz crystal microbalance when mounted in a crystal holder. The center of the quartz is coated with gold electrodes on opposing sides. Gold tabs are connected to the central electrode on opposite sides of the crystal so that the crystal only oscillates between the central electrodes. Electrical connection to the oscillator circuit is made through the terminals of the crystal holder (white ceramic piece at the bottom of image). Silver paint[90] has been applied to the spring clamps on each tab to improve instrument stability.**

symmetrical electrode arrangement is used. Upon application of potential, AT-cut quartz crystals oscillate in thickness shear mode (TSM) meaning that the motion of the disk surface is parallel to the plane of the disc face (see figure 10). The electrode design is important because it can prevent exciting flexural modes in the crystal that can couple with the thickness shear mode and produce spurious frequencies[91]. A thicker electrode (greater than 100 nm) can prevent coupling between the various modes as can contouring the face of one or both sides of the crystal. Besides the crystal, an oscillator circuit is needed to drive the crystal oscillations and a variety of circuits has been used. The frequency change upon loading of the QCM is usually monitored by a frequency counter that can rapidly (msec) measure frequencies with high precision, typically 1 part in 1,000,000 or better.

The first use of a QCM was reported by Sauerbrey[92] who derived a relationship between the mass deposited on the electrode of a quartz crystal

resonator and the change in the frequency of the resonator after mass deposition (eqn 4). In equation 4, $\Delta f$ is the change in frequency from the resonant frequency after mass has been deposited on the electrode surface, $\Delta m$ is the mass change, $f_0$ is the fundamental frequency of the resonator, $\mu_q$ and $\rho_q$ are the shear modulus and density of the quartz, respectively.

**Equation 4. Sauerbrey equation**

$$\Delta f = \frac{-2\Delta m f_0^2}{\sqrt{\mu_q \rho_q}}$$

His equation, now known as the Sauerbrey equation, has been the foundation for developing the QCM into a widely used sensor for monitoring thin metal film

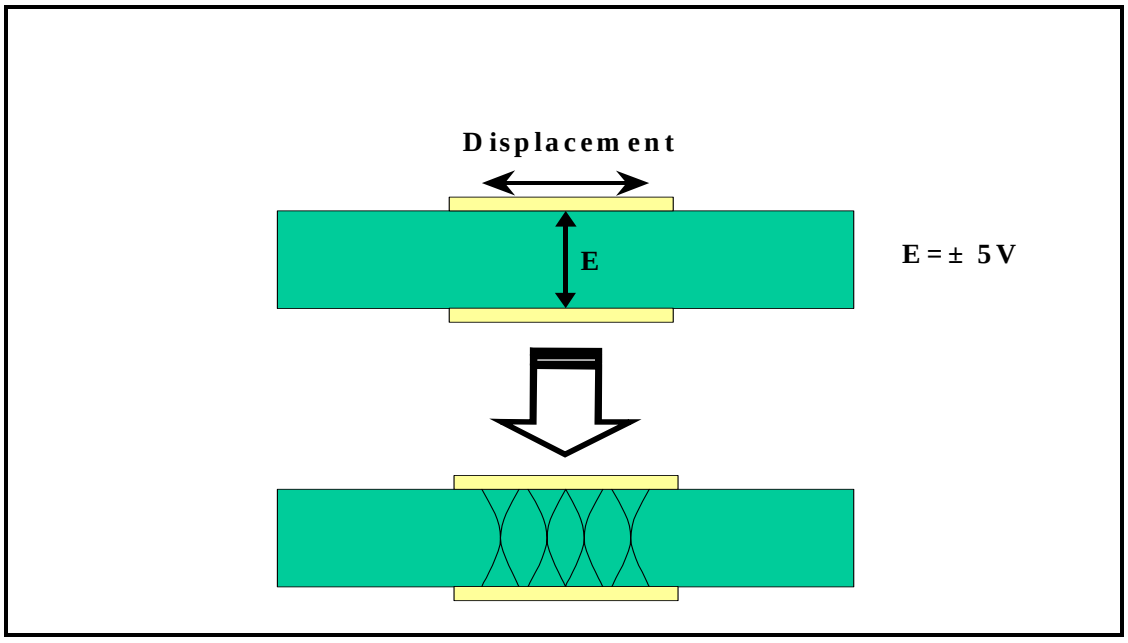


**Figure 10. Application of potential to the electrodes of the quartz crystal resonator sets up standing waves, black arcs, in the quartz which have antinodes at the surface. The gold colored rectangles are gold electrodes vapor deposited onto the green quartz crystal.**

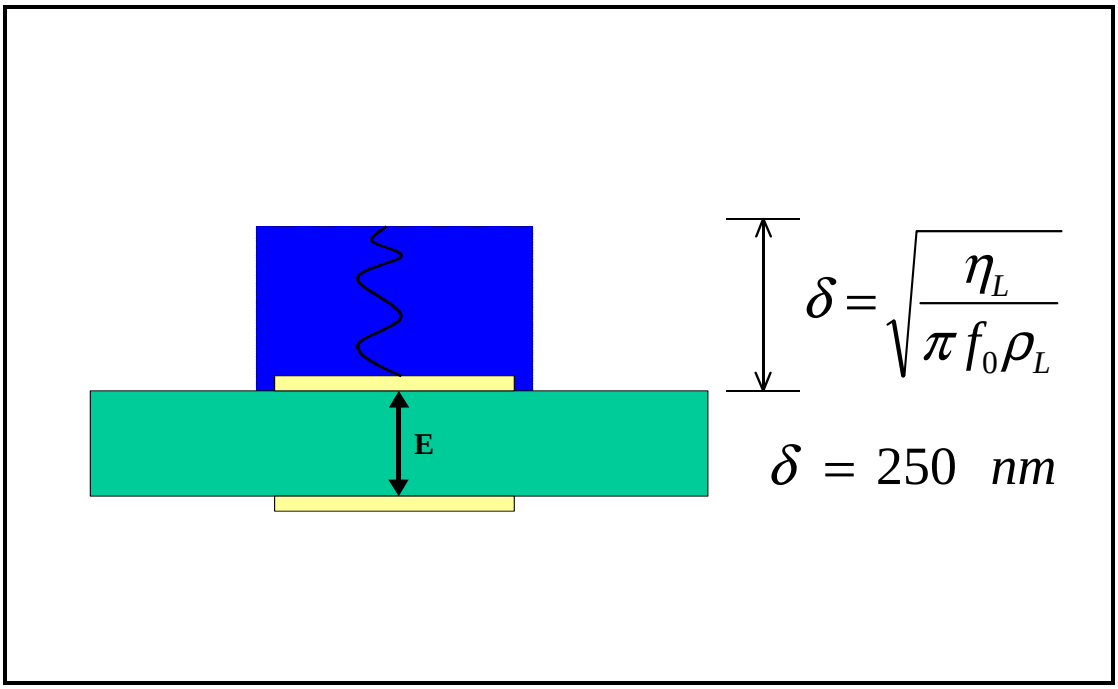


**Figure 11. The shear wave propagates from the quartz crystal resonator into the liquid, blue, via coupling with shear waves generated in the liquid. The equation is explained in the text.**

deposition in vapor deposition chambers. Sauerbrey's equation is strictly applicable only when the deposited material is rigidly coupled to the electrode of the resonator. An additional caveat applies because a thick overlayer of material on the electrode surface generates a non-linear relationship between the frequency change and mass of material deposited on the electrode although corrections have been developed[91]. Until recently, the QCM was limited to use in gaseous environments because it was thought that crystal oscillation would be quenched in liquid environments. Several reports in 1980 showed experimentally that oscillation quenching did not occur when one QCM electrode was exposed in a flow cell to a liquid pumped through the flow cell[93]. Most descriptions of how the quartz crystal oscillation coupled to the fluid were based upon empirical fitting of experimental data. Kanazawa and Gordon at IBM developed a physical model in 1983 that describes the coupling of the elastic shear waves in the crystal with the viscous shear waves in the liquid[95]. Previous models relied upon complicated electrical engineering analysis by invoking a

transmission line analog model[94]. A short description of the physical model they developed is warranted, however the mathematical details are omitted.

### 3.1.1 Kanazawa and Gordon's model of coupling between a liquid and a quartz crystal resonator surface[95]

Application of a potential across the electrodes of the quartz crystal resonator sets up shear waves with antinodes at the surface of the crystal (figure 9). The shear waves in the AT cut quartz crystal are described by the Helmholtz differential equation obtained by combining the stress/strain equation with an equation describing the net force acting on a slab of the quartz crystal. The solution to the Helmholtz equation describes the velocity of shear waves in the quartz crystal resonator in both the positive and negative surface normal directions. In a similar way, the velocity of the fluid at the surface of the resonator can be found from the differential equation developed by combining equations describing the stress/strain of the fluid and the force acting on the fluid. Applying the constraint that the amplitude of the velocity of the shear wave in the liquid equal the amplitude of the velocity of the shear wave in the quartz crystal leads to an equation describing the damping of the propagated shear wave from the quartz crystal surface into the fluid. An important assumption made in Kanazawa and Gordon's derivation is that a small layer of the liquid is rigidly coupled to the quartz resonator surface. Based upon agreement between experimental results and the predictions obtained from the model, this assumption appears valid. The resonance condition can be found by applying Newton's law of equal and opposite forces to the interface between the quartz crystal resonator and the liquid in the limit that the in-phase shear stress component on the liquid side is equal to but opposite that on the quartz side (figure 11). Ultimately, Kanazawa and Gordon's equation relates the viscosity and density of the liquid to the frequency change observed through equation 5

**Equation 5. Kanazawa and Gordon's equation**

$$\Delta f = -f_0^{3/2}\left(\frac{\rho_L \eta_L}{\pi \rho \mu}\right)^{1/2}$$

where $\rho_L$ and $\eta_L$ are the solution density and viscosity, respectively. The fundamental frequency, $f_0$, is the frequency of the quartz crystal resonator and $\rho$ and $\mu$ are the density and shear viscosity of the quartz crystal, respectively. The frequency change, $\Delta f$, is the difference between the fundamental frequency of the quartz crystal when it is unloaded and the frequency when it is loaded. The equation shown in figure 11 describes how far the shear wave propagates in the solution. The variables in the equation are the same as those used in equation 5. The value shown in the figure was that calculated for a 5 MHz AT cut quartz crystal and clearly shows that only a thin layer of the liquid is sensed by the resonator. It is important that the type of quartz crystal used in the resonator be specified since there is a difference between the shear moduli of different cuts of quartz, AT versus BT, for example. AT and BT cut quartz crystal are distinguished based upon the angle at which the crystal is cut with respect to the optical axis.

### 3.1.2 Lin and Ward's extension of the Kanazawa-Gordon equation[96]

Lin and Ward have extended this treatment to cases where the electrode of the QCM is not completely covered by the liquid and this extension is the basis of the contact angle measurement made in these experiments. According to them, the frequency change due to loading the quartz crystal electrode with a liquid film having radius, r, is given by

**Equation 6. Change of frequency due to loading with one fluid**

$$\Delta f_1 = -\frac{\pi}{2}\delta_1\rho_1 K\frac{r_e^2}{\beta}\left[1-\exp(-\beta\frac{r^2}{r_e^2})\right]$$

where $\delta_1 = (\eta_1/\pi f_0\rho_1)^{1/2}$ which is the decay length of the acoustic shear wave propagated into the fluid, K is the maximum sensitivity at the center of the electrode, $r_e$ is the electrode radius and $\beta$ is a constant that defines the steepness of the sensitivity dependence on r. If a drop of fluid 2 is placed in the center of the electrode and is surrounded by the first fluid, the frequency change due to loading by the second drop is given by

**Equation 7. Change of frequency due to loading with 2 fluids**

$$\Delta f_2 = -\left[\int_r^{r_0} K \exp\left(-\beta \frac{r^2}{r_e^2}\right)\delta_1\rho_1(\pi r dr) + \int_0^r K \exp\left(-\beta \frac{r^2}{r_e^2}\right)\delta_2\rho_2(\pi r dr)\right]$$

where $\delta_2 = (\eta_2/\pi f_0 \rho_2)^{1/2}$ which is the decay length of the acoustic shear wave in fluid 2 and $\eta_2$ and $\rho_2$ are the viscosity and density, respectively, of fluid 2. The quantity, $r_0$, accounts for the portion of the quartz crystal that is covered by fluid 1 but is not covered by the electrode. The difference between $\Delta f_1$ and $\Delta f_2$, $\Delta f$, is given by

**Equation 8. Frequency difference**

$$\Delta f = \Delta f_2 - \Delta f_1 = -\frac{\pi}{2} K \frac{r_e^2}{\beta}\left[1 - \exp(-\beta \frac{r^2}{r_e^2})\right]\left[\delta_1\rho_1 - \delta_2\rho_2\right]$$

with all variables previously defined. The numbers one and two refer to fluid one or fluid two. The term $\delta_1\rho_1$ is zero when fluid one is air so equation eight simplifies to

**Equation 9. Frequency difference in air**

$$\Delta f = -\frac{\pi}{2} K \frac{r_e^2}{\beta}\left[1 - \exp(-\beta \frac{r^2}{r_e^2})\right]\left[\delta_2\rho_2\right].$$

Importantly, equation nine is identical to Kanazawa and Gordon's equation in the limit that the entire surface of the quartz resonator is covered with fluid two[97]. At the center of the quartz resonator, the sensitivity function, $\beta$, is relatively flat so the exponential character in equation eight can be disregarded. Then the frequency change is given by

**Equation 10. Frequency change at electrode center**

$$\Delta f = -\frac{\pi}{2} K r^2 \left[\delta_1\rho_1 - \delta_2\rho_2\right]$$

or this equation can be rewritten with $C=-(\pi/2)K\delta_2\rho_2$ as equation eleven

**Equation 11. QCM constant equation**

$$\Delta f = C\left(1 - \frac{\delta_1 \rho_1}{\delta_2 \rho_1}\right) r^2 = Cr^2$$

if fluid one is air. This last equation suggests that a plot of frequency change versus the square of the radius of the fluid drop should be linear with the slope of the line equal to the "calibration constant" of the particular resonator used to make the measurement. A more detailed development is given in Lin and Ward's paper. Figure 12 summarizes this mathematical discussion. As a drop at constant volume wets a surface, the radius of the drop measured from the center of the drop increases covering a larger area of the surface. As the drop covers a larger area of the resonator electrode, the frequency should decrease according to equation 9. For the same drop volume to cover a larger area of the crystal electrode surface, the contact angle made by the drop at the interface must decrease. The contact angle changes because of the changing interactions between surface free energies between the vapor, liquid and solid phases. These last two facts are the basis of measuring the contact angle with the QCM. Experimental evidence demonstrating that the frequency changes with the

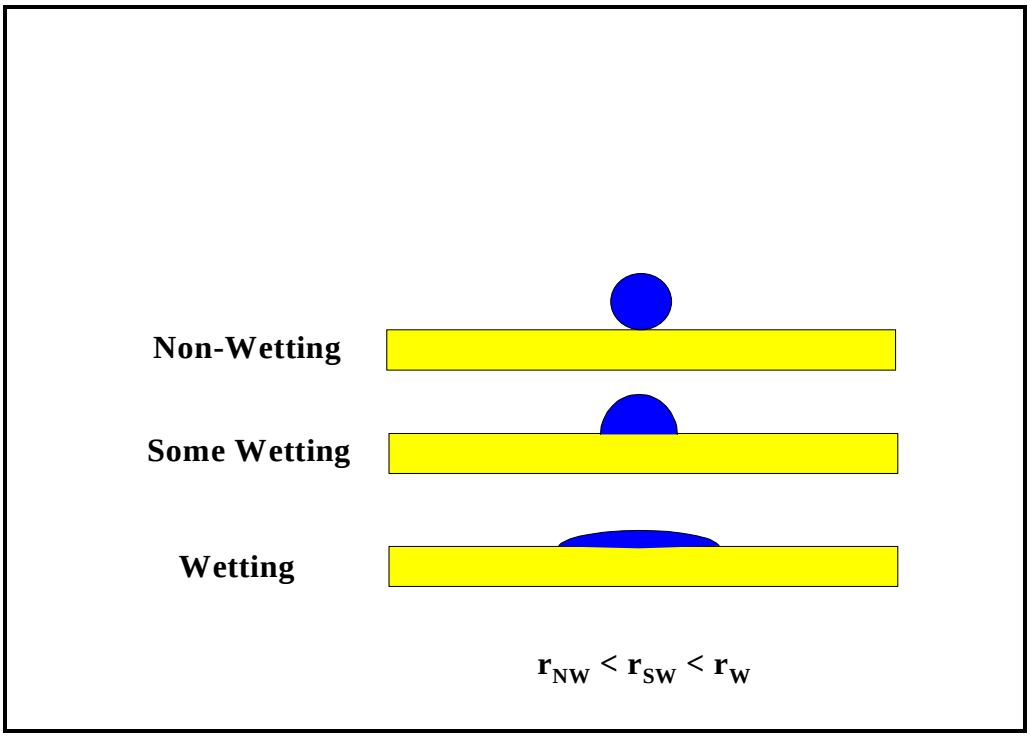


**Figure 12. The drop of probe fluid placed on the QCM electrode decreases the contact angle with the surface as the surface becomes wetted by the probe liquid. The same drop volume is used in all three cases.**

surface free energy of constant volume drops of phenol solutions is shown in figure 21.

### 3.2 The crystal oscillator circuit

To force the crystal to begin oscillation, a potential must be applied across the electrodes of the crystal. The choice of which type of oscillator circuit to use determines the instrument stability, and dictates the type of experiments that can be carried out. Three designs have been published in the chemical literature and at least two books[98] have been published on the subject of oscillator circuits. Bruckenstein and Shay[99] designed a circuit that references the working crystal frequency to an external crystal. This circuit had the disadvantage that the working crystal is not set to true ground. This circuit has the highest signal to noise ratio of the three circuits and has been used to successfully monitor monolayer mass changes. Given the high signal to noise ratio of the circuit, it would seem to be an ideal candidate for the present application except that it is has the ungrounded electrode which might influence the instrument's stability.

Benje[100], *et. al.* used a more conventional oscillator based upon a modified Pierce-Miller oscillator circuit that is frequently used in other electronic applications. This circuit might have been a good choice to use for making contact angle measurements because the oscillator's frequency is relatively insensitive to small changes in resistance or capacitance that might result from ionization processes in electrolyte solutions. In the modified Pierce-Miller circuit, the working electrode is at true ground, which should help promote a stable signal, and the signal amplitude can be increased in the limit of large viscous losses. Unfortunately, the oscillation frequency of this circuit suffers from a temperature dependency that is difficult to correct even when using AT-cut quartz resonators. The modified Pierce-Miller circuit is also sensitive to power supply fluctuation. Finally, Buttry[101] has published a circuit that is stable to better than one Hertz over tens of minutes, and this circuit was built to oscillate the crystal in these experiments. The circuit is insensitive to power supply fluctuations, and the frequency does not have a temperature dependence. A schematic of the circuit is shown in figure 13 and the circuit built based on this schematic is shown in figure 14. The circuit is a simple modification of the circuit used by Kanazawa and Gordon[102] lacking the inductor-capacitor tuning element used to oscillate the crystal at its third harmonic. The circuit is comprised of two Schottky diodes ($D_1$ and $D_2$) which act as limiters to prevent damaging the crystal at large applied voltage. The integrated circuit ($IC_1$) is a Texas Instruments high gain video amplifier with two switching transistors ($T_1$ and $T_2$) which provide signal inversion to start the crystal oscillation. The gain from the amplifier is set to its maximum value and the transistors provide significant gain as well. One output of the amplifier is sent to the frequency counter. The resistor values (see figure 13) are selected to achieve maximum stability of the oscillator circuit. This circuit proved to be very stable in the experiments detailed later allowing frequency differences to be measured at one Hz or better resolution.

### 3.3 Crystal Cell

The quartz crystal was mounted in a cell so that small, liquid drops could be placed in the center of the upper, grounded electrode of the crystal (figures 15

and 16). The crystal is sandwiched between two viton o-rings whose diameters are larger than the electrode diameter but smaller than the crystal diameter. Care must be taken so that the o-rings do not compress the electrode area of the quartz crystal when mounting the crystal. If the o-rings compress the electrodes, the oscillation of the crystal will be damped. The upper o-ring is held in a Plexiglas tube with one-quarter inch of the tube bottom polished so that the electrode is visible when the drop is placed at its center. A central stainless steel tube with a hole bored through its center was mounted in the Plexiglas to guide the syringe needle to the center of the electrode. With this arrangement of cell and guide tube, the solution drop could be reproducibly placed at the center of the electrode. This is important because it has been found that the frequency response of the oscillator to deposited materials is Gaussian with the center of the distribution located at the crystal center. The guide tube was held in place by a setscrew mounted in the guide tube support. This cell design made it easy to dismount the crystal and clean it between experiments or place another crystal in the cell. Most importantly, constant humidity could be maintained in the cavity once the liquid was deposited on the crystal surface. This made possible measurement of contact angles under equilibrium conditions as required by Young's equation.

### 3.4 Importance of using buffered solutions

It might be argued that CATs using buffered solutions would suffer from adsorption of the ions used to prepare the buffer or the base when titrating acid

surfaces. Adsorption of the ions should cause the surface free energy to change,

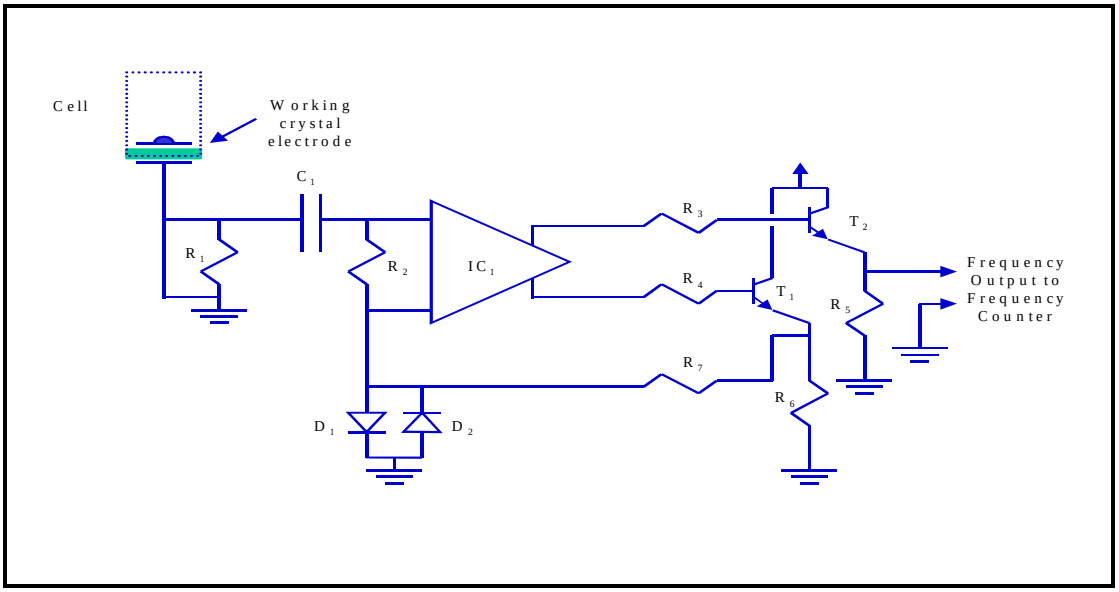


**Figure 13. Schematic of the circuit in figure 12. IC1=Texas Instruments high gain video amplifier R1=2.2 MΩ, R2=200 Ω,R3=R4= R5= R6=180 Ω, R7=220 Ω, C1=0.01 µF, T1 and T2=2N3904 transistors, D1 and D2=HP 5082-2811 Schottky diodes.**

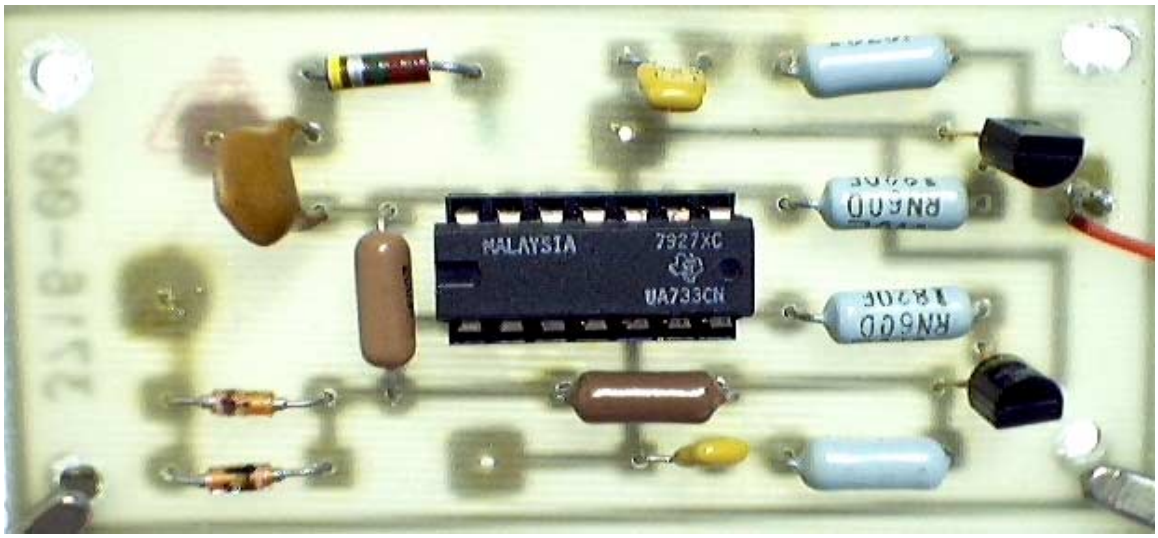


**Figure 14. Image of the circuit used to oscillate the crystal**

which should cause a different contact angle to be obtained. While the ions used to prepare the buffer might adsorb, it does not appear to influence the titration curve. Data collected by Creager and Clark using solutions buffered with diverse salts indicates that the nature of the base and buffering salt does not influence the inflection point observed in the titration curve. Data published by Whitesides' with various bases and salts support Creager and Clark's work. This

experimentally observed fact might be explained by a closer examination of the acid-base reaction between the surface confined acid and the unbuffered base solution. As will be shown later, the number of 3-dodecyloxymercaptophenol molecules adsorbed to the gold substrate is on the order of $5 \cdot 10^{14}$ molecules per $cm^2$. The number of ionizable hydroxyl groups near the surface should equal the number of molecules on the surface, and each could react with an approaching basic hydroxide anion. A 3 μL drop making a contact angle with the surface of 50° would cover about 7.67 $mm^2$ of the surface or about $3.8 \cdot 10^{13}$ ionizable functional groups assuming a hemispherical drop. A 3 μL drop of solution at pH=8 has about $1.8 \cdot 10^{12}$ hydroxide ions in it. These calculations indicate that there are about ten times more acid molecules than hydroxide anions at the interface between the acidic surface and basic solution assuming that the dielectric constant of water at the surface is similar to bulk water

**Figure 15. Base of the cell used to mount the crystal for experiments with a crystal in place. The gold crystal rests on an o-ring whose diameter is larger than the diameter of the central gold electrode. Spring clamps (wires on either side of the crystal) are bound to the electrode tabs using conducting silver paint to increase the stability.**

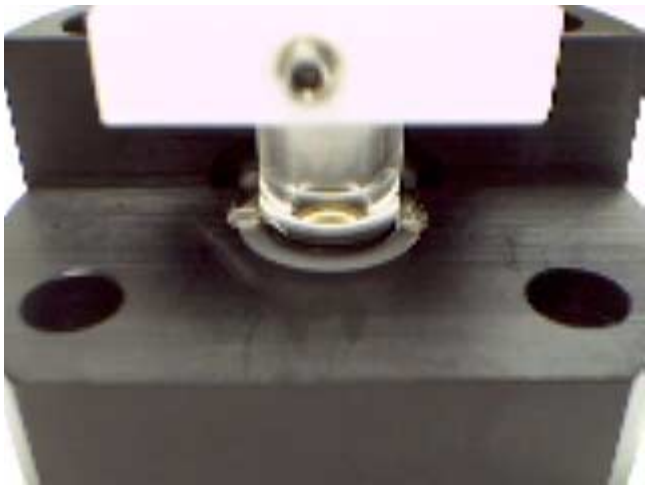

**Figure 16. Fully assembled cell with the Plexiglas tube in place. Delrin was used to fabricate the base and the guide tube support (white square at the top of the figure). A setscrew was used to hold the guide tube in place.**

There is some evidence that the dielectric constant of water at the interface is lower than its bulk value because of the increased ordering of water molecules at the interface[103]. If the dielectric constant of water at the surface were less than bulk water, the number of acid groups at the surface would be even greater than the number of hydroxide anions. This is a buffer capacity argument in essence, and the result suggests that the surface confined acid groups act as their own buffer. Furthermore, a plot of contact angle versus pH for unbuffered solutions would not yield a titration curve in the same sense that a titration curve is obtained in a conventional, solution acid-base titration. The titration curve obtained with unbuffered solutions should show a break point but that break point would be at a solution pH where the number of hydroxide anions equaled the number of acid groups on the surface. This could be a way to roughly count the number of acid groups on a surface if a better method were not readily applicable. For this reason, solutions used in these titrations have all been buffered with 0.02 M buffer capacity.

### 3.5 Theoretical development of the contact angle titration experiment

The inflection point in the titration curves of the surface confined molecules synthesized in chapter 2 should represent a pKa value if the reaction

**Equation 12. Surface acid reaction**

$$SH \Leftrightarrow S^- + H^+$$

is true, SH is a surface acidic group. The free energy of an acid dissociation is given by equation 13, which must be normalized to the area of the acid surface covered

**Equation 13. Reaction free energy of a surface acid**

$$\Delta G/_{Area} = -RT \ln(K_a).$$

Complete ionization of the surface will not occur at every pH so a term must be added to the classical expression to account for processes in which only a portion of the surface acid is ionized where x is the portion of the acid ionized.

**Equation 14. Reaction free energy of ionized and non-ionized surface**

$$\Delta G/_{Area} = -RT \ln(K_a) + RT \ln\left[\frac{[H^+]x}{1-x}\right].$$

Equation 14 demonstrates another reason why buffered solutions should be used for the titration curve measurement. It assumes that the bulk solution pH does not change upon ionization. The probe drop must have sufficient buffer capacity for this to be true. If this equation is integrated over all x, in other words from complete association to dissociation, then the free energy of ionization should be given by equation 15 where T indicates the total free energy of the ionization process.

**Equation 15. Total free energy of ionization**

$$\Delta G_T = nRT \ln(1-x).$$

Since ionization is a function of pH, equation 15 is implicitly a function of pH and as stated earlier, area. In contact angle measurements, Young's equation is used to relate the surface free energies of three interfaces (solid-liquid (SL), solid-vapor (SV) and liquid-vapor (LV)) to the contact angle formed at the solid-liquid-vapor interface (equation 16).

**Equation 16. Young's equation**

$$\cos(\theta) = \frac{\gamma_{SV} - \gamma_{SL}}{\gamma_{LV}}$$

In the case studied here, a reaction occurs between the solid and liquid phases and that reaction would be expected to have some influence on $\gamma_{SL}$ since the surface changes as the reaction proceeds. Based upon this reasoning, an additional term needs to be added to equation 16 to account for the change in $\gamma_{SL}$ during the ionization process. Conveniently, a term has already been identified and gives equation 17.

**Equation 17. Young's equation modified for changes in $\gamma_{SL}$ during ionization**

$$\cos(\theta) = \frac{\gamma_{SV} - (\gamma_{SL} + \Delta G_T)}{\gamma_{LV}}$$

Clearly, this simple development is not rigorous, but it explains the experimental fact that a constant volume of buffered solution wets an acid surface as a function of pH to a greater extent at high pH values than at low pH values. Bain has developed a similar equation.

## 3.6 Contact angle titration curves of 3- and 4-dodecyloxymercaptophenol and 12-phenoxy-dodecane-1-thiol surfaces

In previous sections of this chapter, the general operating principles of a QCM were detailed and an explanation was proffered on how shear waves generated in the crystal are propagated into the solution. The circuit driving the crystal was described, as was the cell in which the following experiments take place. The reason for using buffered solutions in making contact angle titration measurements was detailed and a semi-theoretical description describing the relationship between the contact angle and the extent of ionization of the surface was given. The topic now at hand is to present experimental results obtained when using the QCM to measure the contact angles of solutions buffered from pH=4 to pH=13 on surfaces made from molecules whose synthesis was detailed in chapter two.

### 3.6.1 Experimental

AT cut quartz crystal oscillators (figure 9) were obtained from International Crystal Manufacturing (Oklahoma City, OK) resonant at a fundamental frequency of 5 MHz. The electrode was 100 nm thick and covered 0.25" of the blank which was approximately 0.5" in diameter. An under-layer of chromium was deposited on the polished blank before deposition of the primary metalated layer. Each electrode was coated with a monolayer of the compound of interest by exposing it to a 1 mM solution in $CHCl_3$ for 24 hours. A 10 μL syringe was obtained from Hamiliton and was fitted with a Chaney adapter to reproducibly deliver a set volume of liquid to the center of the quart crystal oscillator. A 10X Loupe was used to set the Chaney adapter at the appropriate volume for the particular experiment carried out. De-ionized water was purified further by a Barnstead Nanopure II water purification system and had a measured resistivity of 17.3 MΩ-cm. Buffer solutions were prepared using phosphoric acid and $NaH_2PO_4$, $Na_2HPO_4$ or $Na_3PO_4$ by adjusting the pH of the solution with 0.1 N NaOH solution in purified water and ranged from 4-13. Sodium chloride or cesium chloride was added to the buffered solutions so that a constant sodium or cesium ion concentration was obtained across all the solutions. Adding these salts to achieve a constant cation concentration should minimize any salt effect that might influence the measurements. Solution pH was measured using a Fisher Scientific Accumet pH meter with a Ag/AgCl/sat. KCl glass membrane electrode at 25° C. The chemicals used were reagent grade and were used as received. The oscillator circuit described earlier was connected to a HP 3932B frequency counter. A gate time was set at 1 sec so that the frequency was measured every second, which permitted measuring the frequency at a resolution of 0.01 Hz. Faster gate times permitted more rapid data acquisition, but decreased the resolution of the measured frequency. Data were collected at different gate times and no dependence on gate time was observed. The frequency counter was interfaced to a computer via a GPI bus (Computer Boards), and the data was collected by a data acquisition program written in-house in Microsoft's Visual Basic v.5.0, SP 3.

### 3.6.2 Calibration of the QCM

To use the QCM to measure contact angles, it must first be calibrated by determining the calibration constant in equation 11. All the calibration data reported here used purified water as the calibration fluid. The calibration constant, C in equation 11, is measured by placing a 1 μL drop of the calibration fluid in the center of the quartz crystal electrode while monitoring the frequency decrease. After the frequency has stabilized, a second drop of the same volume is added while monitoring the frequency response. The procedure is repeated until enough data points have been collected to prepare the calibration curve. Each excursion to lower frequency seen in figure 17 corresponds to the addition of one drop of liquid to the liquid already present on the QCM electrode. Calibration values were measured using both 0.5 μL and 1 μL drop volumes. The smaller drop volume typically gave a calibration curve with a larger linear correlation coefficient, but it was more difficult to work with so most calibration curves were prepared using 1 μL drops. The calibration curve (figure 18) is plotted by calculating the radius of the drop at each incremental volume (expressed in $cm^3$) increase as it is added to the electrode. The radius, r, of the drop volume, $V_d$, is calculated from

**Equation 18. Drop radius**

$$r^2 = \frac{(3V_d/\pi)^{2/3}\left(1-\cos^2(\theta)\right)}{(2-3\cos(\theta)+\cos^3(\theta)^{2/3}}$$

where θ is a known contact angle measured goniometricly. A smaller drop volume was also used but no significant differences were observed between using the smaller or larger drop.

### 3.6.3 Contact angle titration

The contact angles (see figure 19 for diagrammatic definition of the contact angle) used to plot the correlation curve (figure 20) and the titration curves shown in figures 24, 25, 26 and 27 were calculated by numerically solving equation 19 for θ.

**Equation 19. Frequency change as a function of contact angle**

$$\Delta f = C\frac{(3V_d/\pi)^{2/3}\left(1-\cos^2(\theta)\right)}{(2-3\cos(\theta)+\cos^3(\theta)^{2/3}}$$

where θ is the contact angle made by the liquid on the solid surface. Contact angles of phenol solutions were measured using a Rame-Hart NRL contact angle goniometer on a dodecanethiol surface self assembled on a gold substrate. Using the same phenol solutions, the frequency change of the QCM that accompanied deposition of the phenol solution onto the electrode of the QCM was measured. The contact angle of the phenol solution on the dodecanethiol coated QCM electrode was computed by numerically solving Equation 19. The goniometricly determined contact angles and the contact angles from the QCM method were plotted against each other (figure 20). The slope of such a plot should be one. The graph in figure 20 has a slope of 1.008 indicating that there is excellent agreement between the goniometricly determined contact angle and QCM determined contact angle. The raw frequency data used to obtain the data plotted in figure 20 is shown in figure 21. The value of Δf is determined by taking the average of the frequency before deposition and subtracting from it the average of the frequency after deposition. Typically, 30 to 40 frequency values are averaged for the initial frequency and 40 to 60 values are averaged for the final frequency. The same crystal is used throughout one titration from low pH to high pH. One notices in the raw data in both figures 21 and 22 that the initial frequency does not return to the same value from one deposition to the next. The data in figure 21 indicate that this is not due to mass deposition on the electrode surface of the quart resonator. The initial frequency for the solution with the largest amount of phenol dissolved in it is higher than the initial frequency with the solution with the least amount of phenol dissolved in it. If additional mass had been deposited on to the electrode surface of the quartz resonator, the initial

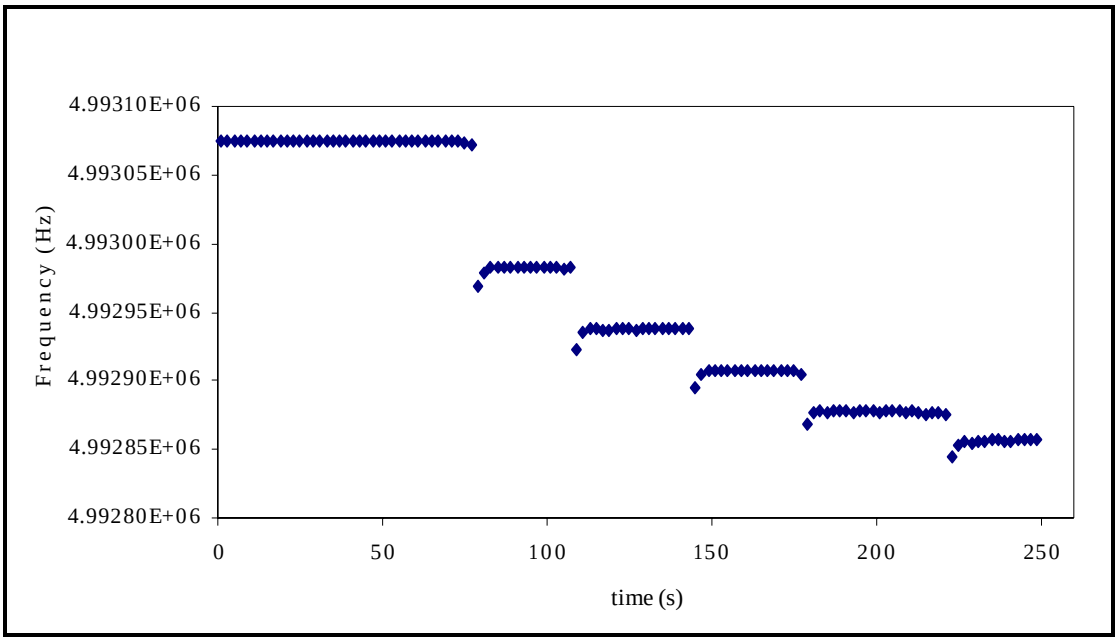


**Figure 17. Frequency response of a 3-dodecyloxymercaptophenol coated electrode surface using water while collecting data to determine the calibration constant, C, of the crystal prior to titration of the acid surface. Each excursion to lower frequency corresponds to the addition of a 0.5 µL drop of $H_2O$ onto the electrode surface. The frequency change is measured from the initial frequency for all drops added to the surface.**

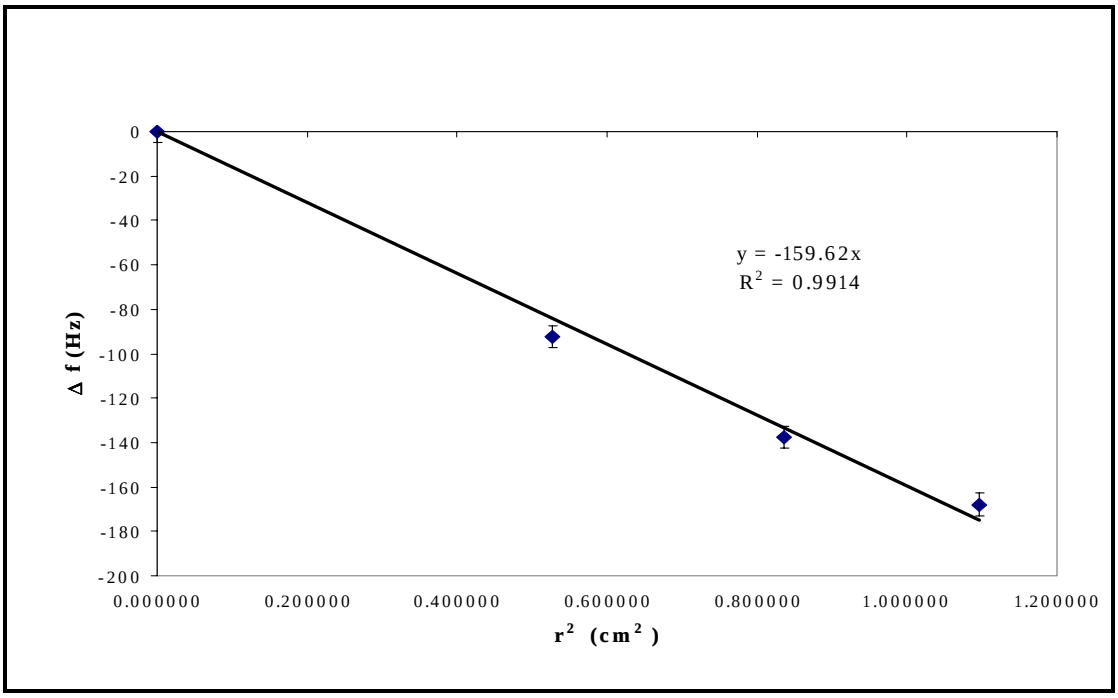


**Figure 18. Calibration curve for a 3-dodecyloxymercaptophenol surface. The slope of the line corresponds to the QCM calibration constant and has units of Hz/mm².**

frequency should drop with each successive solution deposition. Instead, the initial frequency rises with each successive deposition of phenol solution and appears random for buffer solution deposition (figure 22). The phenol solution data might indicate mass loss from the electrode of the quartz resonator, but CV experiments prior to titration and after titration indicated that the same amount of SAM is present in both cases. This suggests that mass is not added or removed from the resonator. The most likely explanation is that when the resonator is remounted, it not remounted in exactly the same way. The resonator must be cleaned after each solution deposition and remounted prior to the next deposition.

The data in figure 23 show the reproducibility of these contact angle measurements. Three different crystals on different days were used to measure the contact angle of pH=9.03 on 4-dodecyloxymercaptophenol surfaces. The contact angle measured was 75±2° resulting from a frequency change of 185±5 Hz.

As mentioned earlier, SAMs of 3- and 4-dodecyloxymercaptophenols and 12-phenoxy-dodecane-1-thiol were prepared on the gold electrodes of the quartz crystal resonator by placing the crystal disc into 1 mM chloroform solutions of the respective compound. The adsorption and assembly process progressed over 24 hours in a temperature controlled (25.0±0.1° C) bath after which the crystal disc was removed from the solution. The disc was rinsed with ethanol and water, dried under a nitrogen stream and this washing process was repeated three more times before remounting the crystal in the spring clamps of the crystal holder. Infrared spectra (see figure 34 and 35 in the next chapter) indicated that a monolayer had formed on the electrode and appeared identical in all respects to monolayers formed on 1”x1” gold coated glass slides. After mounting the crystal in the cell described earlier, the crystal was allowed to stabilize before measurements were made.

No special effort was made to control the temperature of the cell of the QCM during the course of a titration other than the laboratory heating and cooling system. Room temperature was monitored but did not vary over the course of a titration. The chamber temperature of the QCM was not monitored,

but the crystal oscillation should not be affected by the exothermic acid-base reaction occurring at the electrode. For most cuts of crystals, a change of temperature of one degree centigrade changes the resonant frequency by 1 Hz. AT cut quartz crystal is used in these experiments because it has a zero temperature coefficient at room temperature.

The titration curve of 12-phenoxy-dodecane-1-thiol (figure 24) shows no transition at any pH. This expected result suggests that the transition observed in the titration curve of 3-dodecyloxymercaptophenol (figure 25) is consistent with the ionization of the terminal hydroxyl group of the deposited monolayer. If any process other than ionization of the terminal hydroxyl group was responsible for the break point, it should be evident in the titration curve of the 12-phenoxy-dodecane-1-thiol. Two clear plateaus are seen at low and high pH in figure 25. On the other hand, the titration curve for 4-dodecyloxymercaptophenol (figure 26) does not show a plateau at high pH but does show a plateau at low pH. This difference between the titration curves is odd because in bulk solution, the pKa for the second ionization of hydroquinone occurs at 11.32 while the second

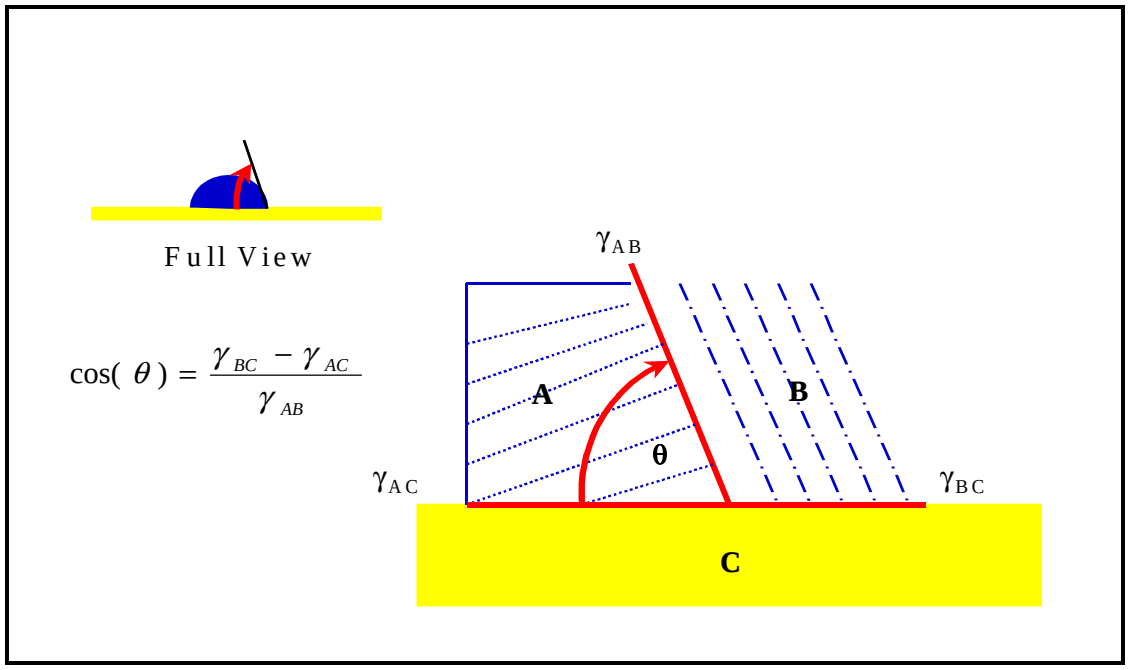


**Figure 19. Diagrammatic definition of the contact angle, θ, between the solid phase, C, and liquid phase, A, in the presence of a gas phase, B. The contact angle is formed where three phases ($\gamma_{AC}$, $\gamma_{BC}$, $\gamma_{AB}$) are in equilibrium (thermal and mechanical) with each other.**

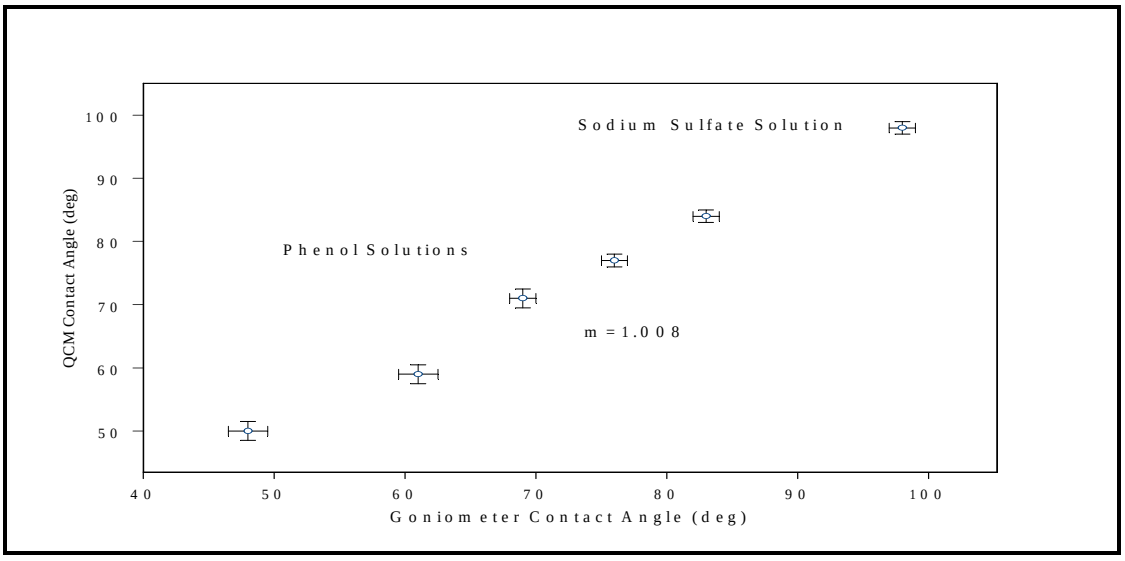


**Figure 20. QCM determined contact angle plotted against the goniometricly determined contact angle. The slope of the line indicates excellent agreement between the two methods.**

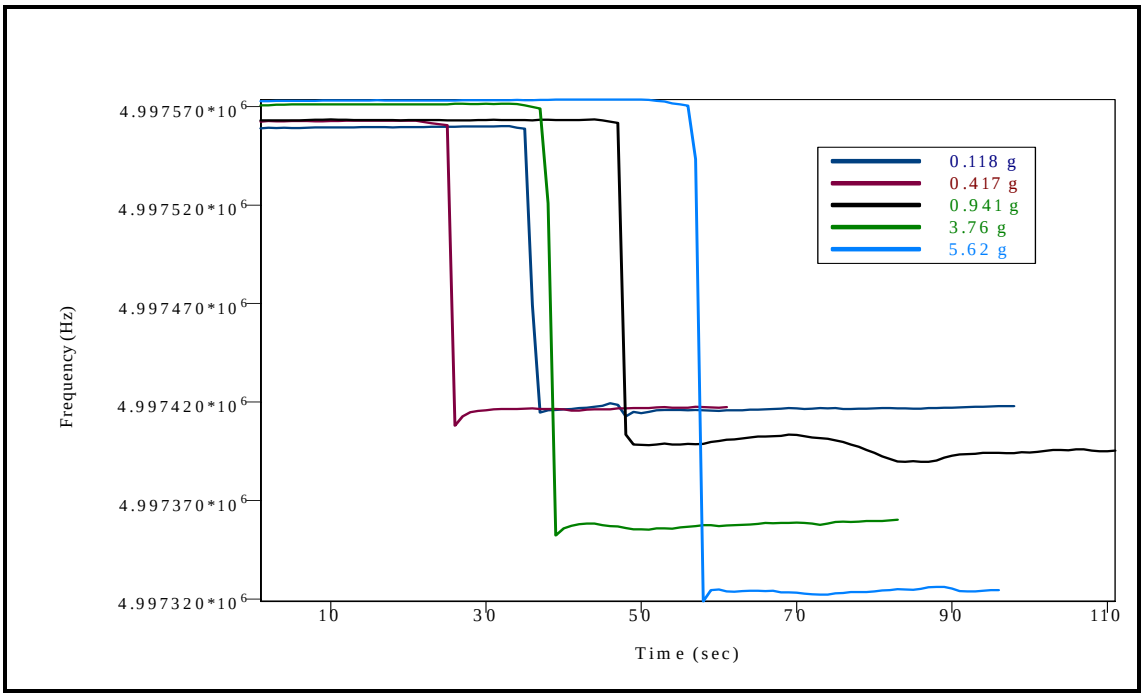


**Figure 21. This chart shows the raw frequency response of the QCM to the deposition of solutions, made by adding different masses of phenol to water, onto a dodecanethiol SAM assembled on the gold electrode of the quartz resonator of the QCM. At the highest phenol concentration, the frequency decrease is the largest indicating that the phenol solution wets the surface to a greater degree than the do the other solutions. This is the expected result since the free energy of the more concentrated solution more closely matches the surface free energy of the monolayer. A 3 μL sessile drop of the solution was used in all five cases. This is experimental confirmation of figure 12.**

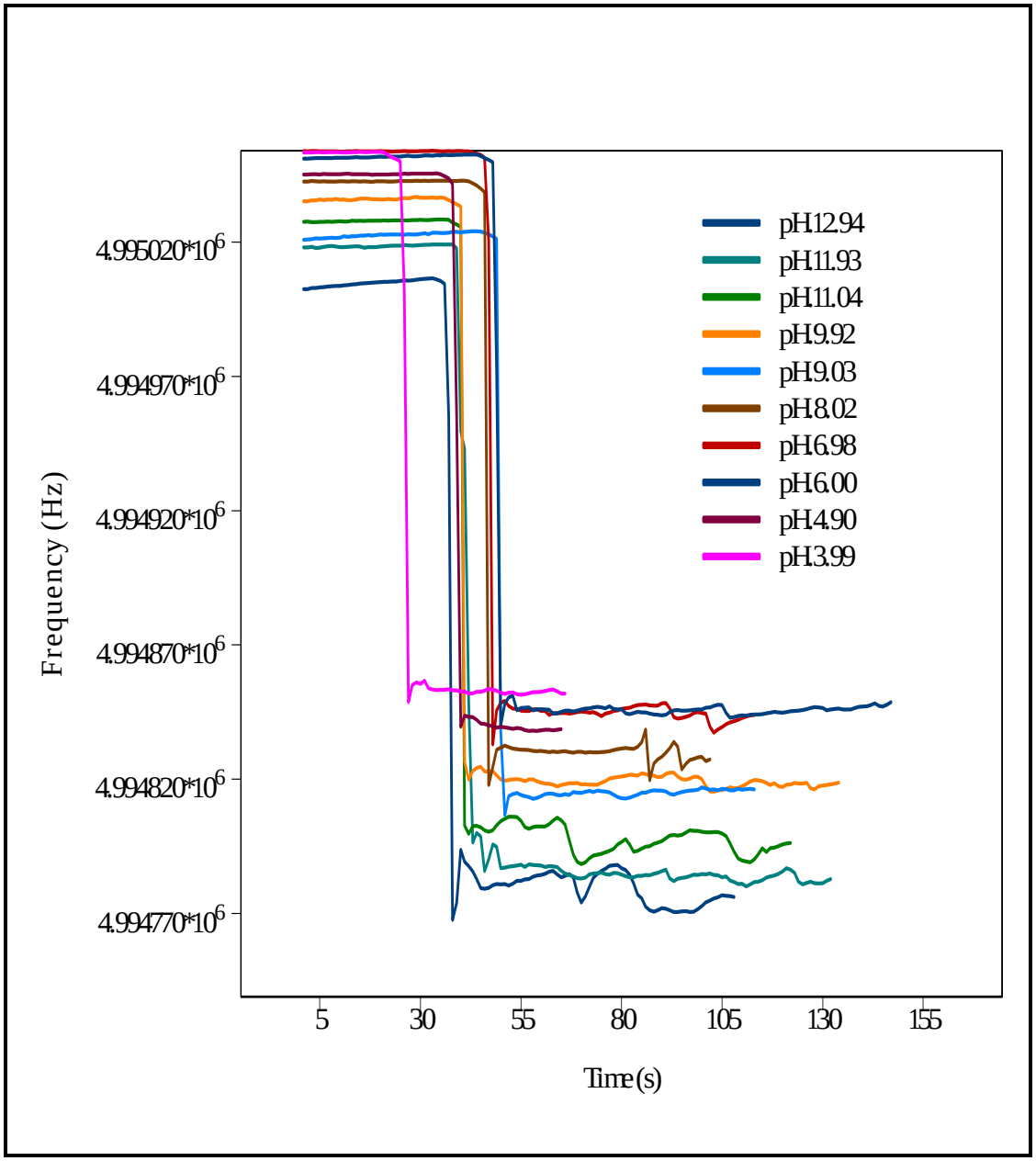


**Figure 22. Raw frequency data for the titration of 4-Hydroxythiophenol. Only half of the data is presented for clarity. The difference in frequency is determined by averaging the initial frequency and subtracting from it the average of the final frequency.**

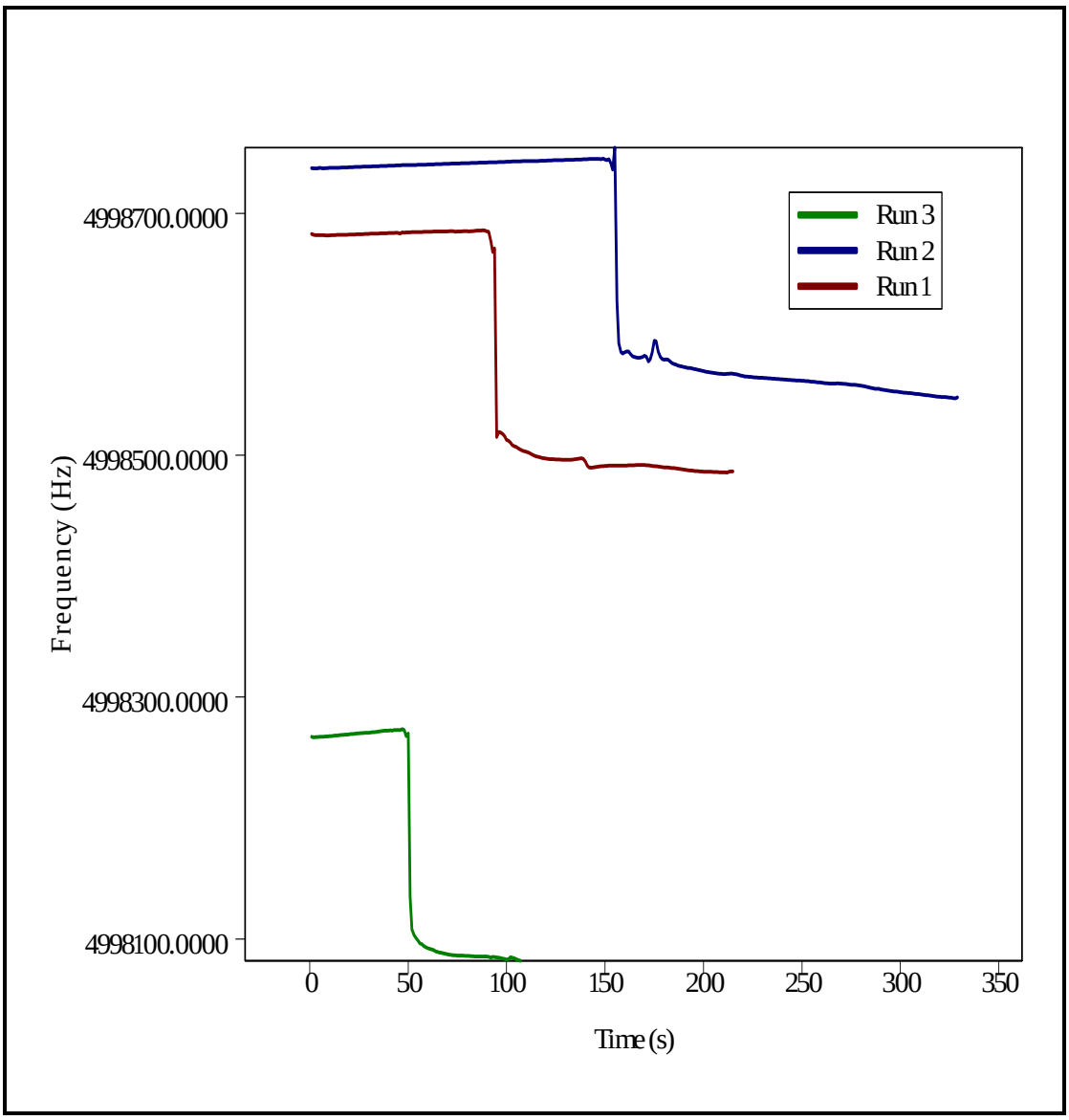


**Figure 23. Reproducibility of the change in the frequency response upon depositon of pH=9.03 solution to a 4-dodecyloxymercaptophenol surface. The data was collected on three different days and three different crystals. The frequency difference is 185±5 Hz and the computed contact angle is 75±2°.**

ionization of resorcinol occurs at 11.4 pH units. The compounds 3- and 4-dodecyloxymercaptophenols are synthesized from resorcinol and hydroquinone, and the hydroxyl groups would be expected to demonstrate acid behavior similar to resorcinol and hydroquinone. Comparison of figures 26 and 27 also highlight the unusual behavior of 4-dodecyloxymercaptophenol compared to 4-hydroxythiophenol (4-HTP). The much smaller compound, 4-HTP, should experience a much larger surface potential than 4-dodecyloxymercaptophenol because it is much closer to the metal substrate. Despite this, plateaus are seen at both limits of the pH scale in 4-HTP but not in 4-dodecyloxymercaptophenol. So surface potential effects do not explain the differences between the titration curves of 3-dodecyloxymercaptophenol and 4-dodecyloxymercaptophenol. The difference between the acid behaviors of these three compounds clearly lies in the differences in their structures at the solid-liquid interface. The contact angles in the titration data itself hint at this. The 4-HTP surface has a maximum contact angle of approximately 58° in its unionized state at low pH values, and the 3-dodecyloxymercaptophenol surface has a maximum contact angle of approximately 59° at low buffer solution pH values. These low contact angles with aqueous solution suggest that the surface is relatively hydrophilic. In contrast, 4-dodecyloxymercaptophenol makes a contact angle with an aqueous solution of approximately 72° in the unionized state. This larger contact angle value suggests that the surface of a 4-dodecyloxymercaptophenol monolayer has an appreciable hydrophobic component present. The $pK_{1/2}$ of 3- and 4-dodecyloxymercaptophenol appear to differ as well, although it is difficult to say this with certainty because 4-dodecyloxymercaptophenol lacks a clear plateau at

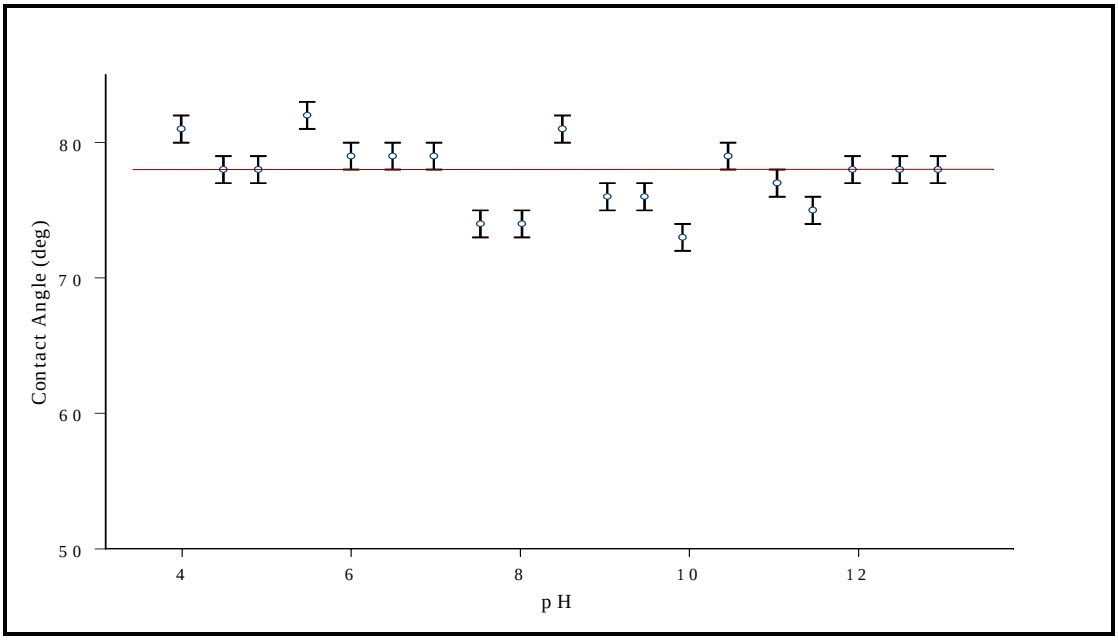


**Figure 24. Contact angle titration curve for 12-phenoxy-dodecane-1-thiol. No sharp transition from low to high pH is seen. This suggests that the buffered solution has little impact on the SAM. The line is meant to guide the eye.**

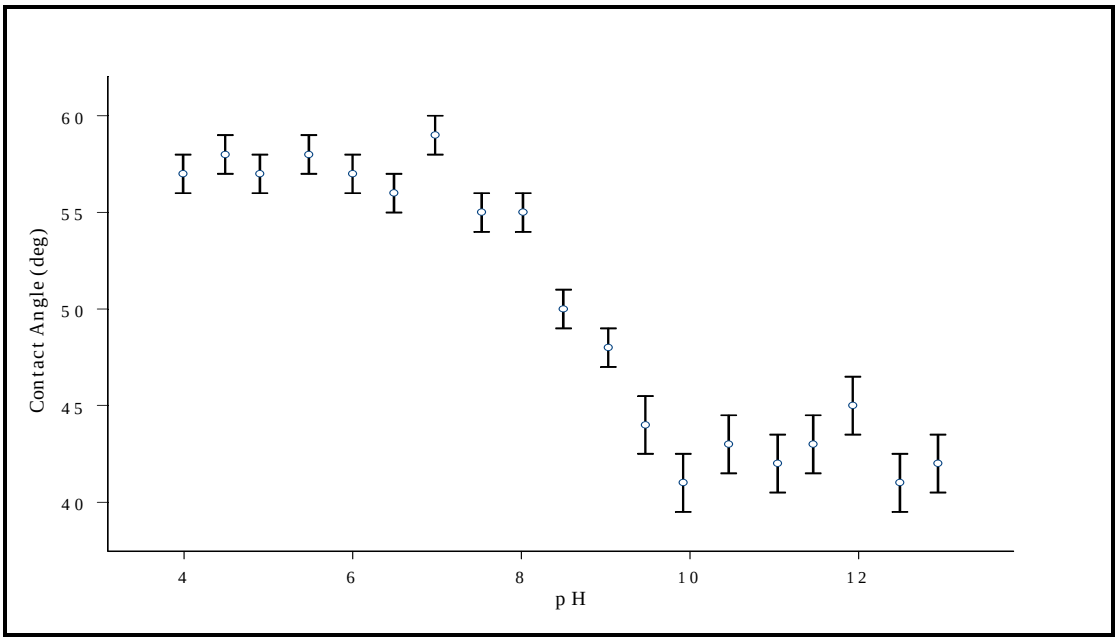


**Figure 25. Titration curve of 3-dodecyloxymercaptophenol. A clear transition from low pH to high pH is seen with plateaus at low and high pH values.**

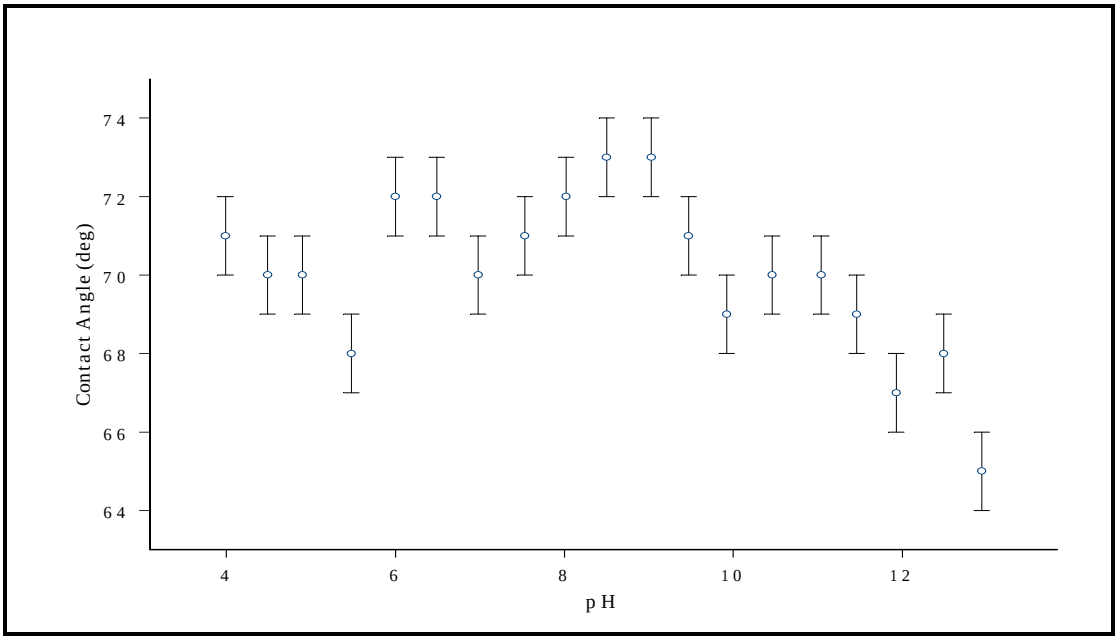


**Figure 26. Titration curve for 4-dodecyloxymercaptophenol. A transition for low pH to high pH is evident but no plateau exists at high pH.**

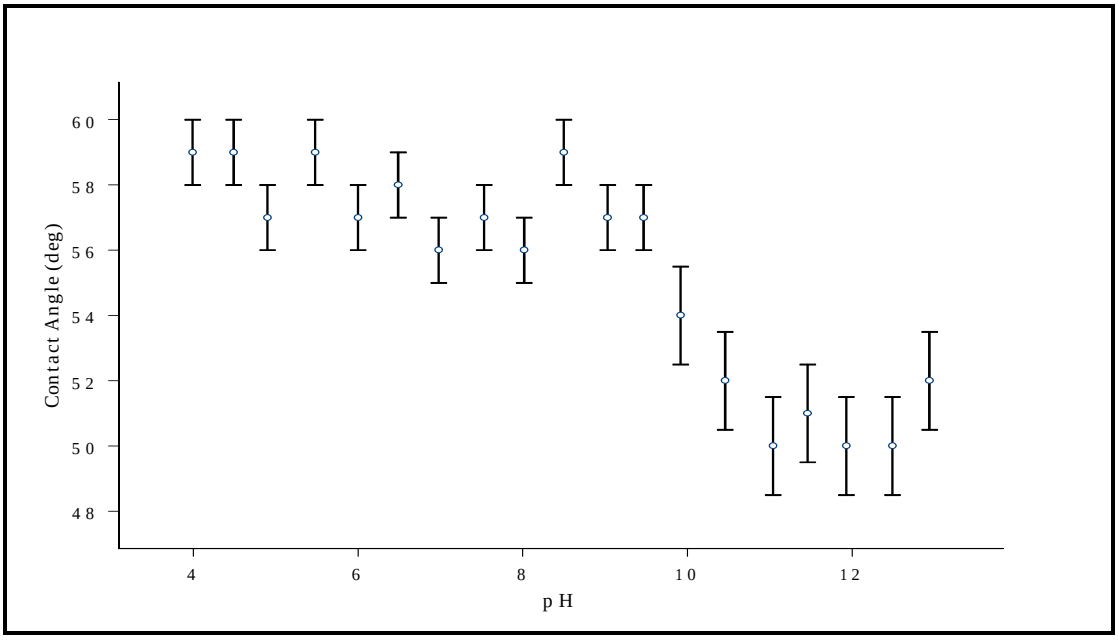


**Figure 27. Contact angle titration curve for 4-hydroxythiophenol. The hydroxyl group of this molecule is projected into space almost parallel with the surface normal and is much closer to the metal surface.**

high pH. The $pK_{1/2}$ of 3-dodecyloxymercaptophenol appears at approximately 8.75 solution pH units, but 4-dodecyloxymercaptophenol appears to have a larger $pK_{1/2}$. This might be explained by differences between the intermolecualr interaction of the hydroxyl groups in 3- and 4-dodecyloxymercaptophenol.
In the next chapter, surface infrared spectroscopy and electrochemistry will be used to examine the differences in the structure of 3-dodecyloxymercaptophenol and 4-dodecyloxymercaptophenol. Electrochemistry will be used to measure the differences in intermolecular interactions between the molecules that make up the monolayer surface.

# 4.0 Surface Molecular Orientation and Interactions

This chapter is concerned with determining the orientation of the benzene rings bearing the hydroxyl groups making up the surfaces shown in figure 5. The electrochemistry of the SAMs will also be discussed as it was used to measure the intermolecular interactions between the chains. General remarks about experimental details will be presented first followed by a brief theoretical section describing the important aspects of surface infrared spectroscopy that make orientation measurements possible. The next topic presented deals with the spectroscopic method used to determine the orientation of the hydroxyl groups at the surface. Finally, a discussion of the electrochemistry of monolayers of 12-phenoxy-dodecane-1-thiol and 3- and 4-dodecyloxymercaptophenol will be presented.

## 4.1 Experimental details

Monolayers of 3- and 4-dodecyloxymercaptophenols and 12-phenoxy-dodecane-1-thiol were prepared from 1 mM chloroform solutions of each compound by placing a gold substrate into the solution. Prior to placing the substrate into the solution, it was cleaned in “piranha” solution as described in chapter 1. The substrate was a 1”x1” glass slide coated with 50Å of Cr as an adhesive layer. Gold (1000 Å) was deposited onto the Cr metal layer. These slides were purchased from Evaporated Metal Films (Ithaca, New York). Infrared spectra were collected using a Nicolet Model 710 Infrared Spectrometer equipped with a Spectra-Tech Model FT-80 fixed grazing angle specular reflectance sample

apparatus (see figure 28) at an incident angle of 80°. The infrared source light was p-polarized using a ZnSe wire-grid polarizing filter (Cambridge Physical Sciences, IGP228) so that the incident infrared radiation's **E** field vector was oriented normal to the sample surface. Spectral acquisition and data processing were carried out using Nicolet's Omnic (version 3.1) data acquisition software. Transmission and reflection infrared spectra were collected at 2 $cm^{-1}$ resolution using boxcar apodization, and a minimum of 512 interferometer scans were averaged for each spectrum. All infrared spectra were referenced to a clean, gold slide treated in the same manner as the monolayer coated slide except that a monolayer was not deposited on the reference slide. The sample chamber of the spectrometer was purged with $CO_2$ and $H_2O$ free air supplied from a Balston Filter Products type 75-60 system.

CV experiments were conducted using an EG&G Princeton Applied Research model 270 Galvanostat/Potentiostat. A specially designed and built three electrode glass electrochemical cell was used (see figure 29). A Ag/AgCl/sat. KCl reference electrode was used in all the experiments, as was a Pt counter electrode. Electrolyte was drawn into the cell with a syringe via a syringe port. Where appropriate, a SAM free slide was used as a reference. The working electrode was the SAM coated gold substrate. The geometric area of the working electrode was defined by the area of the o-rings holding the electrolytic solution in place, which was 0.646 $cm^2$. The potential was swept from –0.200 V to –1.2 V at a rate of 100mV/sec. Data acquisition and processing were carried

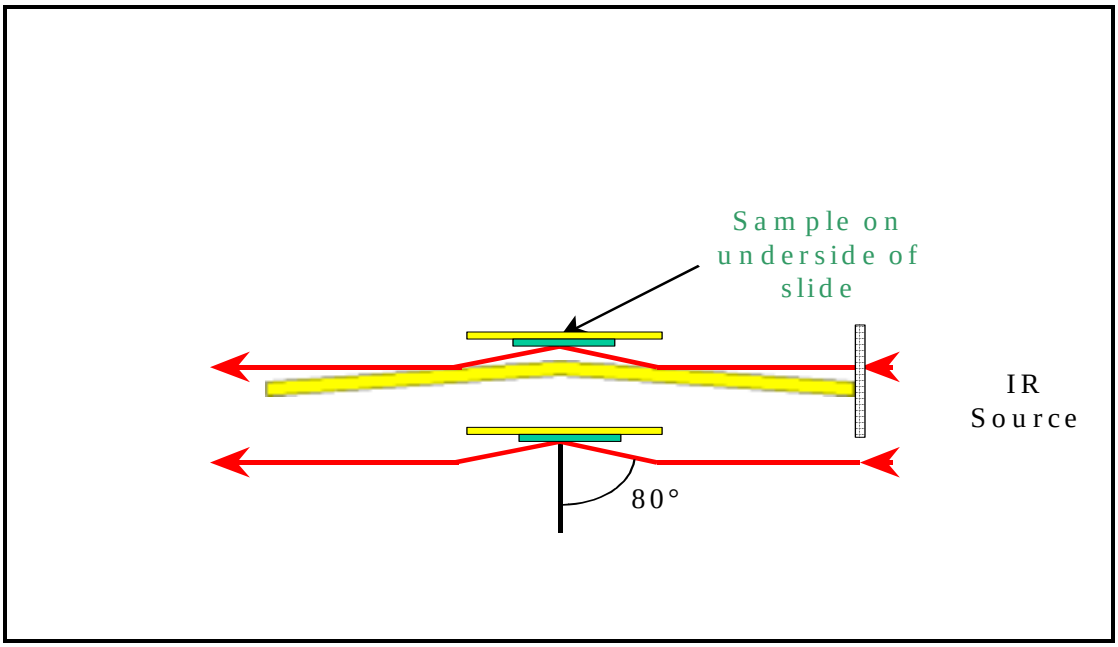


**Figure 28. A sample is place on top of a reflection attachment which directs light tot he sample. The metal mirror substrate then reflects the light back to the attachment which reflects the light to the detector.**

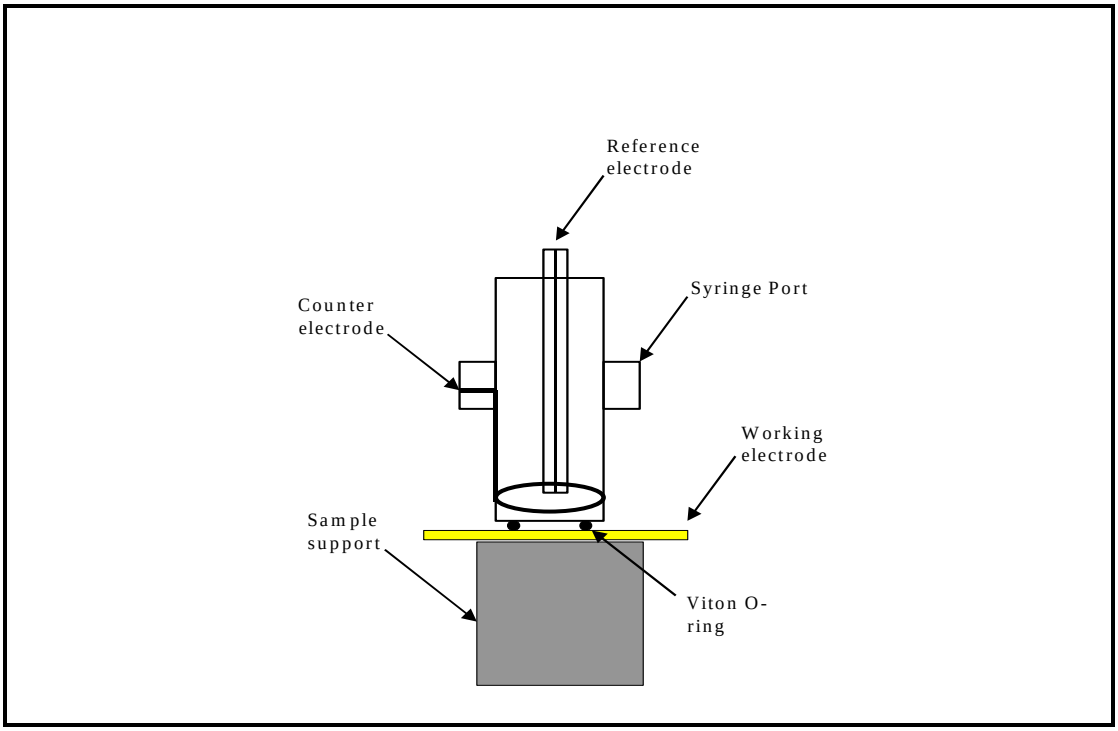


**Figure 29. Electrochemical cell used for the CV experiments. The electrolyte was contained within the cell by compression of the o-rings.**

out using the software package supplied by EG&G. Electrolyte solutions were prepared from KOH that was reagent grade and used as received in nano-pure $H_2O$. All solutions were deaerated for 30 minutes prior to use with a nitrogen bubbler.

### 4.2 Theoretical aspects of surface infrared spectroscopy

In the last chapter it was suggested that the structure of the interface contributed significantly to the different acid properties observed in the titration curves of 3-dodecyloxymercaptophenol and 4-dodecyloxymercaptophenol. Surface infrared spectroscopy is a tool frequently used to probe monolayer structure. More particularly, infrared reflection adsorption spectroscopy is used to obtain a reflection spectrum of monolayers deposited on metal mirror substrates. Several comprehensive review articles have been published in the literature covering the scope of surface infrared spectroscopic techniques. These techniques include reflection-adsorption infrared spectroscopy (RAIRS), polarization modulation infrared reflection spectroscopy and attenuated total reflectance spectroscopy among other techniques. RAIRS is also called external reflection spectroscopy. In general, light from an infrared source is reflected onto a monolayer coated metal substrate with the aid of a reflection attachment placed in the optical path of an infrared spectrometer. The angle of reflection is critical and more will be said about this later. Infrared spectroscopy is so frequently applied because of the extensive theoretical development that relates the direction of the TDMs of various normal vibrational modes to the intensity of infrared adsorption bands. Greenler first applied optical theory to the reflection adsorption experiment to determine the optimal conditions for obtaining a reflection-adsorption spectrum[104]. He showed that only the component of the **E** field vector normal to the surface is apt to excite a dipole-active vibration. He showed further that this excitation is only likely to occur at high incidence angles, which is why a grazing angle must be used. This last finding gave rise to the development of the metal surface selection rule stating that absorbed energy is lost only through those vibrations having a component of their TDM perpendicular to the surface. The infrared reflection spectra for (4-

mercaptophenyl)-phthalimide (4MPP) and (3-mercaptophenyl)-phthalimide (3-MPP) clearly demonstrates this effect (figure 30). The asymmetric vibration of the C=O groups in the imide I band is shown in both the 3-MPP and 4-MPP spectra in the figure. The molecules 3-MPP and 4-MPP differ in that the thiol is substituted at the 4 position in 4-MPP and at the 3 position in 3-MPP which is a difference of 60° between these two substitution patterns. When the molecule adsorbs onto the substrate to form the SAM, the orientation of functional groups within the compound should be different because of the different substitution patterns of the thiol head-groups. In the case of 3-MPP, the carbonyl groups are aligned with the surface normal or perpendicular to the surface plane, but the carbonyl groups are more parallel to the surface plane for 4-MPP molecules. According to the surface selection rule, the vibration with its TDM more perpendicular to the surface, 3-MPP imide I, should show an intensity enhanced signal. The peak from the vibration whose TDM is less normal with the surface, 4-MPP imide I, will either not appear in the spectrum or be much diminished in intensity. The spectra in figure 30 clearly show this effect.

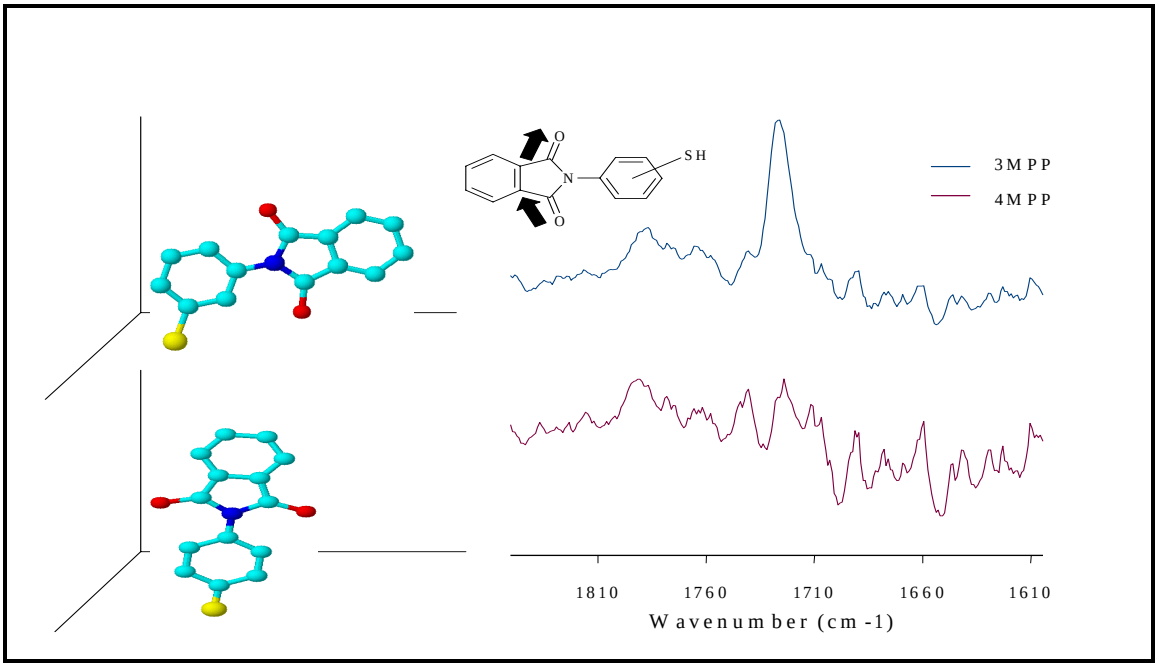


**Figure 30. Experimental evidence of the surface selection rule. See text for an explanation. Both spectra are shown at the same scale. The imide I vibration appears at approximately 1720 $cm^{-1}$.**

Another finding of Greenler's work is that only p-polarized radiation will excite a transition dipole moment. Radiation that is p-polarized has its **E** field vector normal to the surface or parallel with the plane of incidence (figure 31). Upon reflection, p-polarized light adds vectorially to its emitted vector, which almost doubles the amplitude of the incident vector. In contrast, the other polarization state, s, has its **E** field vector perpendicular to the plane of incidence or parallel with the surface. Upon reflection, s-polarized light's emitted vector phase shifts by 180 degrees and destructively adds to the incident vector. This is almost a restatement of the metal surface selection rule. The subtle difference between the two statements is that in the surface selection rule the TDM of the molecule is of concern while the **E** field vector that excites the TDM is paramount in selecting the polarization state of the incident light. A consequence of the polarization state of the light is that only TDMs of "A" character symmetry will produce an IR active signal in infrared reflection spectroscopy. In this symmetry type, the TDM is aligned with the surface normal that is also aligned with the **E** field vector, p polarized light, that excites the TDM[105]. This rule in combination with the rest of group theory of molecular vibrations show that the only point groups allowed for surface confined molecules are $C_1$, $C_s$, $C_2$, $C_{2v}$, $C_3$, $C_{3v}$, $C_4$, $C_{4v}$, $C_6$, and $C_{6v}$[106]. However, the metal surface selection rule diminishes the number of signals that will be observed in the reflection IR spectrum as discussed earlier. The combination of the metal surface selection rule, p-polarized light and analysis of the normal coordinate vibrations provides the tools for measuring the orientation of molecules on surfaces.

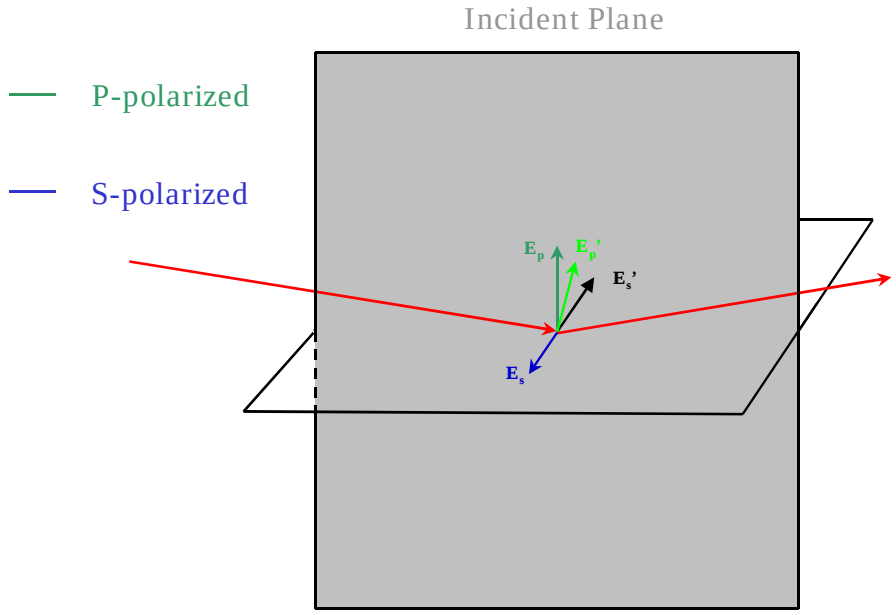


**Figure 31. Diagrammatic definition of s and p polarized light. S polarized light's E field is perpendicular to the incident plane but parallel with the surface. P polarized light's E field vector is perpendicular to the surface but parallel with the incident plane. Upon reflection, p polarized light's emitted vector, $E_p'$; green vector, adds constructively to the incident vector leading to a stronger E field at the surface. On the other hand, s polarized light's incident E field vector is phase shifted by 180°. Thus the emitted vector, $E_s'$; black vector, destructively interferes with the incident vector. The red vector is the source infrared light.**

### 4.3 Orientation of 3- and 4-dodecyloxymercaptophenols on Au metal

At least two methods exist for determining the orientation of molecules on surfaces. The first method developed was due to Allara[107] who combined the work of Greenler[104], Heavens[108], Berryman[109], Francis and Ellison[110] and others to measure the orientation of polymer chains. He later refined his method for application to SAMs. Some effort was initially expended to apply Allara's method to the work of this thesis, so a brief discussion of his method is warranted. However, this method was ultimately abandoned for reasons explained later.

Allara's optical method uses Heavens' model of the monolayer/substrate that treats each bulk layer as possessing unique complex refractive indices. This model allows Maxwell's equations to be applied at each boundary that when solved allow a theoretical spectrum to be computed. To solve Maxwell's

equations, the refractive index and extinction coefficient of the substrate and monolayer must be known. These quantities are also called the complex refractive index or optical constants. The optical constants for most compounds are not known so a Kramers-Kronig transform[111] must be used to extract this information from a bulk, isotropic transmission spectrum. Unfortunately, the optical method is programming intensive and for this reason, the method was abandoned, at least for this thesis. Besides the programming that was done for the Kramers-Kronig calculation, additional programming would have been necessary to completely calculate the theoretical spectrum. Instead, another method, equivalent to Allara's optical method though generally less applicable and much easier to implement, was identified and used.

Miller[112] showed that in some cases the metal surface selection rule could be used to quantitatively determine the orientation of molecules on surfaces. For Miller's method to apply, the molecules studied must have TDM that are perpendicular to and parallel to the long molecular axis of the molecule and in and out of the molecular plane. These bands must be present in both the bulk isotropic transmission spectrum and the reflection spectrum. If this is the case, then equations 20 and 21 can be solved simultaneously to determine the tilt and twist angles of the adsorbed molecules. All terms in equations 20 and 21 are previously defined.

**Equation 20. First of 2 equations used to compute the tilt and twist angle**

$$\frac{A_{prR}}{A_{pdRo}} - \left[ \frac{A_{prT}}{A_{pdTo}} \cdot \frac{(\cot(\theta))^2}{(\sin(\phi))^2} \right] = 0$$

**Equation 21. Second of 2 equations used to compute the tilt and twist angle**

$$\frac{A_{prR}}{A_{pdRi}} - \left[ \frac{A_{prT}}{A_{pdTi}} \cdot \frac{(\cot(\theta))^2}{(\cos(\phi))^2} \right] = 0$$

Figure 32 shows the laboratory coordinate system with the z-axis defined as the surface normal while x and y lie in the plane of the surface. The angle between the long axis of the molecule and the z-axis is defined as the tilt angle, $\theta$, of the surface adsorbed molecule. Figure 33 shows how the twist angle is defined. The long axis of the molecule, $\mu$, is projected onto the x-y plane, $\mu'$, and the angle made by the plane of the molecule with respect to the z-$\mu'$ plane is the twist angle, $\omega$. With the coordinate system defined, it is now possible to compute the tilt and twist angle of the benzene ring of 3- and 4-dodecyloxymercaptophenol.

The bulk transmission spectrum and the reflection spectrum of a monolayer of 4-dodecyloxymercaptophenol is shown in figure 34. The reflection spectrum has been multiplied by 10 times for scaling purposes in the figure. Several prominent bands are visible in both the transmission and reflection spectra. However, only a few bands are relevant to this discussion and those bands are shown in figure 36. Band assignments were made using Wavefunction's Titan molecular modeling software. All computations were carried out using density functional theory at the 6-31G* level. For purposes of determining the tilt and twist angles of the benzene ring, the bands at 1518 $cm^{-1}$, 1009 $cm^{-1}$ and 772 $cm^{-1}$ in the transmission spectrum were selected. The corresponding vibrational band was selected in the reflection spectrum as indicated in the figure. The band at 1518 $cm^{-1}$ in both the transmission and reflection spectrum results from the asymmetric stretch of carbons C2, C3 and C5, C6 in the benzene ring as the top graph in figure 36 indicates. This particular stretch is parallel with the long molecular axis of the benzene ring. The intensity of this band was measured by establishing a baseline using a tangent line technique. It is important to point out that the area of the peak should not be used when using this method to calculate the tilt and twist angles because intermolecular interactions or other band broadening processes could increase the area. Also, the metal surface selection rule only influences the band intensity.

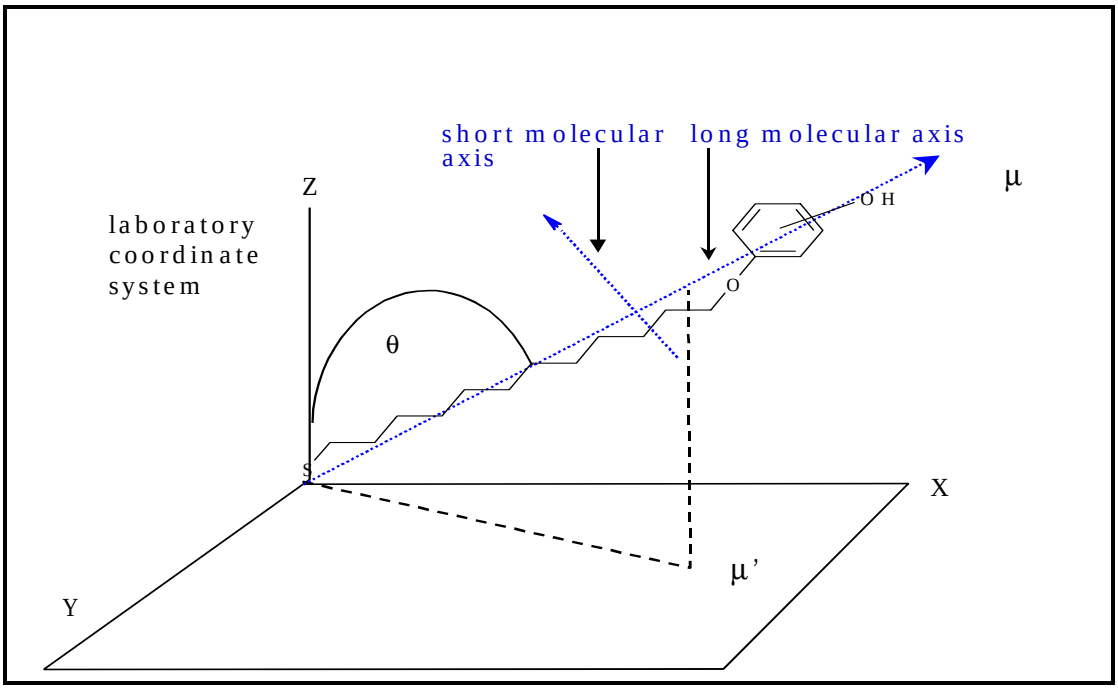


**Figure 32. The tilt angle is the angle, θ, defined by the surface normal and the long axis of the molecule. The long axis, μ, is projected into the X-Y plane in order to define the twist angle.**

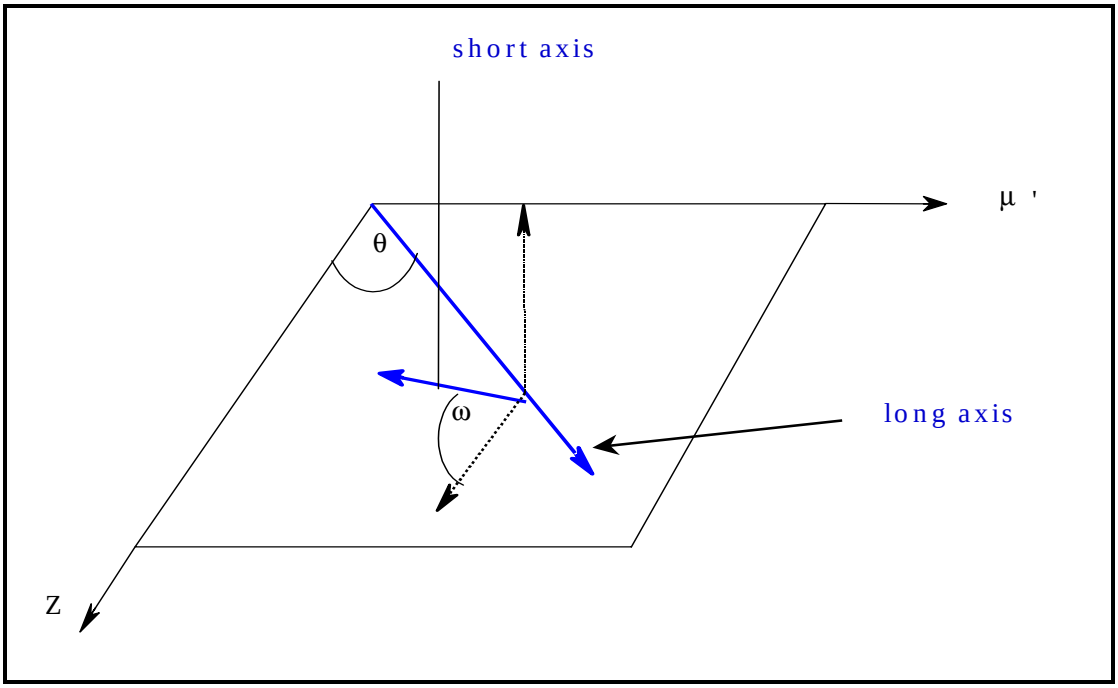


**Figure 33. The twist angle is defined as the angle made by the short molecular axis and the Z-μ' plane.**

The values measured for this stretch established the values of Apr(R) and Apr(T) for use in equations 20 and 21. Baselines were established at the same points in

both the transmission and reflection spectra. The values of Apdi(R) and Apdi(T) were determined by measuring the peak intensity of the bands at 1005 $cm^{-1}$ and 1009 $cm^{-1}$, respectively. This band resulted from the symmetric stretches of C1, C2 and C1, C6 and C4, C3 and C4, C5 as indicated in figure 37. The values of Apdo(R) and Apdo(T) were determined by measuring the intensity of bands at 774 $cm^{-1}$ and 772 $cm^{-1}$, respectively. These bands resulted from CH stretches as indicated in figure 36. The stretch was perpendicular to the long molecular axis and out of the plane of the ring. The orientation of the benzene ring was determined in the same manner for 3-dodecyloxymercaptophenol. The reflection and bulk transmission spectra of 3-dodecyloxymercaptophenol are shown in figure 35. The spectra showing the relevant bands for the tilt and twist angle calculations are shown in figure 37. As in the case of 4-dodecyloxymercaptophenol, a baseline was established by a tangent line method and used in both the reflection and transmission spectra. The assignments and the particular peaks are shown in figure 37. After analysis of the data, the benzene ring of 4-dodecyloxymercaptophenol was found to be tilted from the surface normal by 46° and twisted around the molecular axis by 36°. The tilt angle of 3-dodecyloxymercaptophenol was 55° and its twist angle was 28°. These values are uncertain to ±5° based upon the standard deviation of three separate determinations for the tilt and twist angles. The tilt angle of the benzene ring in 4-dodecyloxymercaptophenol equals the tilt angle of the hydroxyl group since the long molecular axis of the benzene ring is collinear with the 1,4

substitution

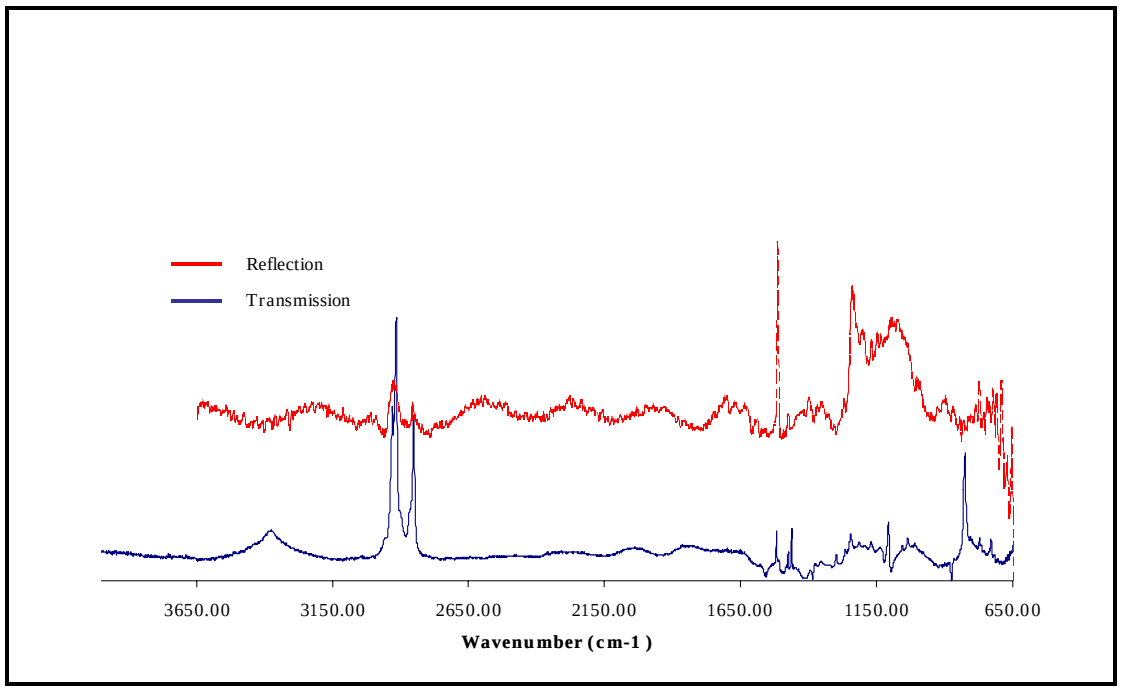


**Figure 34. Reflection and bulk transmission spectra of 4-dodecyloxymercaptophenol. The reflection spectrum is scaled by a factor of 10.**

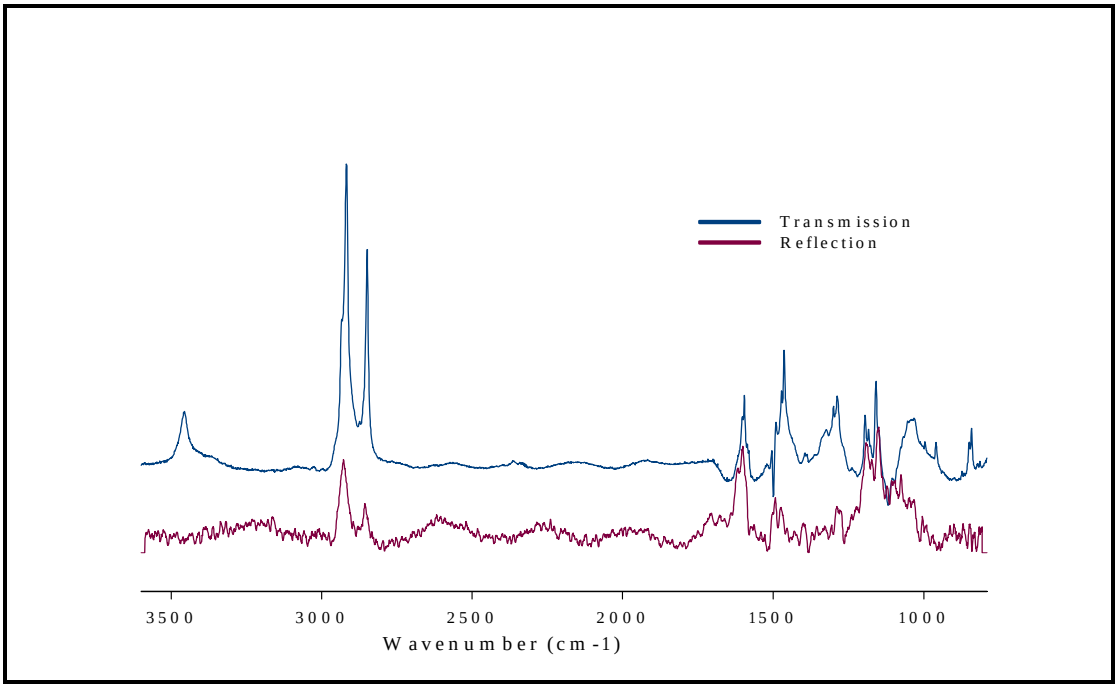


**Figure 35. Reflection and bulk transmission spectrum of 3-dodecyloxymercaptophenol. The reflection spectrum is scaled by a factor of 10.**

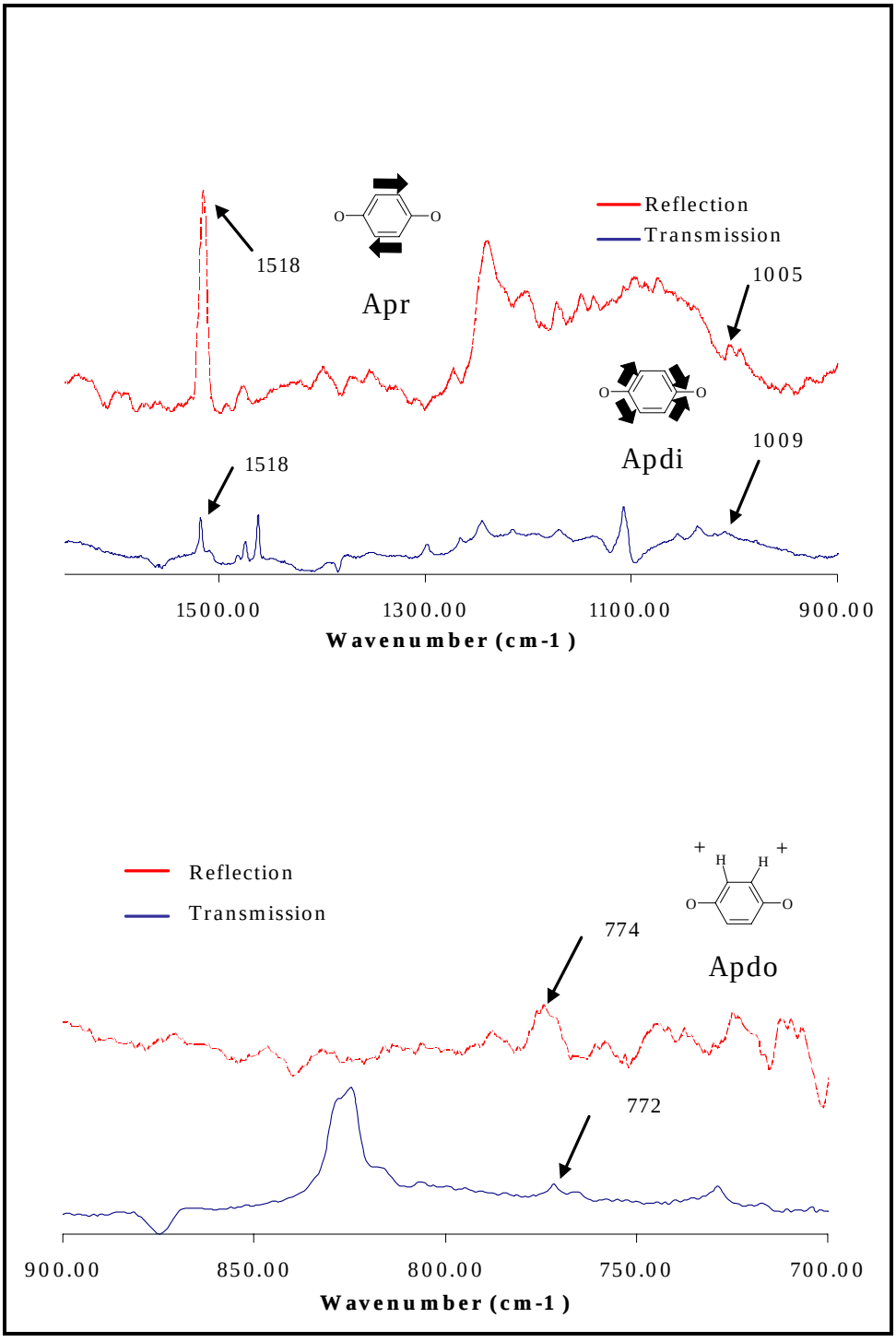


**Figure 36. Reflection and bulk transmission spectra of 4-dodecyloxymercaptophenol showing the bands and their assignments used to determine the orientation of the benzene ring on the surface. The reflection spectra are scaled by a factor of 10.**

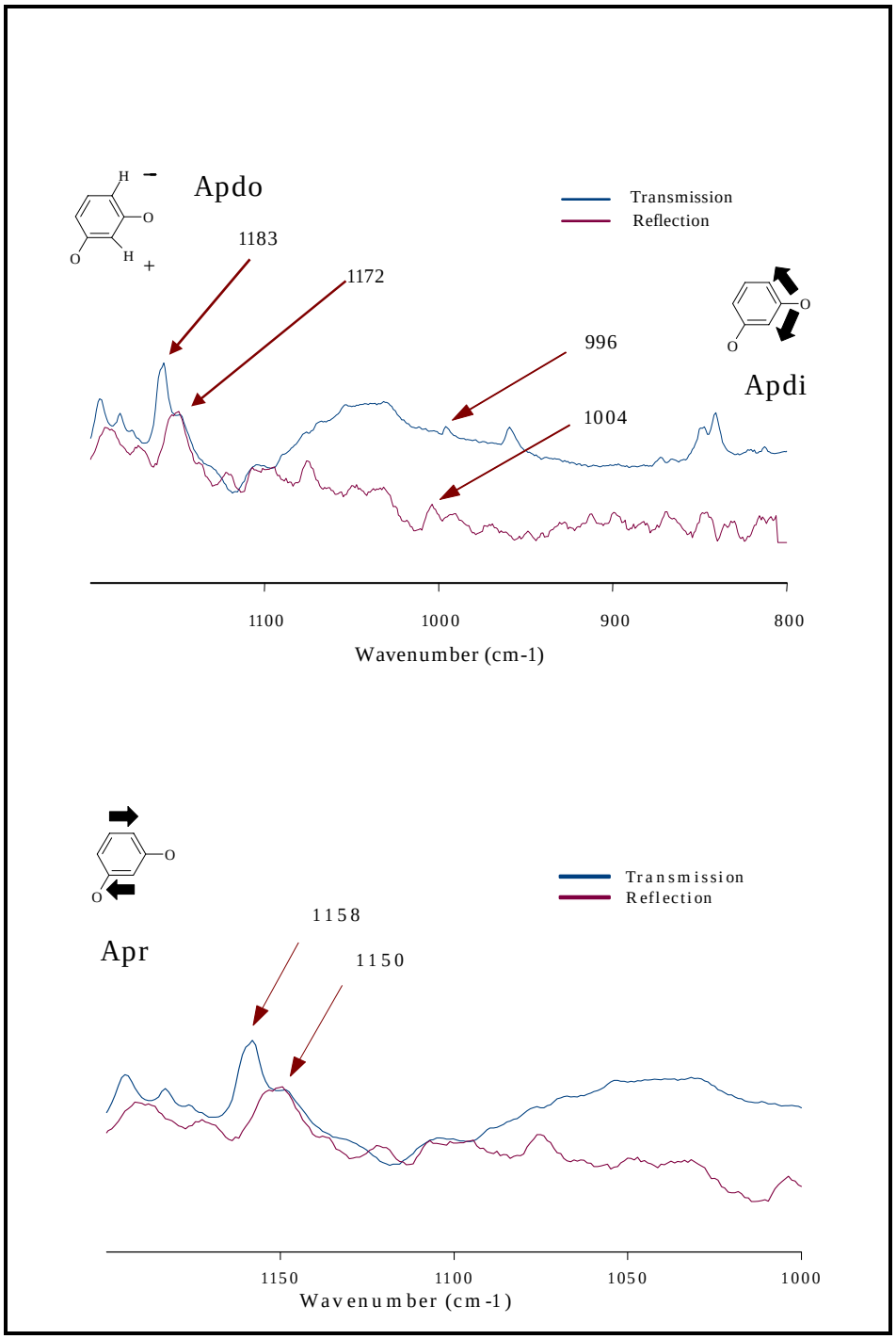


**Figure 37. Reflection and bulk transmission spectra of 3-dodecyloxymercaptophenol showing the bands and their assignments used to determine the orientation of the benzene ring on the surface. The reflection spectra are scaled by a factor of 10.**

pattern of the molecule. This means that the surface of 4-dodecyloxymercaptophenol should have a hydrophobic component present because the edge of the benzene ring has higher altitude than does the hydroxyl group. The contact angle data presented in chapter 3 reflects this because the contact angle at low pH is approximately 71° (figure 26) indicating a somewhat hydrophobic surface. It also suggests that the hydroxyl group is "buried" more in the interface, but the hydroxyl group is still accessible. The contact angles at low pH for 4-dodecyloxymercaptophenol are less than the contact angles at low pH for 12-phenoxy-dodecane-1-thiol indicating a hydrophilic component in the interface. On the other hand, the 1,3 substitution pattern of 3-dodecyloxymercaptophenol places the hydroxyl group 60° from the long molecular axis, which bisects the one and four carbon atoms of the benzene ring in this compound. Therefore, the hydroxyl group is oriented almost perpendicularly to the surface within the experimental uncertainty of the tilt calculations and without considering the twist angle. When the twist angle is considered, the hydroxyl group is no longer normal to the surface, but canted at an angle of 28° above the plane of the surface. The contact angle data presented in figure 25 support this determination as well. The contact angle at low pH averages approximately 58° indicating that the surface is somewhat hydrophilic but still has an appreciable hydrophobic component as well. The twist angle of the benzene ring should have no effect on how the hydroxyl group is presented to the interface in 4-dodecyloxymercaptophenol. The plane of the benzene ring rotates around the long molecular axis that is congruent with the 1,4 substitution pattern in 4-dodecyloxymercaptophenol. This is not true for 3-dodecyloxymercaptophenol because the hydroxyl group is at the edge of the plane of the benzene ring. As the plane of the ring rotates about the long molecular axis, the hydroxyl group rises in conjunction with the rotation.

The difference in orientation of the hydroxyl group at the interface might explain in part the differences in the titration curves between 3- and 4-dodecyloxymercaptophenol. The hydroxyl group of 3-dodecyloxymercaptophenol is more accessible to hydroxide anion than is the hydroxyl group of 4-dodecyloxymercaptophenol. Intermolecular forces probably

play an import role as well. CV experiments have been used to explore the intermolecular forces between the molecules of the SAM.

### 4.4 Cyclic voltammetry of 3- and 4-dodecyloxymercaptophenol and 12-phenoxy-dodecane-1-thiol monolayer on gold

CV is frequently used to study monolayers deposited on gold substrates. Finklea has recently reviewed the CV of monolayer coated electrodes so a review of the literature will not presented here[27]. The working electrode in CV experiments is the substrate on which the monolayer is deposited and is usually referred to as a planar metal electrode. In the experiments presented here, the potential was scanned from –0.200 V to –1.200 V at a scan rate of 100 mV/s. Since the electrochemical active species is already at the electrode, no kinetic effects should be apparent in reductive desorption experiments. To confirm this slower scan rates were examined which produced results equivalent to results obtained at faster scans. Porter[18] has shown that the electrode reaction studied here is as shown in equation 22

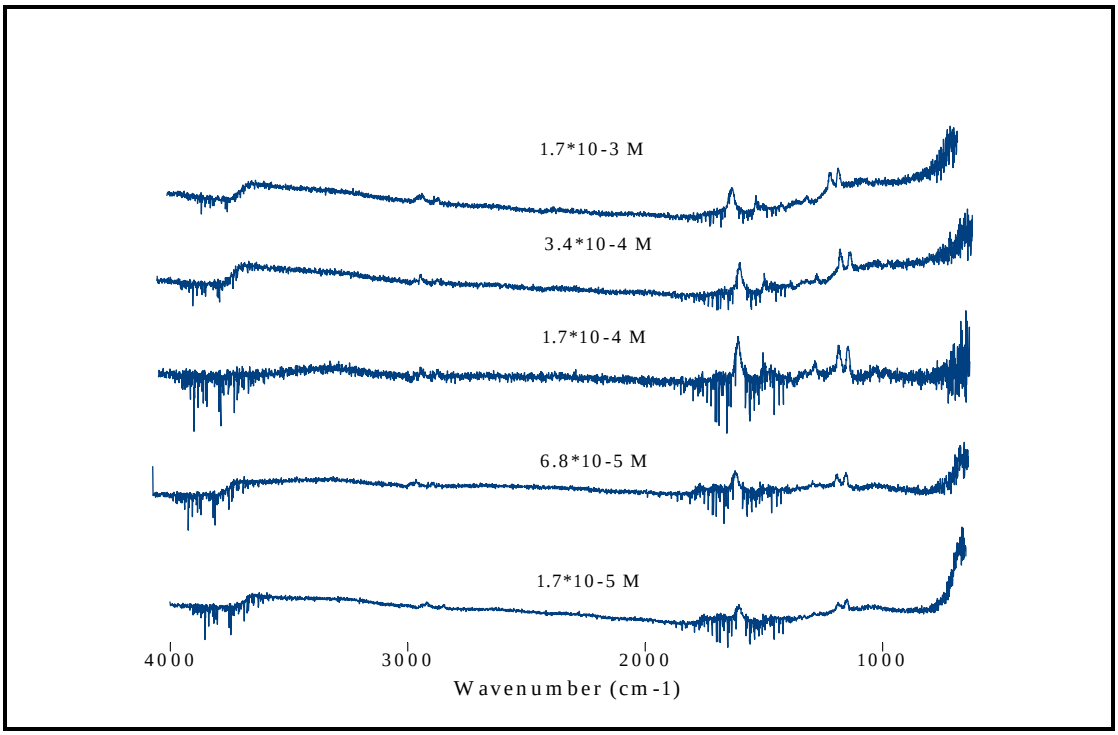


**Figure 38. RAIR spectra of monolayers prepared by exposing the gold substrate to solutions of 3-dodecyloxymercaptophenol whose concentration is indicated in the figure. The methylene peak intensity decreased as the solution concentration of the thiol decreases. The spectra have not been smoothed or processed in any fashion.**

**Equation 22. Electrode Reaction**

$$Au{-}S{-}R + e^- \longrightarrow Au + S^-{-}R$$

in which one electron is used to reduce the gold-sulfur bond creating gold metal and a thiolate anion. This reaction indicates that reductive desorption of the thiol occurs upon application of potential to the electrode.

Intermolecular forces were examined by preparing SAMs having different surface coverages of the molecules on gold metal substrates. The surface coverage of the thiol was varied by exposing the substrate to different solution concentrations of the thiol for a period of two hours at 25.0°±0.1° C. Figure 38 shows the RAIR spectra of each surface after exposure to solutions of 3-dodecyloxymercaptophenol whose concentrations are indicated in figure 38 above each spectrum. The intensity of the C-H stretch of the methylene groups decreases as the solution concentration decreases indicating that fewer molecules are present on the surface. Generally, the number of molecules on the surface can not be quantified using RAIRS because of the metal surface selection rule. When fewer molecules are adsorbed on the surface, the orientation of the molecule can change. Some bands can become more intense at lower surface coverage because the TDM changes its orientation with respect to the surface. Qualitatively, the spectra suggest that fewer molecules are present. CV can be used to quantitatively measure the number of molecules present on the surface by integrating the area under the desorption peak in the cyclic voltammagram and using equation 22. Figure 39 shows the RAIR spectra of an electrode before

a CV desorption experiment and after the CV experiment. The features present in

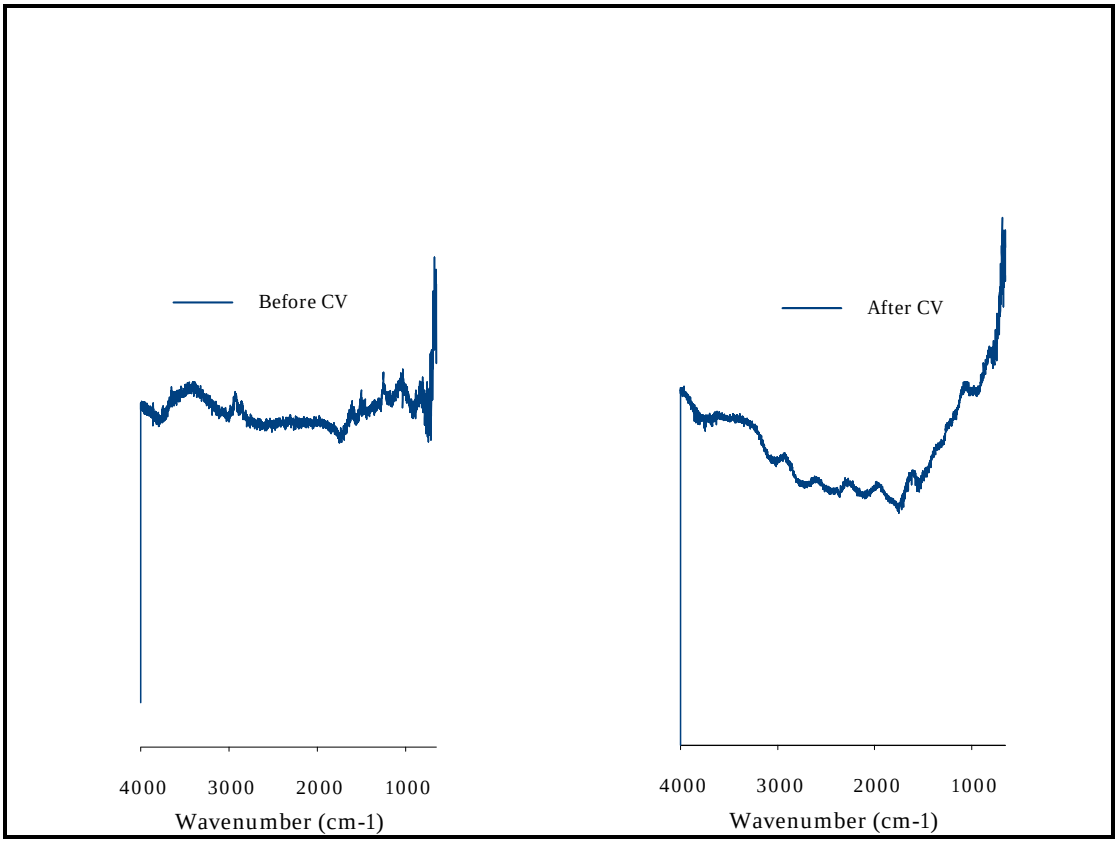


**Figure 39. RAIR spectra taken of a planar, gold metal electrode prior to and after a CV desorption experiment. The spectrum on the right indicates that the SAM has been completely desorbed from the electrode. The spectra were not processed in any way.**

the spectrum obtained before the CV experiment show the monolayer is adsorbed on the surface. The same features present prior to the experiment have disappeared after the CV experiment indicating that the monolayer has been desorbed.

The cyclic voltammagrams of an uncoated electrode and 3-dodecyloxymercaptophenol at high, low and intermediate surface coveragess are shown in are shown in figure 40. The CVs show interesting features. As the surface cooverage decreases, the desorption peak potential shifts to more positive values. Since fewer molecules are present on the surface, as indicated by the lower peak area of each CV, it is reasonable to assume that the intermolecular interactions between the chains making up the monolayer decreases as the average distance between surface molecules increases. This shift in peak

potential can be explained if the adsorption process obeys Frumkin's adsorption model which must be the case since intermolecular interactions account for the self-assembly mechanism.

**Equation 23. Frumkin adsorption isotherm equation**

$$\beta_i a_i^b = \frac{\Gamma_i}{\Gamma_s - \Gamma_i} \exp\left(\frac{2g\Gamma_i}{RT}\right)$$

where $\Gamma_i$ is the amount of material adsorbed on the surface per unit area, $a_i^b$ is the activity of *i* in bulk solution. In equation 23, $\Gamma_s$ is the saturation coverage of the electrode, g is a parameter that expresses the way in which increased coverage of the surface changes the adsorption energy of species *i*. R and T have their usual meanings. The quantity $\beta_i$ is given in equation 24

**Equation 24. Esin-Markov coefficient**

$$\beta_i = \exp\left(\frac{-\Delta\overline{G}_i^0}{RT}\right)$$

where $\Delta\overline{G}_i^0$ is the standard free energy of adsorption of species i. Frumkin's model of adsorption explicitly accounts for intermolecular interactions. Frumkin's adsorption model is more general than Langmuir's model because Langmuir's model of adsorption assumes that intermolecular interactions between the adsorbing molecules do not occur once the molecules adsorb. Angerstein-Kozlowska[113] used computer simulations to show that the degree of the contribution of intermolecular interactions to the peak potential for oxide formation on surfaces could be ascertained from a current-overpotential characteristic equation that was shown to reduce to Frumkin's adsorption isotherm equation. This model was refined by Imabayashi[114], *et. al.* for a current-potential relationship and applied to the specific case of thiol adsorption. In electrochemical terms, Imabayashi, *et. al.* showed that the current-potential characteristic could be written as a Frumkin type adsorption isotherm (equation 25)[115]

**Equation 25. Frumkin type adsorption isotherm derived from the current-potential relationship.**

$$Bc\exp\left(\frac{F}{RT}(\Delta E)\right)=\frac{\Gamma_i}{1-\Gamma_i}\exp(-2g\Gamma_i)$$

where $B$ is the adsorption coefficient, $c$ is the surface concentration, $\Delta E$ is the difference in peak potentials, $\Gamma_i$ is the surface coverage and $g$ is the interaction parameter. The variable $g$ is a measure of the degree of interaction between the chains of the SAM.

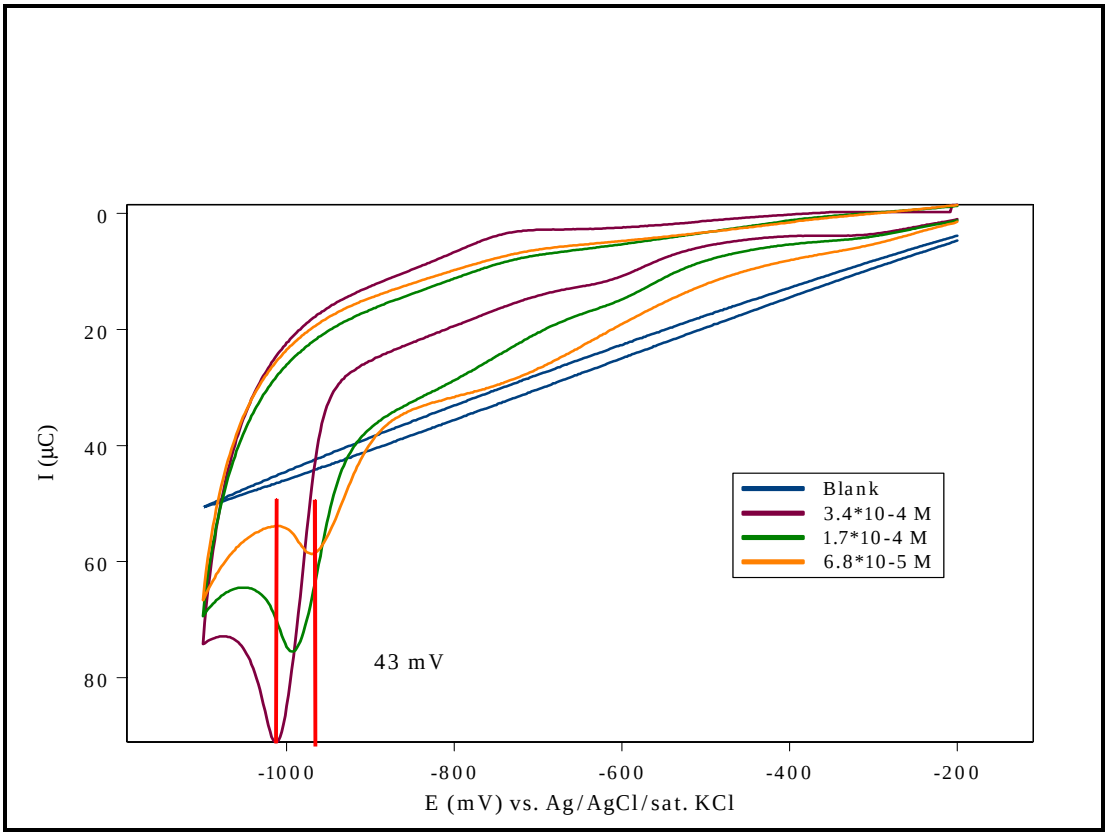


**Figure 40. Cyclic voltammagrams of 4-dodecyloxymercaptophenol at different surface concentrations and an uncoated blank. The separation of the peak potentials at high and low surface concentration is 43 mV. The electrolyte was 0.5 M KOH that had been deaerated. The initial potential was –0.200 V and was swept at 100 mV/s to a final potential of –1.200 V. The area of the electrode was 0.646 cm².**

applied here to measure the degree of intermolecular interactions between the molecules that make up the SAM. As figure 40 shows, the peak desorption potential shifts to more positive values as the surface coverage decreases as measured by the area under the peak. The integrated area under the peak was measured by establishing a baseline on either side of the peak using a tangent line method. At the lowest surface coverage, the peak potential shifts by 43 mV from the peak potential value at the highest surface coverage. Tables 1 through 3 summarize the data from the CV experiments. The data in the tables show that 3-dodecyloxymercaptophenol desorbs at peak potentials more negative than the peak potentials at which 4-dodecyloxymercaptophenol desorb. These data were collected using 0.5 M KOH as the electrolyte which should ionize both 3- and 4-dodecyloxymercaptophenols. Since the compounds are ionized, there should be stronger electrostatic repulsions between ionized hydroxyl groups that are closer together. The peak potential for desorption of 3-dodecyloxymercaptophenol at a surface coverage of $1.064*10^{-10}$ mol/cm$^2$ is shifted by 24 mV more negative than the peak potential of 4-dodecyloxymercaptophenol at a surface coverage of $1.091*10^{-10}$ mol/cm$^2$. This indicates that at nearly constant surface coverage, 3-dodecyloxymercaptophenol is 2.32±0.07 kJ/mol (0.024 V·96484.6 C/mol) more stable than 4-dodecyloxymercaptophenol. In the unionized state, the hydroxyl groups of 4-dodecyloxymercaptophenol would appear to be closer to each other since in the ionized state the 4-dodecyloxymercaptophenol is less stable upon ionization than is 3-dodecyloxymercaptophenol. This suggests that stronger hydrogen bonding

**Table 1*. Desorption results for 4-dodecyloxymercaptophenol. Solution concentration represents the concentration of the solution from which the surface was prepared.**

| Peak Position ±5 (mV) | Area ±0.05 (μC) | $(\Gamma \pm 0.005) * 10^{-10}$§ (mol/cm²) | Solution Concentration (M) |
|---|---|---|---|
| -1013 | 23.07 | 3.701 | $3.4*10^{-4}$ |
| -993 | 13.12 | 2.105 | $1.7*10^{-4}$ |
| -970 | 6.80 | 1.091 | $6.8*10^{-5}$ |
| -960 | 4.69 | $7.53*10^{-11}$ | $1.7*10^{-5}$ |

**Table 2*.** Desorption results for 3-dodecyloxymercaptophenol. Solution concentration represents the concentration of the solution from which the surface was prepared.

| Peak Position ±5 (mV) | Area ±0.05 (μC) | $(\Gamma \pm 0.005) * 10^{-10}$§ (mol/cm²) | Solution Concentration (M) |
|---|---|---|---|
| -1149 | 25.07 | 5.197 | $3.4*10^{-4}$ |
| -1103 | 19.44 | 4.030 | $1.7*10^{-4}$ |
| -1051 | 17.31 | 2.777 | $6.8*10^{-5}$ |
| -994 | 6.63 | 1.064 | $1.7*10^{-5}$ |

**Table 3*.** Desorption results for 12-phenoxy-dodecane-1-thiol. Solution concentration represents the concentration of the solution from which the surface was prepared.

| Peak Position ±5 (mV) | Area ±0.05 (μC) | $(\Gamma \pm 0.005) * 10^{-11}$§ (mol/cm²) | Solution Concentration (M) |
|---|---|---|---|
| -903 | 5.09 | $8.165*10^{-10}$ | $3.4*10^{-4}$ |
| -895 | 3.41 | 5.472 | $1.7*10^{-4}$ |
| -883 | 2.43 | 3.904 | $6.8*10^{-5}$ |
| -875 | 1.82 | 2.932 | $1.7*10^{-5}$ |

* All experiments used deaerated 0.5 M KOH as the electrolytic solution.
§ Unless otherwise indicated.

between the unionized hydroxyl groups in 4-dodecyloxymercaptophenol would occur which could partially explain the absence of a plateau at high pH in the titration curve of this compound. It is difficult to distinguish the chain intermolecular forces from the intermolecular forces of the hydroxyl group. Attempts to measure the effect of the hydroxyl group on intermolecular interactions failed. Experiments with electrolyte solutions of KCl at 0.1 M, 0.5 M and 1.0M did not show desorption peaks in the CVs. The alkyl chains of the monolayer apparently passivated the electrode and prevented desorption.

## 5.0 Summary

Molecules of 3-dodecyloxymercaptophenol, 4-dodecyloxymercaptophenol and 12-phenoxy-dodecane-1-thiol were synthesized using a novel synthetic method. These molecules differ in that 3- and 4-dodecyloxymercaptophenol have ionizable functional groups substituted at different positions on the benzene ring. 12-phenoxy-dodecane-1-thiol was synthesized because it has no ionizable functional group, which allows it to be used as a control surface when measuring the surface acid titration curves. The hydroxyl group substitution pattern on the benzene ring presents the hydroxyl group to the interface at different angles.

A quartz crystal microbalance was built and used to determine the surface acid titration curve for 3- and 4-dodecyloxymercaptophenol. Data was presented demonstrating the equivalence of contact angles measured by the QCM and optical goniometry using phenol solutions. Data was also presented showing the reproducibility of the QCM contact angle measurements. The origin of the transition from low pH to high pH was demonstrated to be the result of ionization of the hydroxyl group in 3- and 4-dodecyloxymercaptophenol. This conclusion was based upon titration of 12-phenoxy-dodecane-1-thiol, which showed no transition from low to high pH. From QCM contact angle measurements, it was found that 3-dodecyloxymercaptophenol had plateaus at both high and low pH while 4-dodecyloxymercaptophenol had a plateau only at low pH. This different behavior was due in part to the different orientations of hydroxyl groups at the interface.

RAIRS was used to measure the *ex situ* angle made by the long molecular axis of the benzene ring with the surface normal. This angle, referred to as the tilt angle, measured 46° for 4-dodecyloxymercaptophenol and 55° for 3-dodecyloxymercaptophenol. The angle that the plane of the benzene ring makes with the surface was also determined and measured 36° for 4-dodecyloxymercaptophenol and 28° for 3-dodecyloxymercaptophenol. These differences in the orientation of the benzene ring presented the ionizable hydroxyl group to the interface in different manners. The hydroxyl group of 4-dodecyloxymercaptophenol was less accessible to buffer solution at the interface compared to the hydroxyl group of 3-dodecyloxymercaptophenol.

Cyclic voltammetry was used to measure intermolecular interactions between the chains of the molecules making up the SAM. It was found that monolayers of 4-dodecyloxymercaptophenol were 2.3 kJ/mol less stable than monolayers of 3-dodecyloxymercaptophenol. The difference in stability of the monolayers was explained in terms of a nearest neighbor argument of the anion. In 4-dodecyloxymercaptophenol, the anions of the ionized monolayer appear to be closer and destabilize the monolayer through electrostatic repulsion compared to 3-dodecyloxymercaptophenol. Since the hydroxyl anions appear to be closer in the ionized monolayer, they may be closer in the unionized form. This would promote greater hydrogen bonding between hydroxyl groups of nearest neighbors and might explain in part the difference in the $pK_{1/2}$ values of 3- and 4-dodecyloxymercaptophenol.

By using infrared spectroscopy to determine the tilt and twist angle of the benzene ring in 3- and 4-dodecyloxymercaptophenol, the position of the hydroxyl group was shown to presented to the interface between the SAM and buffered aqueous solutions in different positions.

The important finding in this thesis is that surface acidity is impacted by the orientation of the acidic functional group on the surface. This raises several questions that could be explored in future experiments. Do more acidic functional groups show a stronger dependence on orientation than do the hydroxyl groups studied here? Do basic surfaces show a similar dependence on orientation as acid surfaces? More fundamental questions could also be probed

using SAMs. By varying the surface composition of the SAM, polar and dispersive contributions to surface free energy could be systematically explored. Past experiments to study these properties have always been limited by the uncertainties of surface composition and structure. As shown in these experiments, the structure of SAMs can be determined from infrared spectroscopy and electrochemistry can be used to quantitatively determine the number of molecules present.

When preparing surfaces for specific purposes, as in surface priming for adhesion applications, the functional group orientation must be considered. In these experiments, the meta substitution pattern is more reactive than the para substitution pattern in terms of the acid-base reactions. The orientation of the functional group at the interface between a SAM and adhesive overlayer, for example, makes substitution reactions in the resole reaction less likely because only one side of the benzen ring is likely to be available. Cross-linking reactions will likely not occur because of this. For the same reason, mechanical interlocking between the SAM and other polmer adhesives will likely not occur as well.

## References


1 J. Comyn, ”Adhesion Science”, Royal Society of Chemistry Paperbacks: Cambridge, 1997.

2 D.L. Allara, R. G. Nuzzo, *Langmuir*, 1, pp 45-52, 1985.

3 D.L. Allara, R. G. Nuzzo, *Langmuir*, 1, pp 52-66, 1985.

4 E. B. Troughton, C. D. Bain, G. M. Whitesides, R. G. Nuzzo, D. L. Allara, M. D. Porter, *Langmuir*, 4, pp 365-385, 1988.

5 C. D. Bain, E. B. Troughton, Y. Tao, J. Evall, G. M. Whitesides, R. G. Nuzzo, *Journal of the American Chemical Society*, 111, pp 321-335, 1989.

6 K. D. Truong, P. A. Rowntree, *Journal of Physical Chemistry*, 100, pp 19917-19926, 1996.

7 Y. Li, J. Huang, R. T. McIver, J. Hemminger, *Journal of the American Chemical Society*, 114, p 2428, 1992.

8 C. A. Widrig, C. Chung, M. D. Porter, *Journal of Electroanalytical Chemistry*, 310, pp 335-359, 1991.

9 E. Livni, M. A. Davis, V. D. Warner, *Journal of Medicinal Chemistry*, 22(5), pp 580-583.

10 C. Beiniarz, M. J. Cornwell, *Tetrahedron Letters*, 34(6), pp 939-942, 1993.

11 T. Kim, R. M. Crooks, *Tetrahedron Letters*, 35(51), pp 9501-9504, 1994.

12 T. Zheng, M. Burkart, D. E. Richardson, *Tetrahedron Letters*, 40, pp 603-606, 1999.

13 L. E. Iglesias, A. Baldessari, E. G. Gros, *Organic Preparations and Procedures International*, 28(3), 319-324, 1996.

14 F. Buckel, P. Persson, F Effenberger, *Synthesis*, 6, pp 953-958, 1999.

15 A. Ulman, *An Introduction to Ultrathin Organic Films:from Langmuir-Blodgett to Self-assembly*, Academic Press, San Diego, 1991.

16 A. Ulman, *Characterization of Organic Thin Films: Materials Characterization Series-Surfaces, Interfaces, Thin Films*, Butterworth-Heinemann, Stoneham, MA, 1995.

[17] Th. Wink, S. J. van Sulien, A. Bult, W. P. van Bennekom, *Analyst*, 122, pp 43R-50R, 1997.

[18] C. J. Zhong, M. D. Porter, *Analytical Chemistry*, 67, pp 709A-715A, 1995.

[19] G. M. Whitesides, P. E. Laibinis, Langmuir, 6, pp 87-96, 1990.

[20] H. O. Finklea, *Electroanalytical Chemistry*, eds. A. J. Bard, I Rubinstein, Marcel Dekker, New York, pp 109-335, 19, 1996.

[21] L. H. Dubois, R. G. Nuzzo, *Annual Review of Physical Chemistry*, 43, pp 437-463, 1992.

[22] A. R. Bishop, R. G. Nuzzo, 'Self-assembled Monolayers: Recent Developments and Applications', *Current Opinions Colloid and Interfacial Science*, 1, pp 127-136, 1996.

[23] D. L. Allara, R. G. Nuzzo, 'Modifications of Properties of Metals', U. S. Patent Application 389/775 (June 18), 1982.

[24] R. G. Nuzzo, D. L. Allara, *Journal of the American Chemical Society*, 105, pp 4481-4483, 1983.

[25] R. G. Nuzzo, f. a. Fusco, D. L. Allara, *Journal of the American Chemical Society*, 109, pp 2358-2368, 1987.

[26] M. D. Porter, T. B. Bright, D. L. Allara, C. E. D. Chidsey, *Journal of the American Chemical Society*, 109, pp 2358-2368, 1987.

[27] H. O. Finklea, S. Avery, M. Lynch, T. Furtsch, *Langmuir*, 3, pp 409-413, 1987.

[28] E. Sabatani, I. Rubinstein, R. Maoz, J. Sagiv, 'Organized Self-assembling Monolayers on Electrodes. Part I. Octadecyl Derivatives on Gold', *Journal of Electroanalytical Chemistry*, 219, pp 365-371, 1987.

[29] E. B. Troughton, C. D. Bain, G. M. Whitesides, R. G. Nuzzo, D. L. Allara, M. D. Porter, *Langmuir*, 4, pp 365-385, 1988.

[30] W. A. Zisman, in *Handbook of Adhesives*, I. Skiest, Ed.,; Van Nostrand: New York, 1977.

[31] Z. X. Lin, R. M. Hill, H. T. Davis, M. D. Ward, *Langmuir*, 10, pp 4060-4068, 1994.

[32] T. Stoebe, R. M. Hill, M. D. Ward, H. T. Davis, *Langmuir*, 13, pp 7276-7281, 1997.

[33] M. E. Napier, H. H. Thorp, *Langmuir*, 13, pp 6342-6344, 1997.

[34] M. A. Reed, C. Zhou, C. J. Miller, T. P. Burgin, J. M. Tour, *Science*, 278, pp 252-254, 1997.

[35] R. G. Nuzzo, L. H. Dubois, D. L. Allara, *Journal of the American Chemical Society*, 112, pp 558-569, 1990.

[36] S. W. Tam-Chang, H. A. Biebuyck, G. M. Whitesides, *Langmuir*, 11, pp 4371-4382, 1995.

[37] R. S. Clegg, J. E. Hutchison, *Langmuir*, 12, pp 5239-5243, 1996.

[38] S. C. Chang, I. Chao, Y. T. Tao, *Journal of the American Chemical Society*, 116, pp 6792-6805, 1994.

[39] Y. T. Tao, C. C. Wu, J. Y. Eu, W. L. Lin, K. C. Wu, C. Chen, *Langmuir*, 13, pp 4018-4023, 1997.

[40] E. Sabatini, J. Cohen-Boulakia, M. Bruening, I. Rubinstein, *Langmuir*, 9, pp 2974-2981, 1993.

[41] T. Kim, R. M. Crooks, M. Tsen, L. Sun, *Journal of the American Chemical Society*, 117, 3963-3967, 1995.

[42] S. B. Bachs, S. P. Dudek, R. P. Hsung, L. A. Sita, J. F. Smalley, M. D. Newton, S. W. Feldberg, C. E. D. Chidsey, *Journal of the American Chemical Society*, 119, pp 10563-10564, 1997.

[43] R. W. Zehner, L. R. Sita, *Langmuir*, 13, pp 2973-2979, 1997.

[44] S. D. Evans, E. Urankar, A. Ulman, N. Ferris, *Journal of the American Chemical Society*, 113, pp 4121-4131, 1991.

[45] C. D. Bain, G. M. Whitesides, *Journal of the American Chemical Society*, 110, pp 5897-5898, 1988.

[46] C. Pale-Grosdemange, E. S. Simon, K. L. Prime, G. M. Whitesides, *Journal of the American Chemical Society*, 113, pp 12-20, 1991.

[47] P. E. Laibinis, C. D. Bain, R. G. Nuzzo, G. M. Whitesides, *Journal of Physical Chemistry*, 99, pp 7663-7667, 1995.

[48] B. Liedberg, Z. Yang, I. Engquist, M. Wirde, U. Gelius, G. Gotz, P. Bauerle, r. M. Rummerl, C. Ziegler, W. Gopel, *Journal of Physical Chemistry B*, 101, pp 5951-5962, 1997.

[49] J. M. Tour, L. J. Jones II, D. L. Pearson, J. J. S. Lamba, T. P. Burgin, G. M. Whitesides, D. L. Allara, A. N. Parikh, S. V. Atre, *Journal of the American Chemical Society*, 117, pp 9529-9534, 1995.

[50] R. G. Nuzzo, L. H. Dubois, D. L. Allara, *Journal of the American Chemical Society*, 112, 558-569, 1990.

[51] M. M. Walczak, C. A. Alves, B. D. Lamp, M. D. Porter, *Journal of Electroanalytical Chemistry*, 396, pp 103-114, 1995.

[52] V. K. Gupta, N. L. Abbott, *Langmuir*, 12, pp 2587-2593, 1996.

[53] W. B. Caldwell, K. Chen, B. R. Herr, C. A. Mirkin, J. C. Hulteen, R. P. Van Duyne, *Langmuir*, 10, pp 4109-4115, 1994.

[54] P. Wagner, M. Hegner, H. J. Guntherodt, G. Semenza, *Langmuir*, 11, pp 3867-3875, 1995.

[55] D. Stamou, D Gourdon, M. Liley, N. A. Burnham, A. Kulik, H. Vogel, C. Duschl, *Langmuir*, 13, pp 2425-2428, 1997.

[56] Y. Golan, L. Margulis, I. Rubinstein, *Surface Science*, 264, pp 312-326, 1992.

[57] P. E. Laibinis, G. M. Whitesides, *Journal of American Chemical Society*, 114, pp 1990-1995, 1992.

[58] P. E. Laibinis, C. D. Bain, G. M. Whitesides, *Journal of Physical Chemistry*, 95, pp 7017-7021, 1991.

[59] P. E. Laibinis, G. M. Whitesides, D. L. Allara, Y. T. Tao, A. N. Parikh, G. G. Nuzzo, *Journal of the American Chemical Society*, 113, pp 7152-7167, 1991.

[60] K. Chen, F. Xu, C. A. Mirkin, R. L. Lo, L. s. Nanjundaswamy, J. P. Zhou, J. T. McDevitt, *Langmuir*, 12, pp 2622-2624, 1996.

[61] A. D. Vogt, T. Han, T. P. Beebe, *Langmuir*, 13, pp 3397-3403, 1997.

[62] Z. Mekhalif, J. J. Pireaux, J. Delhalle, *Langmuir*,13, 2285-2290, 1997.

[63] T. Kondo, M. Takechi, Y. Sato, K. Uosaki, *Journal of Electroanalytical Chemistry*, 381, pp 203-209,1995.

[64] F. P. Zamforini, J K. Campbell, R. M. Crooks, *Langmuir*, 14, pp 640-647, 1998.

[65] G. K. Jennings, P. E. Laibinis, *Journal of the American Chemical Society*, 119, pp 5208-5214, 1997.

[66] J. D. Burgess, F. M. Hawkridge, *Langmuir*, 13, pp 3781-3786, 1997.

[67] H. Ron, S. Matlis, I. Rubinstein, *Langmuir*, 14, pp 1116-1121, 1998.

[68] H. Ron, I. Rubinstein, *Langmuir*, 10, 4566-4573, 1994.

[69] G. E. Poirier, E. D. Pylant, *Science*, 272, pp 1145-1148, 1996.

[70] O. Chailapakul, L. sun, c. Xu, R. M. Crooks, *Journal of the American Chemical Society*, 115, pp 12459-12467, 1993.

[71] J. Liu, A. E. Kaifer, *Israel Journal of Chemistry*, 37, pp 235-239, 1997.

[72] C. Miller, P. Cuendet, M. Gratzel, *Journal of Physical Chemistry*, 95, pp 877-886, 1991

[73] K. A. Peterlinz, R. Georgiadis, *Langmuir*, 12, pp 4731-4740, 1996.

[74] N. Camillone, C. E. D. Chidsey, P. Eisenberger, P. Fenter, J. Li, K. S. Liang, G. Y. Liu, G. Scoles, *Journal of Chemical Physics*, 99, pp 744-747, 1993.

[75] E. Delamarche, B. Michel, Ch. Gerber, D. Anselmetti, H. J. Guntherodt, H. Wolf, H. Ringsfdorf, *Langmuir*, 10, pp 2869-2871.

[76] H. O. Finklea, D. D. Hanshew, *Journal of Electroanalytical Chemistry*, 347, pp 327-340, 1993.

[77] K. J. Stevenson, M. Mithell, H. S. White, *Journal of Physical Chemistry B*, 102, pp 1235-1240, 1998.

[78] D. E. Weisshaar, B. D. Lamp, M. D. Porter, *Journal of the American Chemical Society*, 114, pp 5860-5862, 1992.

[79] D. W. Hatchett, R. H. Uibel, K. J. Stevenson, J. M. Harris, H. S. White, *Journal of the American Chemical Society*, 120, pp 1062-1069, 1998.

[80] S. R. Holmes-Farley, C. D. Bain, G. M. Whitesides, *Langmuir*, 4, pp 921-937, 1988.

[81] G. M. Whitesides, H. A. Biebuyck, J. P. Folkers, K. L. Prime, *Journal of Adhesion Science and Technology*, 5, pp 57-69, 1991.

[82]H.-Z. Yu, N. Xia, Z.-F. Liu, *Analytical Chemistry*, 71, pp 1354-1358, 1999.

[83] H. S. White, J. D. Peterson, Q. Cui, K. J. Stevenson, *Journal of Physical Chemistry B*, 102, pp 2930-2934, 1998.

[84] K. Hu, A. J. Bard, *Langmuir*, 13, pp 5114-5119, 1997.

[85] M. R. Anderson, D. H. Evans, *Journal of the American Chemical Society*, 110, pp 6612-6617, 1988.

[86] S. E. Creager, J. Clarke, *Langmuir*, 10, pp 3675-3683, 1994.

[87] M. A. Bryant, R. M. Crooks, *Langmuir*, 9, pp 385-387, 1993.

[88] A. D. Cort, L. Mandolini, B. Masci, *Journal of Organic Chemistry*, 48, pp 3979-3982, 1983.

[89] G. V. S. Reddy, G. V. Rao, D. S. Iyengar, *Synthetic Communications*, 30, pp 859-862, 2000.

[90] J. H. Teuscher, R. L. Garrell, *Analytical Chemistry*, 67, pp 3372-3375, 1995.

[91] H. Bahadur, R. Parshad, *Physical Acoustics*, 16, pp 37-131, 1982.

[92] G. Sauerbrey, *Z. Phys.*, 155, p 206, 1959.

[93] T. Nomura, M. Iijima, *Analytica Chimica Acta*, 131, p 97, 1981. T. Nomura, T. Nagamune, K Izutsu, T. S. West, *Bunseki Kagaku*, 30, p 494, 1981.

[94] V. Mecea, R. V. Bucur, *Thin Solid Films*, 60, p 73, 1979.

[95] K. K. Kanazawa, J. G. Gordon II, *Analytica Chimica Acta*, 175, pp 99-105, 1985.

[96] Z. Lin, M. D. Ward, *Analytical Chemistry*, 68, pp 1285-1291, 1996.

[97] K. K. Kanazawa, J. G. Gordon II, *Analytical Chemistry*, 57, pp 1171-1172, 1985.

[98] R. J. Mathys, *Crystal Oscillator Circuits*, John Wiley & Sons: New York, 1983. T. M. Adams, *Oscillator Circuits*, Howard W. Sams & Co.: New York, 1964.

[99] S. Bruckenstein, M. Shay, *Electrochemica Acta*, 30, p 1295, 1985.

[100] M. Benje, M. Eiermann, U. Pittermann, K. G. Weil, *Ber. Bunsen – Ges. Phys. Chem.*, 90, p 435, 1986.

[101] D. Orato, D. A. Buttry, *Journal of the American Chemical Society*, 109, p 3574, 1987.

[102] O. Melroy, K. K. Kanazawa, J. G. Gordon, *Langmuir*, 2, p 697, 1987.

[103] G.M. Whitesides

[104] R. G. Greenler, *Journal of Chemical Physics*, 44, pp 310-315, 1965.

[105] Reference to character tables in any book on group theory confirms this statement.

[106] A. M. Bradshaw, *Z. Phys. Chem.*, 112, p 83, 1978.

[107] D. L. Allara, R. G. Nuzzo, *Langmuir*, 1, pp 52-66, 1985.

[108] O. S. Heavens, "Optical Properties of Thin Solid Films", Academic Press, Inc. New York, 1955.

[109] D. W. Berreman, *Physical Review*, 130, p 2193, 1963.

[110] S. A. Francis, A. H. Ellison, *Journal of the Optical Society of America*, 49, p 131-138, 1959.

[111] J. A. Bardwell, M. J. Dignam, *Journal of Chemical Physics*, 83, pp5468-5478, 1985.

[112] V. Cammarata, L. Atanasoska, L. L. Miller, C. J. Kilaskie, B. J. Stallman, *Langmuir*, 8, p 876, 1992.

[113] H. Angerstein-Kozlowska, J. Klinger, B. E. Conway, *Journal of Electroanalytical Chemistry*, 75, pp 45-60, 1977.

[114] S. Imabayashi, M. Iida, D. Hobara, Z. Q. Feng, K. Niki, T. Kakiuchi, *Journal of Electroanalytical Chemistry*, 428, pp 33-38, 1997.

[115] A. J. Bard, L. R. Faulkner, *Electrochemical Methods*, John Wiley & Sons: New York, 1980.

## Vita

The author, Charles Douglas Taylor, was born in 1967 in Livingston, Tennessee and raised in many states of the eastern United States of America. After graduation from Livingston Academy High School in 1985, Doug attended Tennessee Technological University in Cookeville, Tennessee. While at Tennessee Tech, Doug carried out research under the direction of Professor Robert J. Glinkski and published several papers in the area of chemiluminescence spectroscopy. He was married to Tracey Renee Smith and accepted a position with A. E. Staley Manufacturing Company in Loudon, Tennessee after completing Bachelor of Science in Chemistry degree requirements at Tennessee Tech.

He began his studies at Virginia Polytechnic Institute and State University in August 1996 under the direction of Professor Mark R. Anderson. While at Virginia Tech, he studied the affect molecular orientation of surface confined acid groups has on surface acidity and coauthored several papers.

He and Tracey are expecting the birth of their son, Haydn Douglas, in November 2000, and he received his Ph. D. degree in August of the same year. He has accepted employment with Xanthon, Incorporated in Research Triangle Park, North Carolina where he will be developing electrochemical instrumentation for DNA sequencing.